

RÉPUBLIQUE DU CAMEROUN
Paix - Travail - Patrie

UNIVERSITÉ DE YAOUNDÉ I

CENTRE DE RECHERCHE ET DE FORMATION
DOCTORALE EN SCIENCES, TECHNOLOGIES
ET GEOSCIENCES

Unité de recherche et de formation
doctorale en physiques et applications

B.P 812 Yaoundé
Email: crfd_stg@uy1.uninet.cm



REPUBLIC OF CAMEROON
Peace - Work - Fatherland

UNIVERSITY OF YAOUNDE I

POSTGRADUATE SCHOOL OF SCIENCES,
TECHNOLOGY AND GEOSCIENCES

Research and postgraduate training
unit for physics and applications

P.O. Box 812 Yaoundé
Email: crfd_stg@uy1.uninet.cm

DÉPARTEMENT DE PHYSIQUE
DEPARTMENT OF PHYSICS

LABORATOIRE DE MÉCANIQUE, MATÉRIAUX ET STRUCTURES
LABORATORY OF MECHANICS, MATERIALS AND STRUCTURES

**Ultra-short truncated Airy pulses regeneration
and supercontinuum generation in nonlinear
optical waveguides: cases of fiber-optics links and
AsSe₂/As₂S₅-ChRW**

*Thesis submitted and defended in partial fulfillment of the requirements for the awards
of a Doctor of Philosophy (PhD) degree in Physics*

**Specialty: Mechanics, Materials and Structures
Option: Fundamental Mechanics and Complex Systems**

By
HEUTEU Crépin
*Registration number: 09W0136
Master in Physics*

Jury:

President:	ESSIMBI ZOBO Bernard	<i>Professor, University of Yaounde I</i>
Supervisors:	TCHAWOUA Clément	<i>Professor, University of Yaounde I</i>
Examiners :	DIKANDE Alain Moïse	<i>Professor, University of Buea</i>
	DJUIDJE KENMOE Germaine	<i>Professor, University of Yaounde I</i>
	BEN-BOLIE Germain Hubert	<i>Professor, University of Yaounde I</i>
	FEWO Serge Ibraïd	<i>Associate Professor, University of Yaounde I</i>



© Year: 2024



DEPARTEMENT DE PHYSIQUE
DEPARTMENT OF PHYSICS

ATTESTATION DE CORRECTION DE LA THESE DE
DOCTORAT/PhD DE HEUTEU CREPIN

Nous, Professeurs **DIKANDE Alain Moïse**, **DJUIDJE KENMOE Germaine**, **BEN-BOLIE germain Hubert**, **FEWO Serge Ibraïd** et **ESSIMBI ZOBO Bernard**, respectivement Examineurs et Président du jury de la thèse de Doctorat/PhD de Monsieur **HEUTEU Crépin** Matricule **09W0136**, préparée sous la direction du Professeur **TCHAWOUA Clément**, intitulée : « *Ultra-short truncated Airy pulses regeneration and supercontinuum generation in nonlinear optical waveguides : cases of fiber-optics links an AsSe₂/As₂S₅-ChRW* », soutenue le **lundi, 22 Janvier 2024**, en vue de l'obtention du grade de **Docteur/PhD** en Physique, Spécialité **Mécaniques, matériaux et structures**, attestons que toutes les corrections demandées par le Jury de soutenance ont été effectuées.

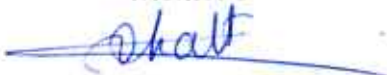
En foi de quoi, la présente attestation lui est délivrée pour servir et valoir ce que de droit.

Fait à Yaoundé le **22 FEV 2024**

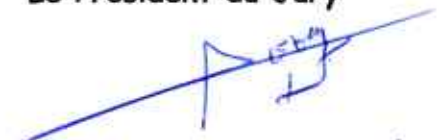
Membre

Membre

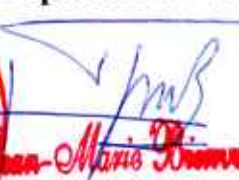
Le Président du Jury


DJUIDJE Kenmoe Germaine


R. BEN-BOLIE


B. Z. ESSIMBI

Le Chef de Département de Physique


Le Chef de Département
Le Chef de Département
Professeur

RÉPUBLIQUE DU CAMEROUN

Paix - Travail - Patrie

UNIVERSITÉ DE YAOUNDÉ I

CENTRE DE RECHERCHE ET DE FORMATION
DOCTORALE EN SCIENCES, TECHNOLOGIES
ET GEOSCIENCES

Unité de recherche et de formation
doctorale en physiques et applications

B.P 812 Yaoundé

Email: crfd_stg@uy1.uninet.cm



REPUBLIC OF CAMEROON

Peace - Work - Fatherland

UNIVERSITY OF YAOUNDE I

POSTGRADUATE SCHOOL OF SCIENCES,
TECHNOLOGY AND GEOSCIENCES

Research and postgraduate training
unit for physics and applications

P.O. Box 812 Yaoundé

Email: crfd_stg@uy1.uninet.cm

DÉPARTEMENT DE PHYSIQUE
DEPARTMENT OF PHYSICS

LABORATOIRE DE MÉCANIQUE, MATÉRIAUX ET STRUCTURES
LABORATORY OF MECHANICS, MATERIALS AND STRUCTURES

**Ultra-short truncated Airy pulses regeneration
and supercontinuum generation in nonlinear
optical waveguides: cases of fiber-optics links and
AsSe₂/As₂S₅-ChRW**

*Thesis submitted and defended in partial fulfillment of the requirements for the awards
of a Doctor of Philosophy (PhD) degree in Physics*

**Specialty: Mechanics, Materials and Structures
Option: Fundamental Mechanics and Complex Systems**

By

HEUTEU Crépin

Registration number: 09W0136

Master in Physics

Jury:

President: ESSIMBI ZOBO Bernard

Professor, University of Yaounde I

Supervisors: TCHAWOUA Clément

Professor, University of Yaounde I

**Examiners : DIKANDE Alain Moïse
DJUIDJE KENMOE Germaine
BEN-BOLIE Germain Hubert
FEWO Serge Ibraïd**

Professor, University of Buea

Professor, University of Yaounde I

Professor, University of Yaounde I

Associate Professor, University of Yaounde I

© Year: 2024

REPUBLIC OF CAMEROON

THE UNIVERSITY OF YAOUNDE

I

REPUBLIQUE DU CAMEROUN

UNIVERSITE DE YAOUNDE I

FACULTY OF SCIENCE

FACULTE DES SCIENCES

DEPARTMENT OF PHYSICS

DEPARTEMENT DE PHYSIQUE

Laboratory of Mechanics, Materials and Structures

Laboratoire de Mécaniques, Matériaux et Structures

**ULTRA-SHORT TRUNCATED AIRY PULSES REGENERATION
AND SUPERCONTINUUM GENERATION IN NONLINEAR
OPTICAL WAVEGUIDES: CASES OF FIBER-OPTICS LINKS
AND $\text{AsSe}_2/\text{As}_2\text{S}_5$ -ChRW**

Submitted in Partial Fulfillment of the Requirements

for the Degree of Doctor of Philosophy in Physics

Speciality: fundamental mechanic and complex systems

Option: **MECANIQUE**

by

HEUTEU Crépin

M. Sc. in Physics

Registration Number: 09W0136

Under the supervision of:

TCHAWOUA Clément

Professor

Copyright© UYI

academic year 2024

Contents

Declaration	2
Dedications	3
Acknowledgments	4
Abstract	9
Résumé	12
List of abbreviations	15
General Introduction	19
1 Literature review	27
1.1 Introduction	27
1.2 Overview on regeneration	27
1.2.1 Theoretical and physical descriptions	27
1.2.2 Fiber optic transmission system	31
1.2.3 Transmitter and receiver	32
1.2.4 Transmission channel	35
1.2.5 Optical pulse	36
1.2.6 Regeneration technique based on optical fiber	45
1.2.7 Limits of the previous Regeneration mechanism	58
1.2.8 Contributions on the truncated Airy pulses regeneration	61

1.3	Overview on SCG	62
1.3.1	Theoretical and physical descriptions	62
1.3.2	Improvement of the phenomenon: spectral bandwidth enhancement	66
1.3.3	Applications of the SCG	72
1.3.4	Limits of the previous works on SCG analysis	74
1.3.5	Contributions of SCG analysis	76
1.4	Description of the optical waveguides studied in this thesis	77
1.4.1	Fiber-optics links	77
1.4.2	Optical waveguide for SCG	83
1.5	Conclusion	85
2	Methodology: Models and Numerical Methods	86
2.1	Introduction	86
2.2	Propagation modeling: the NLSE	86
2.3	Analytical and numerical treatments of the CDM	98
2.3.1	Analytical treatment of CDM	98
2.3.2	Diagrams of the numerical algorithms/set-up schemes	102
2.3.3	Numerical treatments of CDM technique	106
2.4	Analytical and numerical treatments of SCG	111
2.4.1	Analytical modeling and data conditions	111
2.4.2	Description of the numerical code used and the simulation conditions	115
2.5	Conclusion	118
3	Results and Discussion	119
3.1	Introduction	119
3.2	On the linear CDM inducing regeneration of truncated Airy pulses in fiber-optics links	119
3.2.1	Constant positive (respectively negative) initial chirp with alternation of the GVD	120
3.2.2	Constant GVD (normal or anomalous dispersion) with alternation of chirp	121
3.2.3	Alternation of both the GVD and the initial chirp	122

3.2.4	Effect of the initial chirp on the FEAP regeneration in the linear system	123
3.2.5	Effect of the temporal gap τ_B on the regeneration of SFEAPs in the linear system	125
3.3	On the nonlinear CDM inducing regeneration of truncated Airy pulses in fiber-optics links	128
3.3.1	Effect of the nonlinearity on the regeneration of a FEAP	128
3.3.2	Effect of the nonlinearity on the regeneration of strongly SFEAPs	129
3.4	Highlights and discussion on the CDM technique applied on FEAPs	129
3.4.1	Among the three models discussed, what is the best?	129
3.4.2	Is there an optimal value of the chirp? what about the temporal gap ?	135
3.5	On the SCG of truncated Airy pulses in a cubic-quintic AsSe ₂ /As ₂ S ₅ optical waveguide with rib-like structure	137
3.5.1	Numerical results	137
3.5.2	Discussion	142
3.6	conclusion	146
General Conclusion		148
Bibliography		153
Appendix		178
List of Publications		185

List of Figures

1.1	Eye diagrams at 640 Gbit/s showing the SFG-based pump depletion regeneration of the distorted data signal. (a) Original 640 Gbit/s data signal. (b) Distorted 640 Gbit/s data signal with purposefully added ASE noise to lower the Optical Signal-To-Noise Ratio (OSNR) with 20 dB compared to the original signal. (c) Regenerated signal at 640 Gbit/s with clear noise suppression in the one level and reduced timing jitter. (From [64]. © 2012 IEEE.)	29
1.2	Bit Error Rate (BER) characteristics of the regenerator. Curves show demultiplexed to 40 Gbit/s data signals stemming from the 640 Gbit/s deteriorated signal and the regenerated signal with clear improvement. (From [64]. © 2012 IEEE.)	30
1.3	Diagram of an optical transmission system [64].	31
1.4	Diagram of an optical transmitter [64].	33
1.5	Diagram of an optical receiver [64, 67].	34
1.6	A fiber optic transmission line [64, 67].	35
1.7	Plot of the input profiles : (a) Gaussian, (b) SG for $m = 3$, (c) RC, (d) sech-type. Data : $P_0 = 1W, T_0 = 50fs$	38
1.8	(a) Airy profile, $a = 0.05, P_0 = 1W, \tau_0 = 20ps$; (b) Proposed experimental set-up for obtaining an Airy pulse. [22].	40
1.9	Dynamics of the truncated Airy pulse under the combined action of GVD and TOD with comparable strengths $\varepsilon = -0.5, a = 0.1$ [25].	43
1.10	Evolution of (left column) pulse, and (right column) spectra shapes over a distance of 10 dispersion lengths for an initially unchirped and chirped Airy pulses in the anomalous dispersion regime: $a = 0.1$ [27].	44

1.11	Principle of the three stages of regeneration: (1) reamplification, (2) restoration form, and (3) resynchronization [85].	45
1.12	Principle of 1R regeneration [85].	46
1.13	Principle of 2R regeneration [85].	48
1.14	Regeneration by self-modulation (a) and cross-modulation (b) [91].	49
1.15	Principle of 3R regeneration [91].	50
1.16	(a) Lumped and (b) distributed amplification schemes used for compensating for fiber losses. Tx and Rx stand for transmitters and receivers, respectively [2, 92].	51
1.17	The dynamics of one FEAP in 6 periods of the DM scheme in nonlinear regime with different TOD. (a) $\varepsilon = 1$; (b) $\varepsilon = 1.5$; (c) $\varepsilon = 2$; (d) $\varepsilon = 2.5$ and $\alpha = 0.05$ in anomalous dispersion [25].	58
1.18	Diagram of a PCF or microstructured fiber. The parameters d and Λ represent the hole diameter and the pitch, respectively [121].	63
1.19	Some PCFs : Small core extruded PCF (<i>c</i> -2004 OSA, from Ebendorff-Heidepriem et al see [121, 127]), (b) Single mode tellurite PCF with extremely large mode area (<i>c</i> -2008 OSA, from Feng et al see [121, 128]), (c) Preform structure created by drilling (<i>c</i> -2004 IEEE, from Feng et al see [121, 129]), (d) a Hollow core PCF fabricated by Blazephotonics, image realized in the FEMTO-ST institute of the university of Franche-Comté, France (<i>c</i> – 2004 FEMTO-ST institute, from [130, 131]), (e) zoomed picture of (d)	64
1.20	Illustration of the SF mechanism in the SCG phenomenon : results from numerical simulations showing (a) spectral and (b) temporal evolution for Raman induced fission of an incident 1.25 kW launched 3-OS. Top curves show the output profiles after 0.5 m propagation. (<i>c</i> -2006 APS, from [130])	65
1.21	Illustration of the emission of DWs in a SCG process : (a) Low-amplitude pedestal in the form of DW, (b) NSR in spectral domain under two zero-dispersion conditions where FOD is dominant. (<i>c</i> – 2011 CURRENT SCIENCE, from [140])	67
1.22	Influence of the SCG spectral bandwidth by the pulse width (<i>c</i> – 2006 APS, from [130]) . . .	70
1.23	A SCG-Based experiment in spectroscopy :(a)- Photograph and (b)- experimental layout of a compact multidimensional spectrofluorometer based around a commercially available all-fibre SCG source (<i>c</i> -2010 J. Dudley and R. Taylor, from [121])	73
1.24	A SCG-Based experiment in biophotonic microscopy using a SCG source [121].	74

1.25	(a) - Schematic of a fiber-optic link, with a data transmitter, a long transmission fiber with several fiber amplifiers, and a receiver. The amplifiers can be supplemented with additional components for dispersion compensation or signal regeneration; (b) - Fiber-optic links [67].	78
1.26	Eye diagram for the telecom signal after the fiber [67].	82
1.27	(a) and (b) are for the waveguide cross sections: (a)- Rib structure of the waveguide geometry: $H = 1.98\mu m$ and $W = 5\mu m$; (b) HE_{11} mode at the pumping wavelength $4\mu m$ [38, 40].	84
1.28	(a)- Calculated CDPs of the HE_{11} mode for the considered $AsSe_2/As_2S_5-ChRW$; (b)- Values of each order of the CDP [38, 40].	84
2.1	Plot asymmetric (a) and symmetric (b) Airy pulse. $\tau_B = 8$, $P_0 = 9$, $ C =0.5$	101
2.2	Diagram of the numerical algorithm or the set-up scheme for the first case : constant initial chirp with alternation of the GVD by piece of fiber.	103
2.3	Diagram of the numerical algorithm or the set-up scheme for the second case : constant GVD sign with alternation of the initial chirp by piece of fiber.	104
2.4	Diagram of the numerical algorithm or the set-up scheme for the third case : both the GVD and the chirp signs are alternated by piece of fiber in order to have whether $s \times C < 0$ or $s \times C > 0$	105
2.5	Schematic illustration of the symmetrized split-step Fourier method used de numerical simulations. Fiber-optics link is divided into a large number of segments of width h. Within a segment, the effect of nonlinearity is included at the midplane shown by a dashed line [1, 92].	108
3.1	$ C = 0.5$, $ s = 1$ and $a = 0.05$; (a.1) and (b.1) for 3D-contour plots of the FEAP propagation within the fiber links in the first model of Fig. 2.2; (a.2) and (b.2) for 2D-plots of $\max U ^2$ versus ξ ; The initial conditions are described as: (a.1) and (a.2) starting with the A.I. mechanism $s \times C < 0$; (b.1) and (b.2) starting with $s \times C > 0$	121
3.2	The conditions are the same as in Fig. 3.1 however this simulation corresponds to the second model of Fig. 2.3 : s is constant while C alternates. The initial condition : (a.1) and (a.2) for the A.I. mechanism $s \times C < 0$; (b.1) and (b.2) for $s \times C > 0$	122
3.3	The conditions are the same as in Fig. 3.1 however this simulation corresponds to the third model of Fig. 2.4 : both s and C alternate. The initial condition : (a.1) and (a.2) for the A.I. mechanism $s \times C < 0$; (b.1) and (b.2) for $s \times C > 0$	123

3.4	Effect of initial chirp (change of the initial value of $C \in \{-0.25; -0.5; -0.75; -1\}$): (a.1) to (d.1) for 3D-contour plots of the FEAP propagation within the first model of Figs. 2.2 with the initial condition of the A.I. mechanism $s \times C < 0$ as $s = 1$ and $C < 0$; (a.2) to (d.2) for the 2D-plots of the $\max U ^2$ versus ξ	124
3.5	Effect of τ_B on the regeneration of SFEAPs (change of the value of $\tau_B \in \{1; 2.5; 5; 7.5\}$: (a.1) to (d.1) for 3D-contour plots of the SFEAPs under the configuration of Figs. 2.2, 3.1(a.1) and 3.1(a.2) with the initial condition of A.I. mechanism $s \times C < 0$ and $C = -0.5$; (a.2) to (d.2) for 2D-plots of $\max U ^2$ versus ξ	126
3.6	Same conditions as in Fig. 3.5 but with $C = -1$	127
3.7	Effect of N on the FEAP propagation (change of $N \in \{1; 2; 3; 4\}$): (a.1) to (d.1) for 3D-contour plots of the FEAP under the configuration of Figs. 2.2, 3.1(a.1) and 3.1(a.2) with the initial condition of A.I. mechanism $s \times C < 0$ and $C = -1$; (a.2) to (d.2) for 2D-plots of $\max U ^2$ versus ξ	130
3.8	Effect of N on the SFEAPs regeneration (change of $N \in \{1; 2; 3; 4\}$): (a.1) to (d.1) for 3D-contour plots of the SFEAPs under the configuration of Fig. 3.7 with the initial condition of A.I. mechanism $s \times C < 0$ and $C = -1$; (a.2) to (d.2) for 2D-plots of $\max U ^2$ versus ξ	131
3.9	Zoom on the FEAP propagation through the first three pieces ($f_{i=1..3}$) of optical system described by the first model of Fig. 3.1. The initial condition : (a.1) and (a.2) for the A.I. mechanism $s \times C < 0$, (b.1) and (b.2) for $s \times C > 0$	132
3.10	Zoom on the FEAP propagation through the first three pieces ($f_{i=1..3}$) of optical system described by the second model of Fig. 3.2. The initial condition : (a.1) and (a.2) for the A.I. mechanism $s \times C < 0$, (b.1) and (b.2) for $s \times C > 0$	133
3.11	Zoom on the FEAP propagation through the first three pieces ($f_{i=1..3}$) of optical system described by the third model of Fig. 3.3. The initial condition : (a.1) and (a.2) for the A.I. mechanism $s \times C < 0$, (b.1) and (b.2) for $s \times C > 0$	134
3.12	(a) Plot of $I_{max} = f(C)$ in the case of FEAP following Fig. 3.4; (b) Plot of $I_{max} = f(\tau_B)$ in the case of SFEAPs following Figs. 3.5 and 3.6.	135

3.13 Contour plots of SCG Airy pulse spectral propagation for a $50fs$ input pulse with $10kW$ peak power at a central wavelength of $4\mu m$ along $15cm$ long $AsSe_2/As_2S_5$ - ChRW: (a)- Single CKN, (b)- CKN+TPA, (c)- CKN+QKN in case of cooperating nonlinearities ($\gamma_1\gamma_2 > 0$), (d)- CKN+QKN in case of competing nonlinearities ($\gamma_1\gamma_2 < 0$), (e)- CKN+QKN+TPA in case of cooperating nonlinearities, (f)- CKN+QKN+3PA in case of competing nonlinearities, (g)- CKN+QKN+TPA+3PA in case of cooperating nonlinearities, (h)- CKN+QKN+TPA+3PA in case of competing nonlinearities. 137

3.14 Contour plots of SCG Airy pulse temporal propagation for the different cases of Fig. 3.13. . . 139

3.15 SCG spectra for the FEAP in the anomalous GVD regime for different cases mentioned above.
 $L = 15cm, a = 0.05, t = 50fs, P = 10KW$ 141

3.16 Highlight on the spectral propagation distance $L = 0.05m$ of the effect of QKN in the MIR-SCG of FEAP within the considered optical waveguide: (a) for the single CKN, (b) for the case of $\gamma_1\gamma_2 > 0$, (b) for the case of $\gamma_1\gamma_2 < 0$ 142

3.17 Highlight the effect of TPA for the two cases of QKN in the MIR-SCG of FEAP within the considered optical waveguide. 144

Declaration

I declare that this work "**Ultra-short truncated Airy pulses regeneration and supercontinuum generation in nonlinear optical waveguides: cases of fiber-optics links and AsSe₂/As₂S₅-ChRW**" is my original work and that all the sources I have used or cited have been indicated and acknowledged by means of complete references, and that this document has not been submitted for degree purposes at my other academic institutions.

Heuteu Crépin

Student Number: 09W0136(UY1)

Signed: CH

Date: Janvier 2024

Dedication

*This thesis is dedicated to my parents Mr. Dagobert Ketchakou and
Mrs. Jeannette Ketchakou*

Acknowledgments

The author of this thesis namely **Crépin HEUTEU** first thanks God Almighty for all the blessings throughout his life and studies. He is thankful to individuals who have contributed either directly or indirectly to the finalization of this thesis.

The work presented in this thesis has been made under the label of the Laboratory of Mechanics, Department of Physics, Faculty of Science, University of Yaoundé I.

A particular acknowledgement is addressed to **Pr. Clément Tchawoua** to have been our advisor. He has been our lantern, guiding us and assuming fully his role despite all the other tasks associated to his position within the University of Yaoundé I. This thesis being a result of this laborious work, no word can describe our gratitude, we just hope that he will continue this noble task for the next generation of PhD students. A sentence of our advisor still resounds in our head and has been the conductor line of this work : "Only the perseverance, the seriousness and the rigor allow to reach to the expected results...". This sentence has allowed us to be tenacious and to hope the end of this tunnel. Thank once again **Pr. Clément Tchawoua**.

I am grateful to **Pr. Luc Calvin Owono Owono**, Coordinator of URFD-PA for his teaching in Higher teacher training college. It is also an occasion to thank all the teacher of Department of Physics, Higher teacher training college, University of Yaounde I.

I am grateful to **Pr. Jean Marie Ndjaka**, Head of Department of Physics for having contributed to our introduction in the research work. It is also an occasion to thank all the Department of Physics of the Faculty of Science (University of Yaoundé I).

I am grateful to **Pr. Bernard Essimbi Zobo**, Chairman of the jury's members of the preliminary and final thesis's viva voce of this work.

I am grateful to **Pr. Germain Ben Bolie**, Chairman of the jury's members of the audition thesis for his contribution.

We also thank **Pr. Martin S. Siewe** for his help and advices. We continue with **Pr. Blaise Nana Nbandjo**, **Pr. Germaine Djuidje Aloyem**, for their encouragement.

We acknowledge the jury's members of the preliminary thesis's viva voce of this work .

We acknowledge the jury's members of the final thesis's viva voce.

We are profoundly grateful to our family : my father **Mr. Dagobert Ketchakou** and my mother **Mrs. Jeannette Nyamsi** who are always there for us in any circumstances, spiritually, financially, emotionally. Their support has been a real and decisive turning point for the achievement of this thesis. We send our thanks to **Mr. Charles Ngako** and **Mrs. Irène Nyamsi** for his sincere support. We acknowledge our brothers and sisters **Jonathan Billy Nyanang**, **Fany Tatiana Noussi** and his family, **Jules César Ketchakou**, **Jordy Cabrel Ayombeu** and **Ingrid Davyla Kembeu** who are always there for us in all circumstances. We also think to our large family (uncles, aunts, cousins,...).

We are indebted to our late brother **Jospain Ngueya** and our late grandfather **Augustin Heuteu**. May their souls rest in peace.

We specially thank **Dr. Lucien Mandeng Mandeng** from the National Advanced Engineering school of Yaoundé for having been a must in the achievement of this work, for the useful discussions, advices and collaboration in the study of supercontinuum generation and regeneration mechanism. He has kindly shared his personal and academic experiences with us. He has also proofread this thesis. Very thanks **Dr. Lucien Mandeng Mandeng**.

We are grateful to the constructive discussions with our colleagues who belong to the Laboratory of Mechanics as **Dr. Alain B. M. Togueu** and **Dr. D. T. Tchintang**. Beyond those mentioned above, we also include all the rest of students

under the direction of **Pr. Clément Tchawoua**, both in the PhD and MsC levels.

We sincerely thank **Dr. Cassidi Bitang** and his family, **Dr. Alain Djazet**, **Dr. Dieudonné Zanga**, **M. Jean Lapluy Youtchom** and his family, **M. Marius Nko'o** and his family, **M. S. Kemedane Boukar** and his family, **M. Moïse Tamedjouong** and his family for their encouragement.

We also send our thanks to:

- Our friends **M. Rodrigue Fokom Si** and all his family, **M. Arnold Djoko** and all his family, **M. Darel Tchadji Kamguaing** and all his family, **M. Sinclair Mbounda**, **M. Bertrand Tchouamo**, **M. Patrice Simo** and his family, **M. Wilfried Fomekong** and his family.

- our colleagues in the secondary studies: **Mrs. Sidonie Pascal Telezing** and his family, **M. Pavel Monnif** and his family, **M. Leonard Watchou** and his family, **M. Beaudelaire Ntsafack** and his family, **M. Serge Kanko** and his family, **M. Patrick Lesse** and his family, **M. Samuel Feudjio** and his family, **M. Idriss Tatsingoum** and his family, **M. Vincent Ketchawat** and **M. Cédric Pouatcho** for their encouragement.

- the teachers participating to the "*Groupe Les PUISSANTS*" project since 2015 until now.

- our students in the National Advanced Engineering School of Yaoundé for having allowed us to stay in a state of permanent work which has certainly contributed to the successful achievement of this work.

Finally, the best for the end, a thought is addressed to our darling **Mrs.**

Stéphanie Mebong (and her family); all my children named **Grace Ange Kamga Chekam**, **Gabriel Pharell Tontchepeu Heuteu**, **Annaëlle Léticia Kimberly Nyamsi Heuteu** and **Dave Ethane Ketchakou Heuteu** for having been there for us, with her sincere affection during the last step of our thesis's work.

Abstract

In this thesis, we numerically study regeneration and supercontinuum generation of truncated Airy pulse in fiber-optic links and $AsSe_2/As_2S_5$ with rib-like structure respectively.

Firstly, we introduce another technique of Airy pulses regeneration in fiber links using the interaction between the group-velocity dispersion (GVD) and the initial value of frequency-chirp. This technique, called chirp-dispersion management (CDM), consists to manage the product of $GVD \times chirp$ over each piece of fiber line in the case of zero third-order dispersion (TOD). The alternation of both the initial chirp and GVD that conducts this regeneration followed the work done by **R. Driben and T. Meier [25]** for nonzero-TOD systems. Three diagrams of the numerical algorithm are considered: The first one consists to alternation of the GVD with constant frequency chirp, the second one consists to the alternation of the frequency chirp with a constant GVD and the last one consists to the alternation of both the two parameters. Through numerical results in the linear optical system, we show that the model of the first case with an initial condition $GVD \times chirp < 0$, is the best one able to yield an interesting regeneration both for a single finite energy Airy pulse (FEAP) and for symmetric FEAP (SFEAP) previously defined by **S. Xiaohui et al [29]**. The main parameter which is beneficial

for this kind of CDM-regeneration of Airy pulses in fiber links, is found to be the initial frequency chirp while the temporal gap and the nonlinearity are obtained to have deleterious impact on the regeneration. Moreover, the noise in the regeneration originates from the alternation of the chirp, the simultaneous alternation of both the GVD and the chirp, the drastic increase in chirp, and nonlinearity. Therefore, for weakly nonlinear optical systems with fiber links, considering an absolute strong constant initial chirping with an alternation of GVD, could be a best choice to achieve a convenient regeneration of single truncated Airy pulses while using a small temporal gap is useful for the one symmetric Airy pulses in zero-TOD systems.

At the end of this part, we suggest that to achieve efficiently the regeneration of FEAP through the CDM technique, it is necessary to fulfill only the following points: (a) to choose the best model, which is the first one; (b) to use the initial condition of the A.I. mechanism; (c) in the nonlinear case, the value of cubic Kerr nonlinearity (CKN) should be small; (d) the absolute initial value of frequency chirp should be a little high but not too high to avoid the destruction of the regeneration quality ($|C| \in [1; 3]$), and (e) for SFEAPs, to use a small value of temporal gap.

The second study of this thesis focuses on the numerical study of supercontinuum generation (SCG) using specially Airy pulses in the Mid-infrared (MIR) region of wavelengths through an $\text{AsSe}_2/\text{As}_2\text{S}_5$ optical waveguide with rib-like structures modeled by the cubic-quintic nonlinear Schrödinger equation. We use the waveguide studied by **Diouf et al, J. of Lightwave Tech. 37, 5692 (2019)**, which has been found interesting, as it can generate explosive spectra in the MIR

domain. Through the anomalous dispersion regime, the spectral 20 dB bandwidths obtained have been found to exceed approximately 97250 nm. After this result, we considered the effects on SCG spectra of quintic Kerr nonlinearity (QKN) and nonlinear photon absorptions (NPAs) such as two-photon absorption (TPA) and three-photon absorption (3PA). Without the NPAs, only the cooperative QKN is beneficial for the MIR-SCG. In the temporal domain, the emission of dispersive waves (DWs) is avoided by the presence of NPAs, while the cooperative nonlinearities perform this emission. Furthermore, if, in the cooperative case, we always neglect the 3PA and consider the TPA, we find an interesting spectral intensity (SI) of the SCG, compared with the case of competition between nonlinearities. Surprisingly, the 3PA appears to be a good tool for controlling the TPA because the SI is less reduced when the QKN cooperates with the cubic Kerr nonlinearity (CKN). In particular, if we consider the case of competition, the 3PA enhances the SI compared to the single TPA case (in which the 3PA is neglected) for larger wavelengths.

Keywords: *Regeneration; CDM; Fiber-optics links; SCG; Truncated Airy pulse; QKN; Multiphotons absorption; Chalcogenides glasses; Mir-Infrared region.*

Résumé

Dans cette thèse, nous étudions numériquement les phénomènes de régénération et du supercontinuum des impulsions d'Airy tronquées respectivement dans les liaisons de fibres optiques et dans les guides d'ondes à nervures constitués des verres à chalcogénures $\text{AsSe}_2/\text{As}_2\text{S}_5$.

Nous amorçons cette étude en introduisant une autre technique de régénération des impulsions d'Airy dans les liaisons de fibres optiques modélisées par l'équation de Schrödinger nonlinéaire cubique avec dispersion d'ordre 2. Nous utilisons l'interaction entre la dispersion d'ordre 2 et la valeur initiale du chirp. Cette technique, appelée gestion de la dispersion et du chirp (GDC) consiste à manager le produit $GVD \times \text{chirp}$ sur les morceaux de fibres ne possédant pas la dispersion d'ordre 3. La mise en œuvre de cette technique est réalisée à la suite du travail effectué par **R. Driben et T. Meier [25]** qui eux ont étudié plutôt l'alternance entre la dispersion d'ordre 2 et la dispersion d'ordre 3. Trois approches ont été considérées notamment: la première consiste à alterner la valeur de la dispersion d'ordre 2 tout en maintenant constante la valeur du chirp. La seconde consiste à alterner la valeur du chirp tout en maintenant constante la valeur de la dispersion d'ordre 2 et la troisième consiste à alterner les valeurs des deux paramètres. En régime linéaire, les résultats montrent que la première approche avec la condition

$GVD \times chirp < 0$, est la meilleure option de régénération des impulsions d'Airy tronquées. Ce choix est également adéquat pour l'impulsion symétrique d'Airy précédemment définie par **S. Xiaohui et Cie [29]**. Le paramètre bénéfique pour régénérer les impulsions d'Airy par application de cette technique est le chirp initial tandis que l'augmentation de la nonlinéarité cubique entraîne la destruction du signal lors du processus de régénération. Ainsi, les deux autres approches donnent des résultats de mauvaises qualités et ne sont donc pas appropriées pour la régénération des impulsions d'Airy tronquées dans ladite ligne de transmission optique. Notons aussi que l'augmentation drastique du chirp ainsi que celle du décalage temporel pour l'impulsion symétrique ont des effets néfastes sur la régénération. En effet, une grande valeur du chirp initial détruit la régénération tandis que celle du décalage temporel réduit l'intensité du signal.

A l'issue de ce travail, il ressort que les conditions favorables pour la régénération des impulsions tronquées d'Airy consistent à choisir la première approche incluant la condition $GVD \times chirp < 0$ avec une faible valeur du chirp (la valeur pourra être prise dans l'intervalle [1;3]), de la nonlinéarité cubique ainsi que du décalage temporel pour l'impulsion symétrique d'Airy.

La suite de notre travail dans cette thèse porte sur l'étude numérique de la génération du supercontinuum (GSC) des impulsions d'Airy tronquées dans le domaine du moyen infrarouge avec les guides d'ondes à nervure constitués des verres à chalcogénure. Ce type de guide d'onde est modélisé dans notre étude par l'équation de Schrödinger nonlinéaire cubique-quintique incluant les termes d'absorptions nonlinéaires multiphotoniques. Il a été étudié par **Diouf et Cie [40]** pour la GSC à bande passante explosive dans le domaine du moyen in-

frarouge (MIR) n'incluant pas les termes d'absorptions non linéaires ainsi que la nonlinéarité quintique (NQ). Nous utilisons donc ce guide d'onde tout en incluant l'absorption à 2 et à 3 photons. Comme résultats, nous obtenons en dispersion anormale une bande passante à 20 dB approximativement égale à 97250 nm; en absence des termes d'absorptions non linéaires, les nonlinéarités coopératives augmentent la bande passante spectrale tandis que les nonlinéarités compétitives réduisent celle-ci. L'inclusion des absorptions multiphotoniques est délétère pour le supercontinuum particulièrement en ce qui concerne le cas des nonlinéarités coopératives. En effet, dans le domaine temporel, l'émission des ondes dispersives est stoppée par la présence des termes multiphotons. Plus encore, concernant le cas des nonlinéarités coopératives, l'absorption à 2 photons réduit moins la bande passante spectrale comparativement à sa combinaison avec l'absorption à 3 photons. Le résultat surprenant apparaît ici dans le cas des nonlinéarités compétitives où l'absorption à 3 photons augmente la bande passante spectrale en opposition à l'effet de l'absorption à 2 photons. Ainsi dans ce cas particulier, l'absorption à 3 photons apparaît être un paramètre de contrôle de l'influence de l'absorption à 2 photons.

Mots clés: *Regénération; GDC; Liaisons de fibres optiques; GSC; Impulsion d'Airy tronquée; NQ; Absorption multiphotons; Guide d'onde à nervure; Domaine du MIR.*

List of abbreviations

ASE:	<i>Amplified Spontaneous Emission</i>
BER:	<i>Bit Error Rate</i>
CD:	<i>Coherence Degree</i>
CDM:	<i>Chirp-Dispersion Management</i>
CDP:	<i>Chromatic dispersion profile</i>
ChRW:	<i>Chalcogenide Rib Waveguide</i>
CKN:	<i>Cubic Kerr Nonlinearity</i>
CQNLSE:	<i>Cubic-Quintic NLSE</i>
CSS:	<i>Cubic SS</i>
CW:	<i>Continuous wave</i>
DCF:	<i>Dispersion Compensating Fiber</i>
DM:	<i>Dispersion management</i>
DRR:	<i>Delayed Raman Response</i>
DW:	<i>Dispersive Waves</i>
EAM:	<i>Electro-Absorption Modulator</i>
EDFA:	<i>Erbium-Doped Fiber Amplifier</i>
FBG:	<i>Fiber Bragg Grating</i>
FCA:	<i>Free Carrier Absorption</i>
FCD:	<i>Free-Carrier Density</i>

FEAP:	<i>Finite Energy Airy Pulse</i>
FEM:	<i>Finite Element Method</i>
FFT:	<i>Fast FT</i>
FT:	<i>Fourier Transform</i>
FVFEM:	<i>Full-Vectorial Finite Element Method</i>
FWHM:	<i>Full Width at the Half Maximum</i>
FWM:	<i>Four Wave Mixing</i>
GFFA:	<i>Gain-Flattened Fiber Amplifiers</i>
GHTJ:	<i>Gordon-Haus Timing Jitter</i>
GNLSE:	<i>Generalized NLSE</i>
GVD:	<i>Group Velocity Dispersion</i>
HNLF:	<i>Highly Nonlinear Fibers</i>
HOD:	<i>Hydro-Optic Disinfection</i>
HOS:	<i>Heater-on-Slab</i>
IPRS:	<i>Intra-Pulse Raman Scattering</i>
LCPCF:	<i>Liquid-Core Photonic Crystal Fiber</i>
MA:	<i>Multiphotons Absorption</i>
MatLab:	<i>Matrix Laboratory</i>
MI:	<i>Modulational instability</i>
MIR:	<i>Mid-Infrared Region</i>
MLLESP:	<i>mode-locked laser emitting soliton pulses</i>
MOF:	<i>Microstructured Optical Fiber</i>
MZI:	<i>Mach-Zehnder Interferometer</i>
MZM:	<i>Mach-Zehnder Modulator</i>

NDLSE:	<i>Normalized Dimensionless Linear Schrodinger Equation</i>
NFK:	<i>Negative Frequency Kerr</i>
NIR:	<i>Near-Infrared Region</i>
NLSE:	<i>Nonlinear Schrödinger equation</i>
NNLSE:	<i>Normalized Nonlinear Schrödinger Equation</i>
NPA:	<i>Nonlinear Photons Absorption</i>
NRZ:	<i>Non-Return-to-Zero</i>
NSR:	<i>NonSolitonic Radiation</i>
OOK:	<i>On-Off-Keying</i>
OSNR:	<i>Optical Signal to Noise Ratio</i>
OTDM:	<i>Optical Time-Division Multiplexing</i>
PB:	<i>Photonic Bandgap</i>
PCF:	<i>Photonic Crystal Fiber</i>
PPLN:	<i>Periodically Poled Lithium Niobate</i>
PTS:	<i>Polydiactylene Toluene Sulfonate</i>
QKN:	<i>Quintic Kerr Nonlinearity</i>
QPSK:	<i>Quadrature Phase Shift Keying</i>
QSS:	<i>Quintic SS</i>
RC:	<i>Raised-Cosine</i>
RZ:	<i>Return-to-Zero</i>
SAFEAB:	<i>self-accelerating finite energy Airy beams</i>
SCG:	<i>SuperContinuum Generation</i>
SF:	<i>Solitonic Fission</i>
SFEAP:	<i>Single FEAP</i>

SFG:	<i>Sum-Frequency Generation</i>
SG:	<i>Super-Gaussian</i>
SI:	<i>Spectral Intensity</i>
SMF:	<i>Single-Mode optical Fiber</i>
SNR:	<i>Signal-to-Noise Ratio</i>
SPM:	<i>Self-Phase Modulation</i>
SRS:	<i>Stimulated Raman Scattering</i>
SS:	<i>Self-Steepening</i>
SSFBG:	<i>Super-Structured Fiber Bragg Grating</i>
SSFM:	<i>Split-Step Fourier Method</i>
SOA:	<i>Semiconductor Optical Amplifier</i>
SOI:	<i>Silicon-On-Insulator</i>
TF:	<i>Tapered Fibers</i>
THG:	<i>Third Harmonic Generation</i>
TOD:	<i>Third Order Dispersion</i>
TPA:	<i>Two Photon Absorption</i>
WDM:	<i>Wavelength-division multiplexing</i>
XPM:	<i>Cross-Phase Modulation</i>
ZDW:	<i>Zero Dispersion Wavelength</i>
3PA:	<i>Three Photon absorption</i>

General Introduction

The study of short pulses in the field of nonlinear optics is subject to a large scientific and technological interest. The applications arising from the use of short and ultra-short pulses transcend high-speed optical telecommunications, ultra-fast physical phenomena, spectroscopy, coherent tomography, photonics, etc...[1]. These pulses propagating in a waveguide, one of the problems in optics consists to clearly define the characteristics of the latter in order to better understand the various linear or nonlinear phenomena likely to occur there. Among these phenomena, we can cite among others temporal pulse compression [1-3], modulational instability (MI) [4, 5], four-wave mixing (FWM), stimulated Raman and Brillouin scattering, regeneration, supercontinuum generation (SCG), etc... All these phenomena mentioned above require that we introduces at the input of the waveguide a pulse having a certain shape. We underline the symmetric and asymmetric pulses. With regard to the symmetric pulses, namely the hyperbolic secants, Raised-cosine and Gaussian impulses, they are generally used in most of the phenomena mentioned above. Recently, a focus has been made on new optical beams known as Airy beams/pulses that are attracting a greatest interest because of their special propagation properties. Sure enough, Airy beams/pulses are now known through their high stability properties in a stable soliton-like behavior

when propagating inside a linear medium. Their origin goes back to 1979, when Berry and Balazs [6] predicted in quantum mechanics that a wavepacket probability density propagating in free space without distortion and having a constant acceleration without external influence, should have an Airy function form. From that moment, the research associated with these waves had almost faded until 2007 when G.A. Siviloglou and D.N. Christodoulides studied accelerating finite energy Airy beams, reviving the interest in these waves in the context of nonlinear optics [7, 8]. Since then, Airy waves have attracted more attention because of their special properties, among which one can quote self-healing, dispersion resistance, acceleration on propagation of their dominant intensity peaks, obliquity in bidispersive optical systems, and soliton shedding [7-11]. Based on all these first studies, Airy waves were proposed for various applications including generalized tomographic maps [12], pulse compression in silicon waveguide [13], plasmonic routing [14, 15], optical light bullets [16, 17], soliton manipulation [18], etc.

In the theoretical aspect of research in nonlinear optics specially in studies of propagation within nonlinear optical waveguides, many works having ended to Ph.D theses, were conducted in the Department of Physics of the Faculty of Science (University of Yaoundé I). For instance S. I. Fewo studied the dynamic of the propagation of solitons in systems modeled by the complex Ginzburg-Landau equations using the collective variables (CVs) and the classical variational approaches [19].

Subsequently, J. Atangana examined the propagation of ultra-short pulses in optical fiber systems under strongly perturbed environmental conditions [20] and C. G. L. Tiofack investigated the MI phenomenon and the ultra-short pulses propa-

gation in Erbium doped fibers modeled by GNLSE with higher order effects both in the linear and in the nonlinear part [21].

Later, L. M. Mandeng analytically and numerically described the phenomena of pulse compression and spectral broadening which manifest themselves during the propagation of ultra-short pulses in common used optical waveguides, namely silicon-on-insulator (SOI) waveguides, single-mode optical fibers (SMFs) in wavelength-division multiplexing (WDM) systems, photonic crystal fibers (PCFs) [22]. Others works were also made.

After the review of these works, it was observed that with the great interest aroused by the optical pulse regeneration and the spectral broadband continua according to their wide applications, a research path oriented on their achievement was missing considering the department of Physics of the Faculty of Science (University of Yaoundé 1). That is why, this thesis comes to be added to the previous ones with a focus on the mentioned phenomena as a study beyond the previous analyses. Particularly, we focus on the Airy pulse regeneration with chirp-dispersion management (CDM) and theirs supercontinuum generation (SCG) in $\text{AsSe}_2/\text{As}_2\text{S}_5$ with chalcogenide rib waveguide:

★ Regeneration of truncated Airy pulses

R. Driben et al [23] and W. Cai et al. [24] discovered the asymmetric inversion (A.I.) mechanism of single finite energy Airy pulses (FEAPs) induced by the interaction between group velocity dispersion (GVD) and third-order dispersion (TOD), and one year later in 2014, R. Driben and T. Meier [25] regenerated FEAPs in SMF links using dispersion management (DM). During the same year, L.M. Mandeng et al. [26] introduced the A.I mechanism using the interaction

between the initial chirp and GVD, while in 2015, P. Zhang et al. [27] presented its numerical and analytical study. The physical explanation and comparison with the nonzero-TOD systems were provided in 2016 by L. M. Mandeng and C. Tchawoua [28]. Indeed, the A.I. mechanism obtained in Refs. [23, 24] differs from the one induced by the interaction chirp-GVD presented in Refs. [26-28]. It was found that the A.I. mechanism occurs here when the GVD regime is opposite to the initial chirp: $chirp \times GVD < 0$. Under these conditions, a compact and symmetric profile as Gaussian, hyperbolic secant, or raised-cosine pulse should only be compressed [1, 3, 25, 27, 28], while an asymmetric profile as a FEAP beyond the temporal compression also undergoes an A.I mechanism. After, S. Xiaohui et al. [29] showed that it is possible to inject symmetric FEAPS (SFEAPs), which also undergo the A.I. mechanism in SMFs under the effect of initial chirp. In the case of propagation of Airy pulses under the DM technique, before the regeneration done in Ref. [25], the evolution dynamics of Airy pulses in optical fibers with periodic dispersion modulation were numerically studied by S. Wang et al [30]. They were able to manage the optical transmission of Airy pulses by a DM technique through the GVD and TOD having periodic profiles in sine and cosine functions.

Following this path of research in this thesis, instead of using the interaction between GVD and TOD as in Refs. [25, 30], we conduct the regeneration of single FEAPs and SFEAPs in fiber links induced by the initial chirp called the CDM technique. This technique of regeneration consists managing the product of $chirp \times GVD$ over each piece of fiber line in the case of zero-TOD systems, contrary to R. Driben and T. Meier [25]. Three models are developed: the first consists of alternation of the GVD with the chirp being constant, the second

consists of the alternation of the chirp with a constant GVD, and the third consists of the alternation of both the two parameters. As results:

- we show that only the first one allows to achieve a more stable regeneration of Airy pulses with an initial condition of $chirp \times GVD < 0$ corresponding to the A.I. mechanism.
- The beneficial parameter is found to be the initial chirp, while the temporal gap (only for SFEAPs) and the nonlinearity have deleterious impacts on this regeneration.
- We would like to remind the reader here that unlike the work done by R. R. Driben and T. Meier [25] who regenerated FEAP using the A.I. mechanism with $GVD \times TOD < 0$, we rather achieve the regeneration using the A.I. mechanism with $chirp \times GVD < 0$.
- Contrary to Ref. [29], instead of achieving the evolution of SFEAPs within one continuous fiber, we proceed to the regeneration of SFEAPs in an optical system with several pieces of different fibers through the alternation of GVD.

★ Supercontinuum generation of truncated Airy pulses

Airy pulses have been used to generate supercontinua in optical fibers. For instance, in 2011, Ament et al [31] studied the SCG of a self-healing Airy pulse both numerically and experimentally through a microstructured or photonic PCF. In 2016, Mandeng et al [28] investigated the drastic spectral broadening of a FEAP through a highly dispersive and nonlinear optical waveguide, such as a liquid-core PCF (LCPCF). This specific PCF had CS_2 as liquid material in its core in order to enhance its nonlinearity by a hundred (100) times compared to that of silica [32]. This kind of fiber had already been studied by Raja et al [33], who modeled it

using a cubic saturable nonlinear Schrödinger equation (NLSE). Thus, Mandeng et al [28] showed by a comparative study that the choice of an FEAP with a weak truncation coefficient, a convenient high energy, and an initial chirp under the anomalous group-velocity dispersion (GVD) regime is more appropriate for coherent supercontinuum generation (SCG) in this kind of fiber, instead of the common compact and symmetric profiles. Classical microstructured optical fibers (MOFs) that are still used for SCG are now to be replaced by the introduction of chalcogenide glasses, which will lead to very explosive, ultra-broadband, and coherent spectra in the mid-infrared region (MIR) [34-40]. In addition, one can also quote Karim et al [41], who demonstrated the possibility of obtaining a wider spectral range, from 1.8 to $6\mu m$, when using a $1cm$ – long channel waveguide made of $Ge_{11.5}As_{24}Se_{64.5}$ glass with MgF_2 glass in the lower cladding. Moreover, T. S. Saini et al [42] demonstrated an SCG spectrum ranging from 2 to $15\mu m$ in a rib waveguide with MgF_2 glass in the upper cladding, As_2Se_3 glass in the core, and SiO_2 glass in the lower cladding. One year later, they also generated an SCG spectrum spanning from 1.2 to $7.2\mu m$ in a rib waveguide structure including As_2Se_3 chalcogenide glass [43-49]. The pulse shaping technique still has a place in the process of further improving the SCG phenomenon. It consists of enhancing the input pulse characteristics for this purpose. This technique encompasses the management of the profile, the time width, the power, and other parameters, such as the initial chirp [4, 28]. In SCG studies, the overwhelming majority of prior studies already cited above [4,34-41,43-49] have utilized intense optical pulses with symmetric and compact temporal profiles, such as Gaussian or sech-type pulses, while the only ones that focused on Airy pulses are those of references [28, 31, 50].

This observation reveals that there are still open questions in this area that should be explored. Moreover, the impact of the quintic Kerr nonlinearity (QKN) on the SCG has already been discussed in reference [28], in which L. M. Mandeng et al [51] showed that the SCG spectra produced with a sech-type input profile were slightly compressed in the cooperative case, compared with the competitive case and the results obtained in [52, 53]. Also, in reference [54], A. Sharafali et al observed that the QKN increased MI for cooperative nonlinearities, while it suppressed the MI for competitive nonlinearities.

Following this path of research, in the second part of this thesis, we report a numerical study of SCG using specially truncated Airy pulses in the mid-infrared (MIR) region of wavelengths through an $\text{AsSe}_2/\text{As}_2\text{S}_5$ optical waveguide with rib-like structures. We consider the effects on SCG spectra of quintic Kerr nonlinearity (QKN) and nonlinear photon absorptions (NPAs) such as two-photon absorption (TPA) and three-photon absorption (3PA). As results:

- the spectra at 20 dB bandwidths could exceed approximately 97250 nm.
- In the case in which the NPA parameters are not taken into account, only the cooperative QKN is beneficial for the MIR-SCG of the truncated Airy pulse within this waveguide.
- In the temporal domain, the emission of dispersive waves (DWs) is avoided by the presence of NPAs, while the cooperative nonlinearities allow this emission.
- In the cooperative case, neglecting the 3PA and considering the cooperative QKN and TPA, we find an interesting spectral intensity (SI) of the SCG, compared with the competitive case.
- An interesting surprise concerns the 3PA, which appears to be a good tool for

controlling the TPA.

– Considering, in particular, the competing nonlinearities, the 3PA enhances the SI of the MIR-SCG of the truncated Airy pulse compared to the single TPA case for larger wavelengths.

The presentation of the work and the results emerging from this thesis is done as follows :

- In the first chapter, we make a brief review of literature on the regeneration mechanism and the SCG including NPAs. It includes a short presentation of physical descriptions, applications and the limits of these phenomena. Then, we design with concision the motivations that have conducted our work on these phenomena. Moreover, we also make a description of the different optical waveguides studied in the thesis in the last section of the chapter.

- In the second chapter, we present the numerically treatments of the different models studied. Particularly, we derived the NLSEs investigated and described the methods used to analyze regeneration and SCG phenomenon. A short presentation of the algorithms on which the numerical simulations are based for each phenomenon is also made.

- In the last chapter, we present the results obtained in each study with the considered discussions and conclusions

A general conclusion is done at the end of the thesis highlighting some perspectives for further researches directly linked to the results presented.

1.1 Introduction

This chapter presents a brief overview on the physical phenomena studied in the thesis. It is organized as follows : section 1.2 deals with regeneration phenomenon, section 1.3 focuses on the SCG phenomenon while section 1.4 describes all the optical waveguides studied in this thesis. The last section concludes this chapter.

1.2 Overview on regeneration

1.2.1 Theoretical and physical descriptions

Regeneration of optical pulse means the optical signal restoration in a transmission line. Using optical regeneration, it is possible to extend the transmission reach of a data signal. It is also possible to expand the information spectral density for a link with a given transmission reach, ultimately allowing for reaching the capacity limit given by Shannon's theorem [55-57] when limited by nonlinear effects in the transmission fiber and Amplified Spontaneous Emission (ASE) noise. This goes for both binary direct detection systems as well as coherent detection systems [57]. A challenge for regenerators is to regenerate multiple wavelength channels

without having to split up the individual wavelengths and regenerate them separately, as the latter holds no clear advantage over $o/e - 3R - e/o$. For regenerators, the benefit in terms of energy efficiency comes when many bits are processed simultaneously in the same device, i.e. when fewer power hungry components are required [58]. This could be the case for very high bit rate signals [58] such as multi-100s Gbit/s OTDM signals [59] or for high-order modulation formats such as 16 QAM or 16 PSK [60]. Recently, a number of impressive schemes for regenerating optical phase modulated signals have been conceived and demonstrated, e.g. [60-62] and methods for scaling these to higher order formats are under way. However, over the last 10 years, Optical Time-Division Multiplexing (OTDM) regeneration has also been demonstrated in various forms, and merging the two efforts of high symbol rate and high-order modulation regeneration may double the benefit in terms of energy efficiency. As most demonstrated phase-sensitive regenerators rely on parametric effects in highly nonlinear fiber, this should also be applicable to ultra-high-speed (OTDM) data signals carrying higher order modulation. An example of a parametric effect used for Quadrature Phase Shift Keying (QPSK) on a high symbol rate is described in [63], where serial-to-parallel conversion of a 640 Gbaud signal is demonstrated using FWM. As for regeneration, so far only a single demonstration has reached 640 Gbit/s (640 Gbaud), and this is based on the use of a Periodically Poled Lithium Niobate (PPLN) device [64]. Again, an ultra-fast parametric effect is used, namely sum-frequency generation with pump depletion under the quasi-phase matching condition. In [64], $3R$ regeneration of a 640 Gbit/s On-Off-Keying (OOK) data signal is demonstrated. A 640 GHz clean clock signal is used to generate a SFG product together with the data

signal. This process requires one photon from each, and hence both the clock and the original data signal will experience pump depletion. Filtering out the output clock signal, a logically inverted replica of the original data is obtained on a clean clock signal. The power transfer curve of this Sum-Frequency Generation (SFG) pump depletion process reveals a step-like shape, such that the zero and one level noise distribution will be redistributed favorably, i.e. yielding a regenerated data signal.

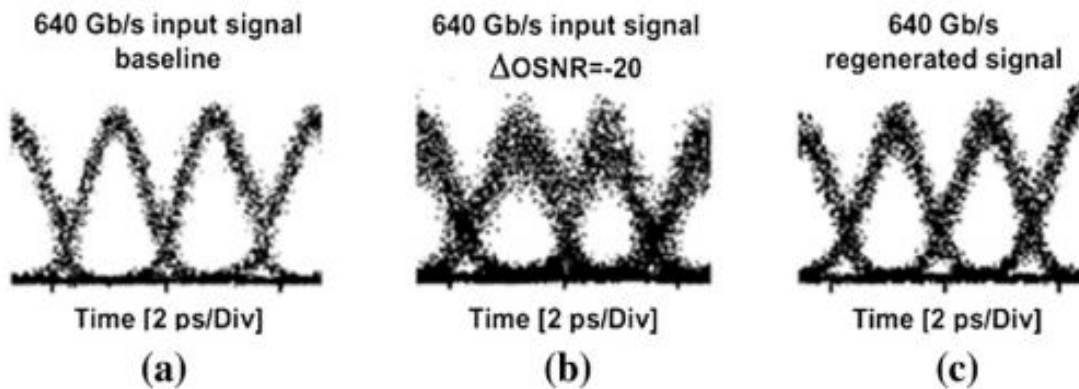


Figure 1.1: Eye diagrams at 640 Gbit/s showing the SFG-based pump depletion regeneration of the distorted data signal. (a) Original 640 Gbit/s data signal. (b) Distorted 640 Gbit/s data signal with purposefully added ASE noise to lower the Optical Signal-To-Noise Ratio (OSNR) with 20 dB compared to the original signal. (c) Regenerated signal at 640 Gbit/s with clear noise suppression in the one level and reduced timing jitter. (From [64]. © 2012 IEEE.)

Fig.1.1 shows regeneration results in terms of eye diagrams. The distorted 640Gbit/s data signal is clearly cleaned up, yielding a significantly opened eye diagram. The biggest noise suppression takes place on the one level, due to the characteristics of the power transfer curve of the regenerator [64]. The sides of the eyes are also cleaned up, due to the data transfer to the clean clock signal with low jitter. Fig.1.2 shows the BER performance of the regenerator. The leftmost curve shows the original data signal and the regenerated signal, revealing a very

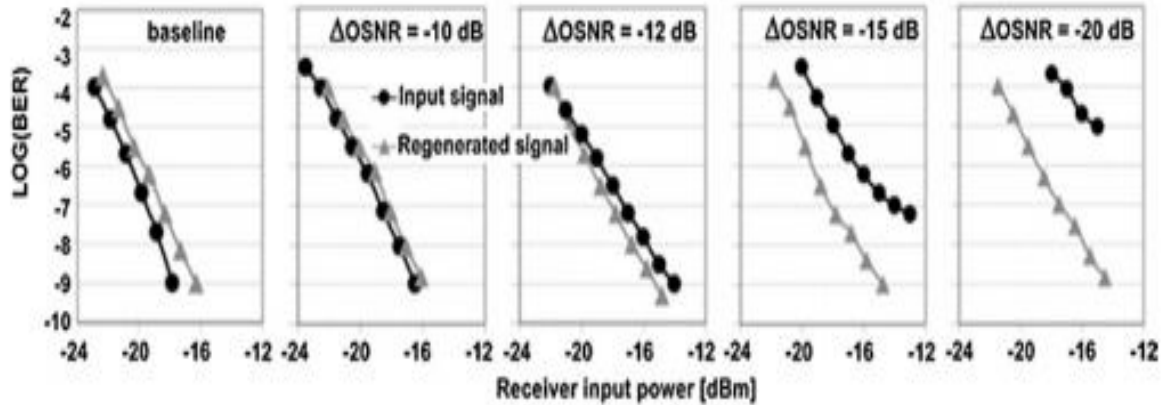


Figure 1.2: Bit Error Rate (BER) characteristics of the regenerator. Curves show demultiplexed to 40 Gbit/s data signals stemming from the 640 Gbit/s deteriorated signal and the regenerated signal with clear improvement. (From [64]. © 2012 IEEE.)

small penalty. When the OSNR of the input signal is lowered, the BER curve of the regenerated signal remains pretty much the same, showing an improvement of the BER curve at 12 dB OSNR deterioration. At 20 dB, corresponding to the eye diagrams in Fig.1.1, the deteriorated signal cannot get below $BER 10E - 5$, but the regenerated signal is pretty much the same as always, demonstrating a very clear regeneration. The regenerated signal has a sensitivity at $BER 10E - 9$ of about -16 dBm and a variation of about 0.5 dB for all the curves in Fig. 1.2. The timing jitter at the output is also kept pretty constant around 40 fs, even when the input timing jitter ranges from 40 fs to 300 fs. So this scheme is very clearly demonstrated to operate well at up to 640 Gbit/s. It would be desirable to keep the signal at the same wavelength, though, so with the above scheme, an additional wavelength converter is required. Though the above results are the only ones at 640 Gbit/s, several other approaches, which should be scalable, have been demonstrated. These include the following two based on polarization rotation in a Kerr switch based on Highly Nonlinear Fibers (HNLF) [65, 66]. In

[65], a full 160 Gbit/s $3R$ regeneration is demonstrated by switching the data onto a clean clock signal in the Kerr switch. The data is first made float-top-like by transmission through a short piece of highly birefringent fiber. The regenerated signal is now on another wavelength, as above, and a Self-Phase Modulation (SPM)-based wavelength shifter is added to obtain a regenerated signal at the same wavelength as the original data. In [66], retiming is demonstrated keeping the same wavelength in a single device. Again, an HNLF-based Kerr switch is used, and the data is made flat-top by the use of a Super-Structured Fiber Bragg Grating (SSFBG) filter. A clean clock signal is used as pump to switch out the central part of the broadened flat-top data pulses, resulting in a retimed output at the same wavelength as the original data.

1.2.2 Fiber optic transmission system

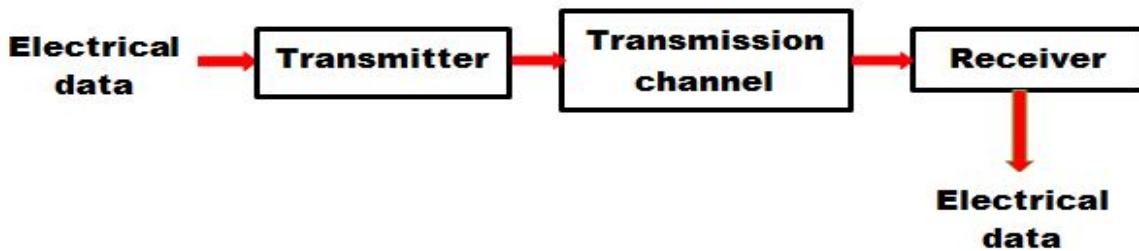


Figure 1.3: Diagram of an optical transmission system [64].

Fig. 1.3 represents the diagram of an optical transmission system called point-at-point, where information is transmitted from point to point while remaining within the domain optical. Like all information transmission systems, the optical transmission system consists of a transmitter, a transmission channel and a receiver. The transmitter generates an optical signal from the electrical digital information signal to be transmitted. The optical signal propagates in the trans-

mission channel to the receiver. To the transmission line, a receiver converts the optical signal back into the electrical field. Optical transmission systems can be listed in two categories: guided transmission, and unguided transmission. In this thesis, we are only interested in guided transmission using fiber optics as transmission medium. In the next subsection, we introduced transmitter and receiver.

1.2.3 Transmitter and receiver

The optical transmitter and receiver are the two elements at the ends of a line of optical transmission. The role of the transmitter is to encode the electrical data to be transmitted on an optical carrier. The receiver performs the reverse operation, i.e. detects the optical signal transmitted and decode it to recover the initial information. Before describing the principle of these components, we will approach the modulation formats.

Transmitter

The main element of a transmitter is the light source which will carry the information. Semiconductor laser sources have proven advantageous for transmissions over fiber optics for several reasons: small footprint, low power consumption tick, good wavelength selectivity, low intensity noise, and ability to modulate optical power via the polarization flow. Direct modulation via the laser bias current can significantly reduce the cost of an optical transmission system. However, it is rarely used for transmission systems over long distances and at data rates greater than 10 Gbit/s due to the variation of the instantaneous frequency (chirp) induced by the modulation of the laser flow. In the specific case of long distance and very high transmissions flow rate, an optical transmitter therefore consists of

an optical source followed by a external modulator as shown in Fig. 1.4.

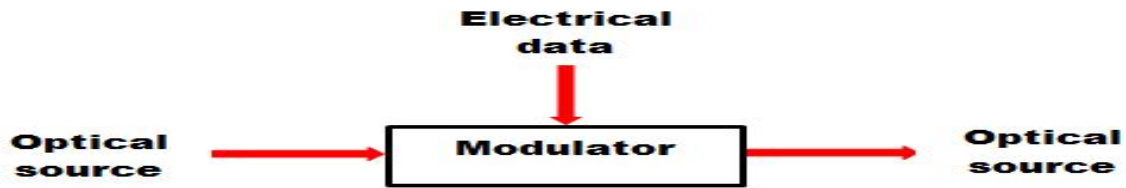


Figure 1.4: Diagram of an optical transmitter [64].

Two types of electro-optical modulators were used: the modulator electro-absorption (EAM for Electro-Absorption Modulator) and the modulator based on Mach-Zehnder interferometer type Lithium Niobate ($LiNbO_3$) ((MZM for Mach-Zehnder Modulator). The first modulator uses the Franz-Keldysh effect where the variation of the optical absorption of a semiconductor is induced by a voltage. This modulator has several advantages: possibility of integrating it with a laser source, which reduces the size of the the source and the external modulator; an extinction ratio of 15 dB can be achieved with a control voltage of a few volts and a modulation bandwidth that can go up to 100 Gbit/s. Despite its advantages, there is still a residual chirp. The second type of modulator uses the electro-optical effect in $LiNbO_3$ where the signal phase is modulated by a control voltage. By integrating the $LiNbO_3$ in a Mach-Zehnder interferometer (MZI), it is possible to achieve a modulation amplitude from this phase modulation.

Receiver

The Fig. 1.5 illustrates the principle of a receiver. it is made up primarily of a photodiode whose bandwidth should theoretically be greater or equal than to half information flow to meet the Nyquist criterion. This photodiode converts the opti-

cal binary signal to electrical binary signal. It reproduces identically the fruiting of optical power in flow fruiting. However, under certain conditions the photodiode can also add amplitude fruiting related to thermal effects or the quantum nature of photons [67]. The electrical signal is then sent to a limiting amplifier whose role is to maintain a constant electrical voltage by output over a certain input voltage. To do so, it adapts its gain by detecting the average input power. This amplifier makes it possible to avoid fruiting of the average optical power which affects the average voltage of the binary signal, and then requires an adjustment of the voltage threshold for decision making. The receiver experimental that we used has a limiting amplifier. A fraction of the signal is sent on a clock recovery in order to recover the rate of information. After having recovered a clock synchronized to the data we come to the decision circuit. This decision circuit is controlled by a threshold voltage and the recovered clock. With the clock we determine the instant of decision which is most from the optimal time to the center of bit time. The voltage of the received signal at the moment of decision will be compared to the threshold voltage. If the received voltage is below (above) the threshold, then the decision latch generates a symbol $\langle 0 \rangle$ ($\langle 1 \rangle$ respectively). The electrical data transmitted is then retrieved at the level of the receiver. In the next subsection, we underlined Transmission channel.

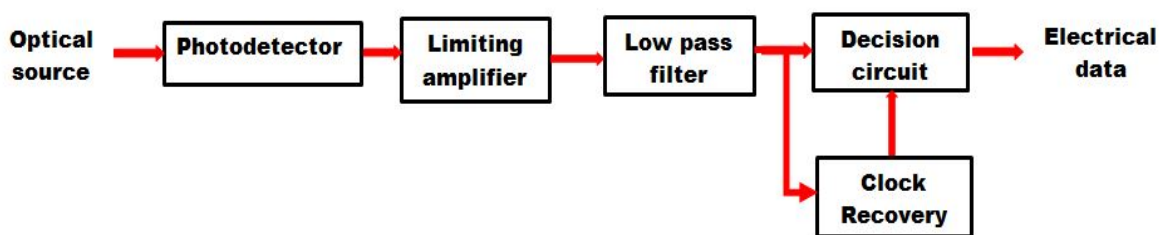


Figure 1.5: Diagram of an optical receiver [64, 67].

1.2.4 Transmission channel

The role of a transmission channel is to transmit the optical signal from the transmitter to the receiver with the least possible distortion. Fig. 1.6 shows a fiber optic transmission line. The main advantage of fiber optics for transmission is their low losses, down to 0.2 dB/km for optical telecommunication wavelength (1550 nm). Despite this advantage, the optical power transmitted is only 1 percent after 100 km of transmission. For this reason, after a certain propagation distance the signal must necessarily be re-amplified by the optical amplifier (OA), or even regenerated by regenerators (R). Another source of optical signal degradation is fiber dispersion leading to a broadening of the pulses during the propagation. When a pulse is expanded more than the dedicated bit time, the signal is degraded. The dispersion problem is predominant for multi-mode fibers due to different group speeds for different fiber modes (typically 10 ns/km). Therefore single mode fiber is used practically in all optical transmission systems since the 80s. In the

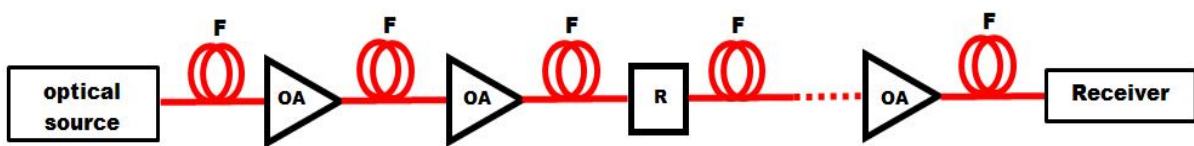


Figure 1.6: A fiber optic transmission line [64, 67].

next subsection, we underlined optical pulse.

1.2.5 Optical pulse

Optical pulses from femtosecond lasers represent some of the shortest physical events ever observed and their high instantaneous powers allow them to be focused to intensities that can heat and compress matter to resemble the extreme conditions found in a nuclear explosion. The extreme units of time and power needed to describe this area of physics can easily distract from the simple and elegant techniques by which femtosecond pulses can be generated. The review presented here is divided into two main subsections. The first subsection show the symmetric optical pulse and the second show the asymmetric optical pulse.

Symmetric optical pulse

- *The Gaussian profile*

It has the following analytical form

$$u(0, \tau) = \sqrt{P_0} \exp\left(-\frac{1}{2} \frac{\tau^2}{\tau_0^2}\right), \quad (1.1)$$

where $u(0, \tau)$, τ , P_0 and τ_0 represent the slowly varying amplitude of the electrical field pulse envelope, the retarded frame of time, the peak power of the pulse, and the pulse half-width (at the $1/e$ - intensity point), respectively. The full width at the half maximum (FWHM), T_{FWHM} , is commonly used instead of τ_0 . For a Gaussian pulse, it is defined by

$$T_{FWHM} = 2(\ln(2))^{1/2} \tau_0 \approx 1.665 \tau_0, \quad (1.2)$$

- *The super-Gaussian (SG) profile*

In some lightwave systems, pulses with steeper leading and trailing edges broaden more rapidly with propagation due to the input wider spectrum of pulse. So, a Super-gaussian profile models the effects of the steep leading and trailing edges on the broadening. The analytical form is given as :

$$u(0, \tau) = \sqrt{P_0} \exp \left[-\frac{1}{2} \left(\frac{\tau}{\tau_0} \right)^{2m} \right], \quad (1.3)$$

The quantity \mathbf{m} represents the coefficient which controls the degree of edge sharpness of the SG pulse. The FWHM is defined as $2(\ln(2))^{1/2m} \tau_0$. The rise time T_r defined as the duration on which the intensity goes from 10 to 90 percent of its maximal value can be written as follows :

$$T_r = (\ln(9)) \frac{\tau_0}{2m} \approx 0.728 \frac{\tau_0}{m}, \quad (1.4)$$

One generally uses this relation to calculate the parameter m .

- ***The raised-cosine (RC) ansätze profile***

The generation of Gaussian-shaped pulses suitable for high bit rate is not easier [68, 69]. Indeed, the output of the commonly used Mach-Zehnder pulse carvers is rather close to RC profiled pulses. A RC profile could be modeled analytically as :

$$u(0, \tau) = \frac{\sqrt{P_0}}{2} \left[1 + \cos \left(\frac{\pi \tau}{\tau_0} \right) \right], \quad (1.5)$$

Its FWHM is defined as:

$$T_{FWHM} = \frac{4}{\pi} \arccos[(1/2)^{1/4}] \tau_0 \approx 0.728 \tau_0, \quad (1.6)$$

- ***The hyperbolic-secant or sech-type profile***

In experiments, one always uses the Gaussian shape because many lasers emitted approximately this form of input pulses. However, in the case of some mode-locked lasers and naturally in the optical soliton context, one often reaches the

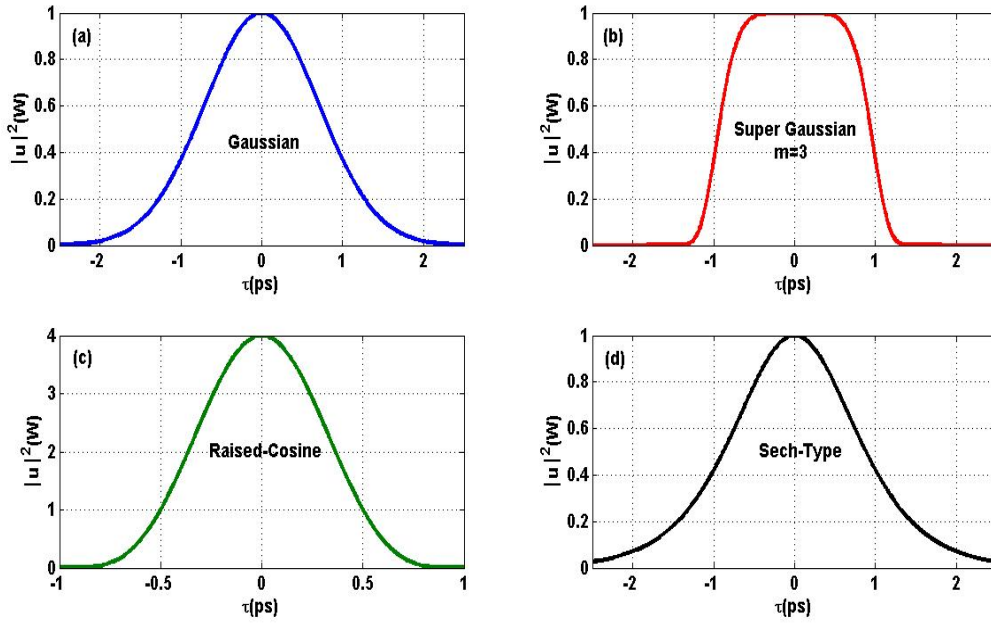


Figure 1.7: Plot of the input profiles : (a) Gaussian, (b) SG for $m = 3$, (c) RC, (d) sech-type. Data : $P_0 = 1W$, $T_0 = 50fs$.

hyperbolic secant of sech-type profile described as:

$$u(0, \tau) = \sqrt{P_0} \operatorname{sech} \left(\frac{\tau}{\tau_0} \right), \quad (1.7)$$

Generally, the Gaussian and the sech-type profiles are nearly identical following their features when undergoing the guide dispersion. One can also define as :

$$T_{FWHM} = 2 \operatorname{arccosh}(\sqrt{2}\tau_0) = 2 \ln(1 + \sqrt{2})\tau_0 \approx 1.763\tau_0, \quad (1.8)$$

An illustration of these profiles is shown on fig. 1.7.

Asymmetric optical pulse: The Airy profile

• Definition

Recently, a focus has been made on new optical beams known as Airy beams and pulses that are attracting a greatest interest because of their special propagation properties [7, 8]. Sure enough, Airy beams/pulses are now known through

their high stability properties in a stable soliton-like behavior when propagating inside a linear medium. Their origin goes back to 1979, when Berry and Balazs predicted in quantum mechanics that a wavepacket probability density propagating in free space without distortion and having a constant acceleration without external influence, should have an Airy function form [6]. These beams tend to reconstruct themselves despite the severity of perturbations that they undergo inside the medium. This reconstruction is understood through their internal transverse power flow [70-72]. The special propagation properties of Airy beams/pulses : the self-healing, the dispersion resistance and the acceleration on propagation of their dominant intensity peaks. A temporal input Airy profile is described in general as [73]:

$$u(0, \tau) = \sqrt{P_0} A_i \left(\frac{\tau}{\tau_0} \right) \exp \left(\frac{a\tau}{\tau_0} \right), \quad (1.9)$$

where P_0 is the peak power and a the truncation coefficient. $A_i(\tau)$ represents the temporal Airy function. The presence of the parameter a allows to ensure that for a positive quadratic dispersion coefficient, one shall obtain a positive dispersion [73].

The asymmetric nature of this pulse implies that, it is not interesting to define a FWHM unless one gives an interest to the main or dominant peak. Basically in practice, as discussed in [2], an input Gaussian profile propagating in a quasi-linear SMF (where the nonlinear effects are neglected comparatively to the linear ones) near its Zero Dispersion Wavelength (ZDW) around $1.31\mu m$ (where the Third Order Dispersion (TOD) β_3 becomes important comparatively to the Group velocity dispersion (GVD) β_2) transforms into an Airy profile. In [31], an input

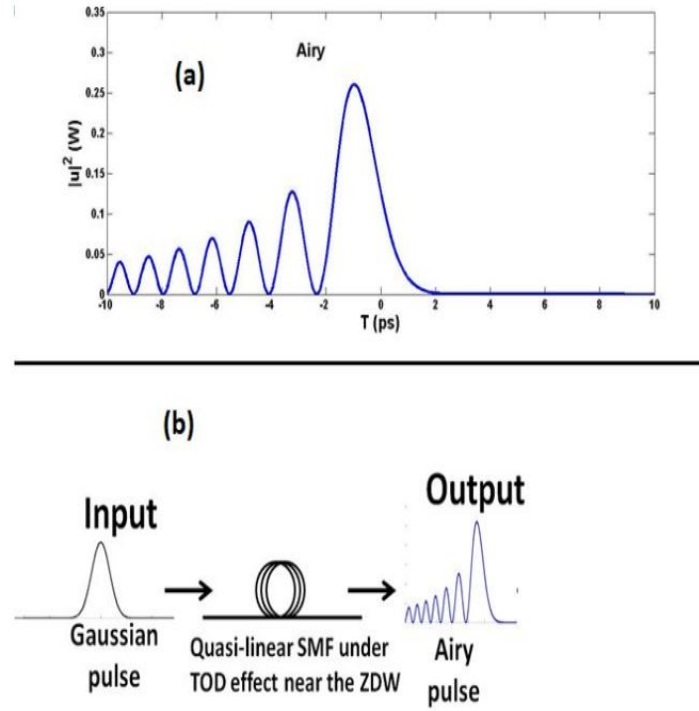


Figure 1.8: (a) Airy profile, $a = 0.05$, $P_0 = 1W$, $\tau_0 = 20ps$; (b) Proposed experimental set-up for obtaining an Airy pulse. [22].

Gaussian pulse was generated by a modelocked Ti-sapphire laser oscillator operating at $800nm$ center wavelength and $80MHz$ pulse repetition frequency and a computer-controlled pulse shaper were used to impose a cubic spectral phase onto these transform-limited Gaussian pulses leading to the generation of an Airy pulse. So, we can suggest the design of a general set-up as illustrated in Fig.1.8. Many other works have been devoted these last years on Airy beams/pulses in different kind of systems [74-82].

- **The chirping process**

Generally when an optical field propagates within a waveguide, its phase varies across the pulse at any distance of propagation z , and following the time τ . So, it appears a difference $\delta\omega$ between propagation induced frequency shift and the central initial frequency ω_0 . In this case, one says that the pulse becomes chirped

[2]. In linear systems, the induced frequency chirp changes linearly across the pulse i.e the waveguide imposes a linear frequency chirp on the pulse depending on the considered dispersion order term. However, in nonlinear systems, the chirp is induced by the wellknown nonlinear Kerr effect leading to a spectral broadening of the pulse. In fact, the SPM compresses the pulse in the time domain, phenomenon which is more pronounced in the anomalous dispersion regime. Consequently, in the spectral domain, it broadens the pulse [2]. The qualitative features of these induced frequency chirps depend on the pulse shape. Often, one imposes an initial frequency chirp on an input profile. This operation is modeled analytically by multiplying the initial profile with the term $\exp(\pm iC\tau/2\tau_0^2)$ where the parameter C is the imposed frequency chirp. In the next subsection, We will talk about the Asymmetric Inversion phenomenon in optical fiber.

Asymmetric Inversion mechanism

- **Asymmetric inversion of truncated Airy pulse induced by interaction between GVD and TOD.**

The propagation acceleration properties of the dominant peak intensity of the truncated Airy pulse generally lead to their destruction. Therefore, some researchers such as W. Cai et al [24] and R. Driben and T. Meier [25] have focused on this problem. they found a way by studying the dynamics of truncated Airy pulses launched into a fiber close to its zero-dispersion point, under the action of the GVD and TOG. In particular, we report new features driven by the dominant positive TOD, which were not reported in the publication dealing with negative TOD [83]. The evolution of truncated Airy pulses, which are launched in the form of $u(0, \tau) = A_0 A_i(\tau) \exp(a\tau)$ with a truncation parameter $a > 0$, obeys the

normalized nonlinear Schrödinger equation (NNLSE):

$$i \frac{\partial u(\xi, \tau)}{\partial \xi} + \frac{\text{sgn}(\beta_2)}{2} \frac{\partial^2 u(\xi, \tau)}{\partial \tau^2} - i \frac{\varepsilon}{6} \frac{\partial^3 u(\xi, \tau)}{\partial \tau^3} + N |u(\xi, \tau)|^2 u(\xi, \tau) = 0, \quad (1.10)$$

where $\xi = z |\beta_2| / \tau_0^2$ and a relative TOD strength parameter, $\varepsilon = \beta_3 / (|\beta_2| \tau_0)$, where β_2 and β_3 are GVD and TOD parameter of and fiber and τ_0 is the pulse's width. The Kerr nonlinearity is represented by the last term. The linear pulse dynamics was studied in an analytical form of Eq. 1.10:

$$i \frac{\partial u(\xi, \tau)}{\partial \xi} + \frac{\text{sgn}(\beta_2)}{2} \frac{\partial^2 u(\xi, \tau)}{\partial \tau^2} - i \frac{\varepsilon}{6} \frac{\partial^3 u(\xi, \tau)}{\partial \tau^3} = 0, \quad (1.11)$$

the Fourier transform method or Marcuse formalism [84] presented for the first time in 1981 as:

$$u(\xi, \tau) = \frac{1}{2\pi} \int_{-\infty}^{+\infty} k(0, \omega) \exp \left(i \frac{\text{sgn}(\beta_2)}{2} \omega^2 \xi + i \frac{\varepsilon}{6} \omega^3 \right), \quad (1.12)$$

where $k(0, \omega)$ is the Fourier transform of the input Airy pulse $u(0, \omega)$. The obtained pulse amplitude $u(0, \omega)$ at the length ξ is given by [23]:

$$|u(\xi, \tau)|^2 = A_0 \exp \left(-2\alpha\Theta\tau + \frac{4}{3}\alpha^3\Theta^2 - \Theta^2\alpha\xi^2 \right) \times \Theta^{2/3} \left| \text{Ai} \left[-\Theta^{1/3} \left(\tau + \frac{\Theta}{4}\xi^2 - \alpha^2\Theta + i \text{sgn}(\beta_2)\alpha\Theta\xi \right) \right] \right|^2, \quad (1.13)$$

where $\Theta = 1/(\varepsilon\xi/2 + 1)$. Fig. 1.9 show dynamic of the truncated Airy pulse under the action of GVD and TOD of comparable strengths. In this regime, the focal point extends to a finite area where the truncated Airy pulse experiences an acceleration reversal. The size of the area depends on the relative strength of the dispersion coefficients. Past this area, the pulse undergoes inversion, and propagates with an acceleration that is opposite [23].

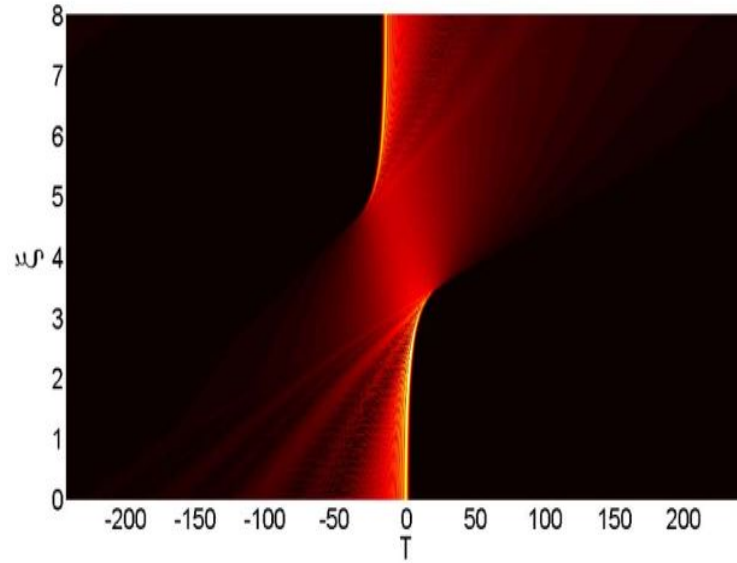


Figure 1.9: Dynamics of the truncated Airy pulse under the combined action of GVD and TOD with comparable strengths $\varepsilon = -0.5$, $a = 0.1$ [25].

- **Asymmetric inversion (AI) of truncated Airy pulse induced by interaction between GVD and initial frequency chirp C.**

Since the property related to β_3 is specific to certain optical systems such as silicon waveguides, it is not easy to apply AI phenomenon of Airy pulse using interaction between β_2 and β_3 in non-zero-TOD systems such as classic fibers made from silica, Bragg grating fibers. Some researchers have therefore asked the following question: What is the parameter of fiber or else the pulse parameter that will allow us to study the AI phenomenon of the Airy pulses in optical fiber mentioned above? Recently, Mandeng et al introduced AI mechanism induced by the interaction chirp-GVD presented in Refs [26-28]. It was found that the A.I. mechanism occurs here when the GVD regime is opposite to the initial chirp: $chirp \times GVD < 0$. Under these conditions, a compact and symmetric profile as Gaussian, hyperbolic secant, or raised-cosine pulse should only be compressed [2, 13, 27, 28, 51], while an asymmetric profile as a FEAP beyond the temporal

compression also undergoes an A.I mechanism. For chirped Airy pulse $u(0, \tau) = A_0 Ai(\tau) \exp(a\tau) \exp\left(i\frac{C\tau^2}{2}\right)$, if we introduced this input in Eq.1.11 assuming that $\varepsilon = 0$, we obtain the analytical solution

$$|U(\xi, \tau)| = A_0 \left| \frac{1}{\sqrt{\theta}} Ai\left(\frac{\tau}{\theta} - \frac{\xi^2}{4\theta^2} + i\frac{a\xi \operatorname{sgn}(\beta_2)}{\theta}\right) \times \exp\left(\frac{a\tau}{\theta} - \frac{a\xi^2}{2\theta^2}\right) \right|, \quad (1.14)$$

with $\theta = 1 - \operatorname{sgn}(\beta_2)C\tau$.

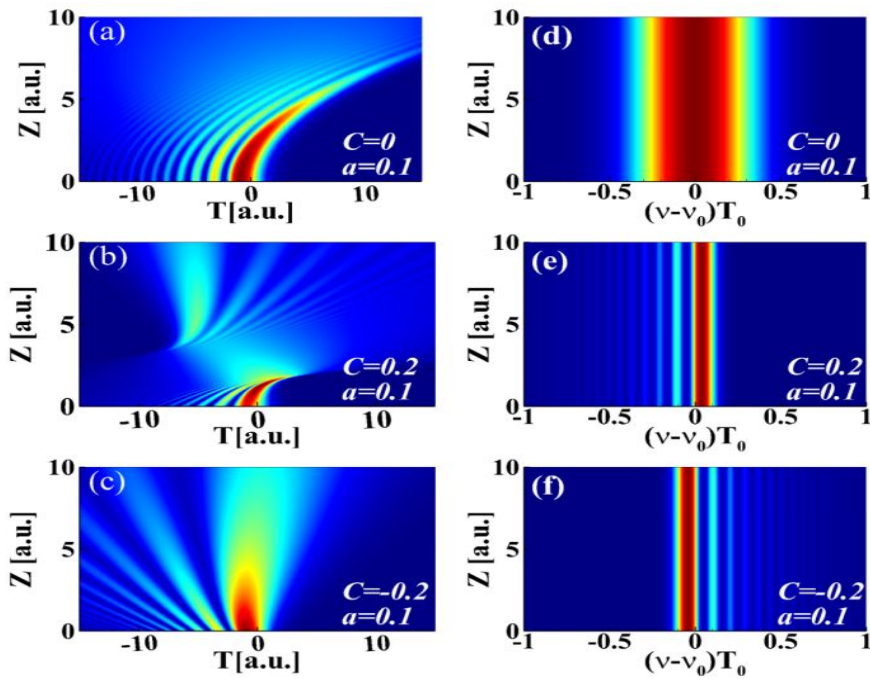


Figure 1.10: Evolution of (left column) pulse, and (right column) spectra shapes over a distance of 10 dispersion lengths for an initially unchirped and chirped Airy pulses in the anomalous dispersion regime: $a = 0.1$ [27].

Fig. 1.10(a) demonstrates the linear propagation of an initially unchirped Airy pulse, showing that it maintains its all remarkable properties of the ideal self-decelerating Airy pulses over an finite propagation distance. It can be seen that in the absence of the chirp, the pulse undergoes an acceleration. On the other hand, in the presence of chirp C , when $C > 0$, we observe the AI mechanism (see fig. 1.10(b)). In the next subsection, we will talk about the different techniques

for regeneration of optical pulse in transmission lines.

1.2.6 Regeneration technique based on optical fiber

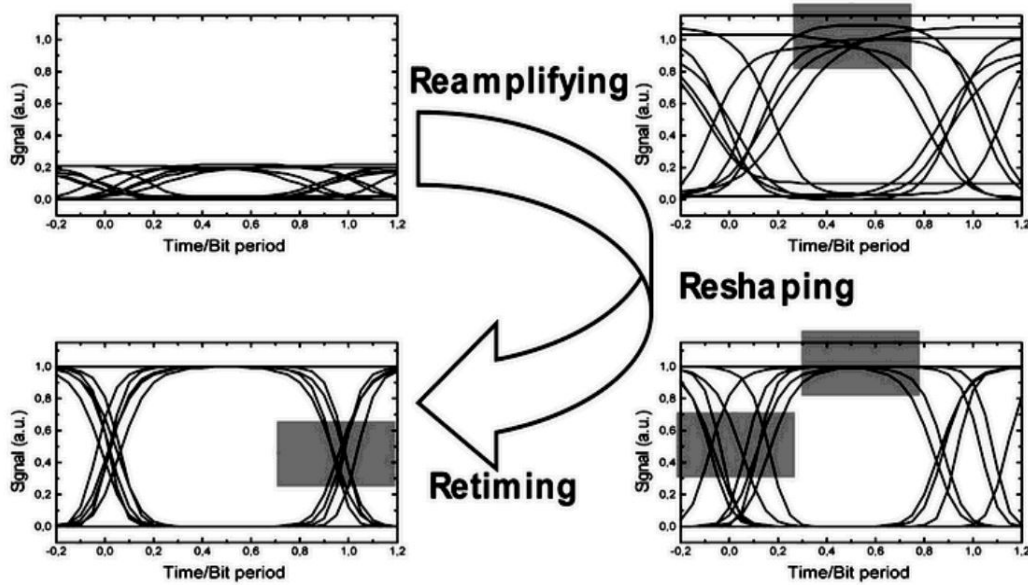


Figure 1.11: Principle of the three stages of regeneration: (1) reamplification, (2) restoration form, and (3) resynchronization [85].

The regeneration consists in dividing the distance of transmission into several segments and to place between these segments regeneration systems ration to maintain signal quality. Three levels and two mechanism of regeneration are defined: $1R$ regeneration (reamplification) to compensate for power attenuation average, the $2R$ regeneration (Reamplification and Reconditioning) to compensate for the attenuation of the average power and the degradations linked to the intensity fluctuations on the symbols, and $3R$ regeneration (Reamplification, Reshaping and Resynchronization) to compensate for impairments related to attenuation, intensity noise and temporal jitter [85], soliton amplification consist to overcome the effect of fiber losses (solitons need to be amplified periodically so that their energy is restored to their initial value)[2], Dispersion management

(DM) scheme consisting of alternating fiber sections with opposite signs of the GVD and TOD [2, 25, 86]. Fig. 1.11 represents the principle of these first three levels of regeneration.

1R Regeneration

1R regeneration consists of a simple amplification of the signal to compensate for the attenuation of the optical fiber. It is therefore the first stage of regeneration which allows to achieve long distance transmissions. Several types of optical amplifiers were developed during the 1980. Semiconductor Optical Amplifier (SOA) have been considered thanks to wide amplification band, gain and their capacity integration [87]. Nevertheless, the nonlinearity of the gain and the phase-

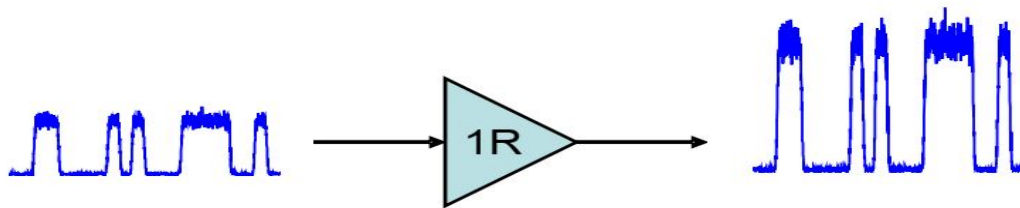


Figure 1.12: Principe of 1R regeneration [85].

amplitude coupling are the weak points which considerably reduce their interest in optical transmission systems. The development of the Erbium-Doped Fiber Amplifier (EDFA) has been considered a technological revolution for optical telecommunications [88, 89]. This type of amplifier consists in obtaining a population inversion in a fiber containing erbium ions thanks to optical pumping at 980 nm or/and 1.480 nm and thus obtain a gain in the radiative transition band around 1550 nm. Today we have a gain up to 40 dB and with high output power, around 30 dBm. Moreover, this type of amplifier has a wide spectral amplification band

(between 1530 nm to 1565 nm), polarization insensitivity, high transition lifetime ($> 1ms$) allowing linear amplification for current transmission rates. These benefits have enabled the EDFA to become a key component in telecommunications optical systems.

The second type of amplifier that combines high gain and low noise is amplifier distributed by the Raman effect [90]. The principle of the Raman amplifier can be described according to the same diagram as an EDFA. The major difference is that the amplification process is not based on an atomic transition but on the molecular vibrations of SiO_2 . This technique makes it possible to obtain distributed amplification directly in a fiber transmission standard without adding dopant, which thus allows a noise factor very weak. Moreover, with a very wide amplification band of 13 THz (i.e. 104 nm in the optical telecommunications spectral band), Raman amplification is a good candidate by combining it with EDFAs to widen the spectral band of amplified optical transmission. The Fig.1.12 gives its principle.

2R Regeneration

The principle of $2R$ regeneration is schematized in Fig. 1.13. To realize signal conditioning, the $2R$ regenerator must have an output power as a function of S-shaped input power.

Thanks to the presence of bearings below and above a given threshold power, the intensity fluctuations are reduced through the device. This reduction in intensity fluctuations is schematized by reducing the variance of symbol power probability distributions 1 and 0 . If on the other hand the ratio of the high and low levels of this nonlinear gate is large enough, it also allows an improvement in the

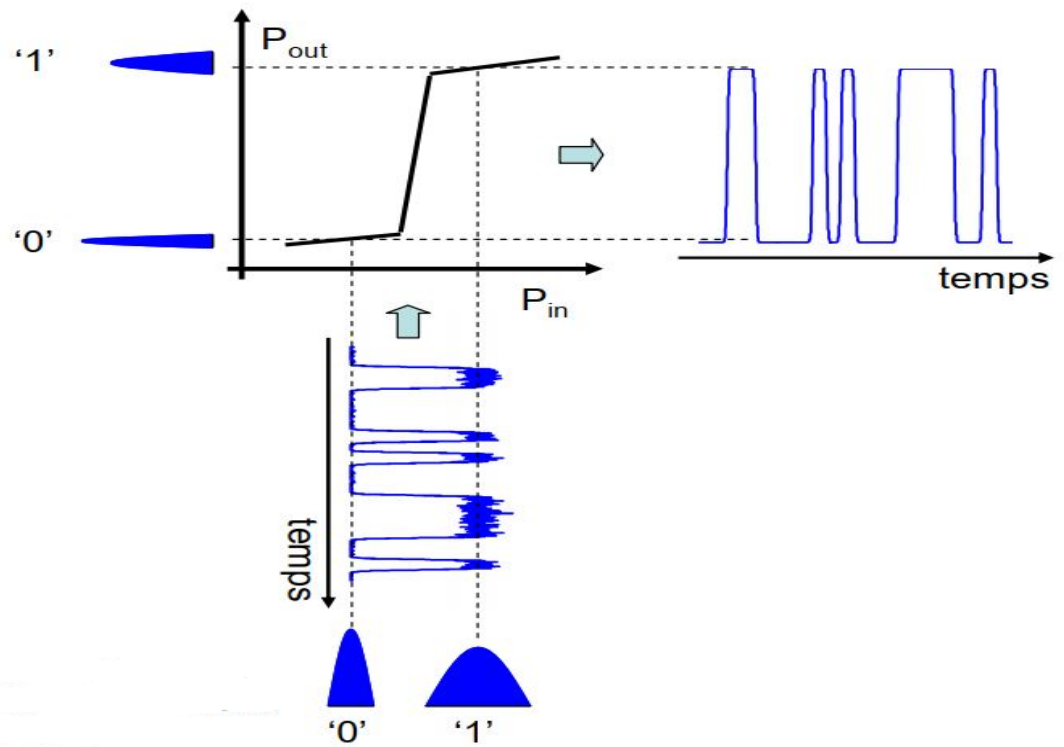


Figure 1.13: Principle of 2R regeneration [85].

rate of extinction of the signal. To obtain this non-linear evolution, it is necessary that the transmission function of the device depends on the input power. 2R regeneration can be achieved through two modulation techniques (Fig. 1.14). The first is said to be self-modulation, i.e. the degraded signal at the control input the nonlinear gate and is regenerated at the output. The second is said to be cross-modulation, where the degraded signal still controls the nonlinear gate which this time modulates a second signal (probe). We therefore transfer data carried by the wavelength λ_1 on a signal of wavelength λ_2 . Regeneration by cross modulation therefore incorporates the wavelength conversion function. However, to continue the initial initial transmission, it is necessary to carry out two successive regenerations to return to the wavelength initial. In this case, regeneration by self-modulation is therefore the simplest solution.

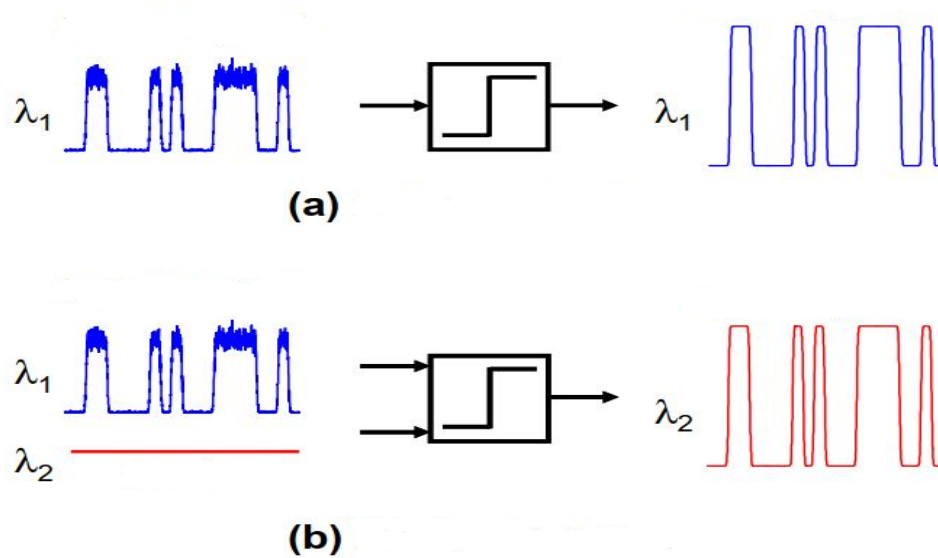


Figure 1.14: Regeneration by self-modulation (a) and cross-modulation (b) [91].

3R Regeneration

The principle of $3R$ regeneration is shown in Fig. 1.15. In addition to the key components for $2R$ regeneration: an amplifier and a nonlinear gate, regeneration $3R$ requires clock recovery to regain data timing. A part of the degraded signal is sent in this clock recovery, which will generate a clock optical or electrical synchronized with the signal. This clock will then modify the transmission of the nonlinear gate, which allows a resynchronization of the signal and thus a reduction of timing jitter.

Soliton amplification

As already discussed, fiber losses lead to the broadening of solitons. Such loss-induced broadening is unacceptable for many applications, especially when solitons are used for optical communications. To overcome the effect of fiber losses, a soliton needs to be amplified periodically so that its energy is restored to its

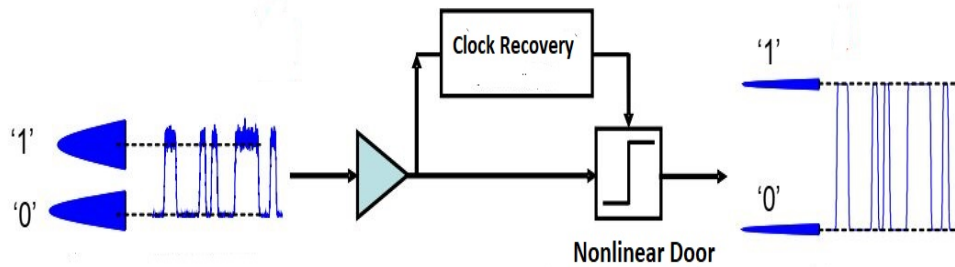


Figure 1.15: Principle of 3R regeneration [91].

initial value. Two different approaches have been used for this purpose [92-101], known as lumped and distributed amplification schemes and shown in Figure 16 schematically. In the lumped scheme [94], an optical amplifier boosts the soliton's energy to its input level after it has propagated a certain distance. The soliton then readjusts its parameters to their input values. However, it also sheds a part of its energy as dispersive waves (continuum radiation) during this adjustment phase. The dispersive part is undesirable and can accumulate to significant levels over a large number of amplification stages. This problem can be solved by reducing the spacing L_A between neighboring amplifiers such that $L_A \ll L_D$. The reason is that the dispersion length L_D sets the scale over which a soliton responds to external perturbations. If the amplifier spacing is much smaller than this length scale, soliton width is hardly affected over one amplifier spacing in spite of energy variations. In practice, the condition $L_A \ll L_D$ restricts L_A typically in the range of 20 – 40 km even when the dispersion length is close to 100 km [94]. Moreover, the lumped-amplification scheme becomes impractical at high bit rates requiring

short solitons ($T_0 < 0ps$) because dispersion length can then become quite short.

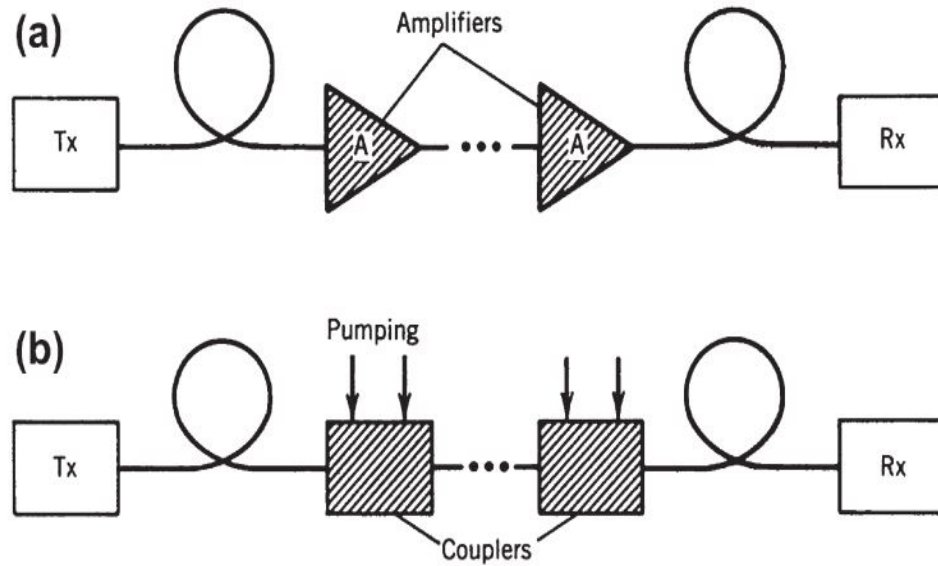


Figure 1.16: (a) Lumped and (b) distributed amplification schemes used for compensating for fiber losses. Tx and Rx stand for transmitters and receivers, respectively [2, 92].

The distributed-amplification scheme often employs stimulated Raman scattering to provide gain. In this approach, a pump beam (up-shifted in frequency from the soliton carrier frequency by nearly 13 THz) is injected periodically into the fiber. For solitons propagating in the $1.55\text{ }\mu\text{m}$ wavelength region, one needs a high-power pump laser operating near $1.45\mu\text{m}$ and emitting power levels in excess of 100 mW. Since the optical gain is distributed over the entire fiber length, solitons can be amplified adiabatically while maintaining N close to 1, a feature that reduces the dispersive part almost entirely [97].

Feasibility of the Raman-amplification scheme was first demonstrated in 1985 in an experiment in which soliton pulses of 10 ps width were propagated over a 10 km long fiber [96]. In the absence of Raman gain, the width of solitons increased by 50 percent because of loss-induced broadening. The Raman gain was obtained by injecting a Continuous wave (CW) pump beam at $1.46\mu\text{m}$ from a color-center

laser in the direction opposite to that of soliton propagation. The pump power was adjusted close to 125 mW such that the total fiber loss of 1.8 dB was exactly balanced by the Raman gain. In a 1988 experiment [98], 55 ps solitons could be circulated up to 96 times inside a 42 km fiber loop without significant increase in their width, resulting in an effective transmission distance of less than 4000 km. The lumped-amplification scheme was used starting in 1989 [99]. With the advent of erbium-doped fiber amplifiers in around 1990, they were used almost exclusively until 2002, in spite of the lumped nature of amplification provided by them. After 2002, the use of distributed Raman amplification has become more prevalent for long-haul lightwave systems.

The condition $L_A \ll L_D$ required for the average-soliton regime can be related to the soliton width T_0 by using $L_D = T_0^2/|\beta_2|$. The resulting condition is

$$T_0 \gg \sqrt{|\beta_2 L_A|}, \quad (1.15)$$

The bit rate B of an optical communication system can be related to T_0 through $T_B = 1/B = 2q_0 T_0$, where T_B is the bit duration and q_0 is the factor by which T_B is larger than the soliton width. Thus, the condition (1.15) can be written in the form of a design criterion:

$$B^2 L_A \ll (4q_0^2 |\beta_2|)^{-1}, \quad (1.16)$$

For typical values $\beta_2 = -0.5 \text{ ps}^2/\text{Km}$, $L_A = 50 \text{ Km}$ and $q_0 = 5$, we obtain $T_0 \gg 5$ ps and $B \ll 20$ Hz. Clearly, the use of amplifiers for soliton amplification imposes a severe limitation on both the bit rate and the amplifier spacing in practice. Optical amplifiers, needed to restore the soliton energy, also add noise originating from spontaneous emission. Amplitude fluctuations, as one might expect, degrade

the signal-to-noise ratio. However, for applications of solitons in optical communications, frequency fluctuations are of much more concern. If the characteristic parameter fluctuates because of amplifier noise, soliton's transit time through the fiber also becomes random. Fluctuations in the arrival time of a soliton are referred to as the Gordon-Haus timing jitter (GHTJ)[102]. Such a timing jitter limits the performance of long-haul systems, but it can be reduced in practice by using a variety of techniques [92, 103, 104].

Dispersion management

Though dispersion management (DM) was applied originally in low-power (linear) transmission systems, it has been discovered recently that this technique is also a very promising way to increase transmission capacity of the soliton-based communication lines. A transmission line constructed from alternated fibers with anomalous or normal dispersion has a low path-averaged chromatic dispersion, but a high local one, thereby suppressing the GHTJ as well as the four-wave mixing efficiency simultaneously. In [105] it has been proposed to incorporate a section of Dispersion Compensating Fiber (DCF) into the standard periodic soliton transmission line, before each amplifier. This was perhaps the first formulation in the literature of the idea of DM soliton transmission, even though a clear theoretical and practical description of this regime was not presented until few years later. It has been shown in [105] that this new (for the soliton systems) technique reduces the power required, compared to an uncompensated (constant dispersion) soliton system, and increases both the maximum transmission distance and the range of pulse width over which operation is possible. In the first related experimental work [106] it has been demonstrated that the dispersion management leads to a

significant reduction of the GHTJ. It should be pointed out that a similar idea of stretched pulses generation in a loop (periodic) laser system with varying dispersion has been proposed in [107]. In [108, 109] the dispersion-managed pulse has been identified as a new information carrier a stable periodic breather with features very different from that of the conventional soliton. A path-average theory and a simple approximate method to describe breathing DM soliton dynamics resulting from the interplay between varying dispersion and nonlinearity has been developed [109]. The energy of the DM soliton is enhanced [108] in comparison with a fundamental soliton (soliton solution of the NLSE) of the same width corresponding to the same path-averaged dispersion. This energy enhancement is the important feature of DM soliton leading to the increase of the Signal-to-Noise Ratio (SNR) with substantial improvement of the system performance [106]. Large variations of the dispersion (strong DM) strictly modify the soliton propagation fundamentally, inducing breathing-like oscillations of the pulse width during the amplification period. This dynamics differs substantially from the path-averaged (guiding-centre) soliton propagation in systems with constant or weakly varying dispersion and from that of the traditional fundamental soliton (the soliton solution of the integrable NLSE [110]). Nevertheless, numerical simulations and experiments have demonstrated that it is possible to observe extremely stable propagation of a breathing soliton in fiber links with strong DM. Pulse dynamics presents rapid oscillations of the power and width on the amplification distance, and slow evolution on the larger scales due the fiber nonlinearity and residual dispersion [109]. In other words, the dispersion management imposes such a strong perturbation that a carrier pulse in this case is no longer the NLSE soliton. In the

case of a weak DM a powerful Lie-transform technique has been applied to describe properties of the carrier pulse (dressed soliton) [111]. Interestingly, reversing the acceleration of Airy waves in spatial domain was recently demonstrated by applying nonlinear TWM process in an asymmetrically-poled nonlinear photonic crystal [112]. It was found that the linear propagation of the truncated Airy wave, which is suitable for a practical realization, in a fiber with SOD leads to a final diversion of the wave [7, 112]. Very recently, R. Driben and T. Meier [25] analyze and compare possibilities to regenerate truncated Airy pulses by the application of a DM scheme consisting of alternating fiber sections with opposite signs of the second order dispersion term similar to [113] with the regeneration possibilities in the new scheme with alternation of the both two leading dispersion terms (β_2 and β_3) using A.I mechanism [23, 24]. In the scheme with the alternation of both the second and the third dispersion terms it will be demonstrated that the acceleration of the Airy pulse will experience multiple reversals which are accompanied by the creation of multiple hot spots in a course of the propagation in the dispersion managed fiber link. The later scheme will reveal a long lasting propagation with multiple tight light concentration hot spots in a course of the propagation. This regime of a tight pulse compression persists in a presence of strong fiber Kerr nonlinearity and provides a possibility to describe the system performance in a quantitative way as a function of the injected light peak power.

The evolution of truncated Airy pulses in lossless fiber links with alternating signs of SOD and TOD of opposite signs is considered. The evolution is governed by the normalized nonlinear Schrodinger equation:

$$i\frac{\partial A}{\partial \xi} + \frac{(-1)^n}{2}\frac{\partial^2 A}{\partial \tau^2} + \frac{i(-1)^{n+1}\varepsilon}{6}\frac{\partial^3 A}{\partial \tau^3} + N|A|^2A = 0, \quad (1.17)$$

An odd integer index- n represents sections with negative SOD and positive TOD, while an even integer index- n stands for fiber sections with positive SOD and negative TOD. The normalized distance is given by $\xi = z|\beta_2|/\tau_0^2$ and the relative TOD strength by the in our scheme always negative parameter $\varepsilon = \beta_3/(\beta_2\tau_0)$, where β_2 and β_3 are the second- and third-order dispersion parameters of the fiber sections, and τ_0 is the pulse width. The Kerr nonlinearity is represented by the last term. In linear regime, $N = 0$. Equation 1.17 became:

$$i\frac{\partial A}{\partial \xi} + \frac{(-1)^n}{2} \frac{\partial^2 A}{\partial \tau^2} + \frac{i(-1)^{n+1}\varepsilon}{6} \frac{\partial^3 A}{\partial \tau^3} = 0, \quad (1.18)$$

By application of the Fourier transform (FT), we obtained:

$$\frac{\partial \tilde{A}}{\partial \xi} = \frac{i(-1)^n}{2} \omega^2 \tilde{A} + \frac{(-1)^{n+1}\varepsilon}{6} \omega^3 \tilde{A}, \quad (1.19)$$

The general solution of Eq. (1.19) is giving by

$$A(\xi, \tau) = \int_{-\infty}^{+\infty} \tilde{A}(0, \omega) \times \exp\left(\frac{i(-1)^n}{2} \omega^2 \xi + \frac{i(-1)^{n+1}\varepsilon}{6} \omega^3 \xi - i\omega\tau\right) d\omega, \quad (1.20)$$

where $\tilde{A}(0, \omega)$ is the Fourier transform of the incident field at $\xi = 0$ and is obtained by using

$$\tilde{A}(0, \omega) = \int_{-\infty}^{+\infty} \tilde{A}(0, \tau) e^{i\omega\tau} d\tau, \quad (1.21)$$

the analytic solution for the pulse evolution in odd and even fiber links reads is giving by:

$$|A(\xi', \tau)|^2 = A_0 \exp\left(2\alpha\Theta\tau + \frac{4}{3}\alpha^3\Theta^2 - \Theta^2\alpha\xi'^2\right) \times \Theta^{2/3} \left| Ai\left[\Theta^{1/3}\left(\tau - \frac{\Theta}{4}\xi'^2 + \alpha^2\Theta + i\alpha\Theta\xi'\right)\right] \right|^2, \quad (1.22)$$

for odd fiber sections with $\xi' = \xi - 2nL$,

$$|A(\xi'', \tau)|^2 = A_0 \exp \left(-2\alpha\Theta\tau - \frac{4}{3}\alpha^3\Theta^2 + \Theta^2\alpha\xi''^2 \right) \times \Theta^{2/3} \left| \text{Ai} \left[-\Theta^{1/3} \left(\tau - \frac{\Theta}{4}\xi''^2 + \alpha^2\Theta - i\alpha\Theta\xi'' \right) \right] \right|^2, \quad (1.23)$$

for compensating even fiber sections with $\xi'' = \xi - (2n + 1)L$. The parameter L represents fiber section's length and Θ is given by: $\Theta = \frac{1}{1-0.5\varepsilon\xi}$. Particularly, in the absence of TOD, the solution 1.22 and 1.23 consistent with that shown in [92] in one piece of fiber, in which self-accelerating finite energy Airy beams (SAFEAB) are proposed in detail. In this case, the FEAP exhibits an approximate diffraction-free behavior. However, in presence of TOD, dynamic of finite energy Airy pulse (FEAP) is different due to the factor Θ . In fact, because the factor Θ changes the sign at $\xi = 2/\varepsilon$, the truncated Airy pulse undergoes in this and continues to propagate with an opposite acceleration. We chose an optimal regime for the system performance to preserve the original pulse width working with each fiber section's length:

$$L = 2/\varepsilon \quad (1.24)$$

and thus one period of DM scheme is $2L$. In the case of nonlinear propagation ($N \neq 0$), the analysis is conducted through numerical simulations. Figure 1.24 explains this scheme. Fig. 2.2(a) gives dynamic of truncated FEAP under the action of equal strength SOD and TOD. We can see that the truncated Airy pulse undergoes an inversion at $\xi = 2$, and then continues to propagate with and a opposite acceleration in one period of DM scheme. This is repeated on all the other pieces of fiber until it comes out of the guide. However, when increasing the TOD (see Fig. 1.17(b), 1.17(c) and 1.17(d)), we find that the inversion length is reduced because here the nonlinear effects are considered. These results are in

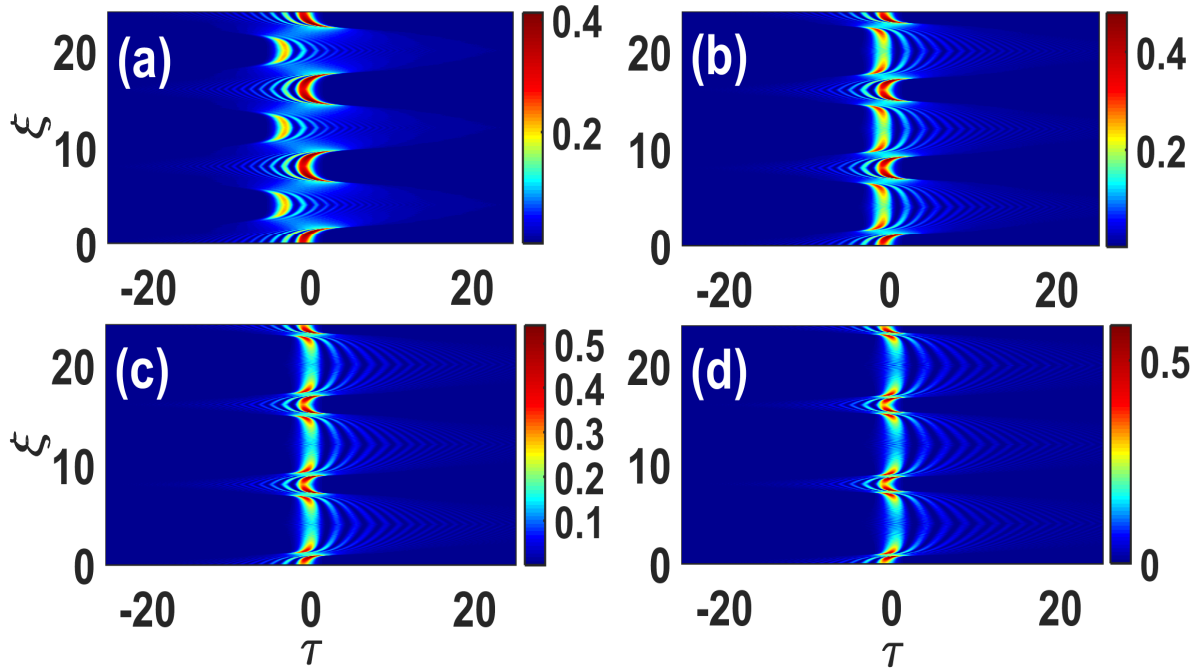


Figure 1.17: The dynamics of one FEAP in 6 periods of the DM scheme in nonlinear regime with different TOD. (a) $\varepsilon = 1$; (b) $\varepsilon = 1.5$; (c) $\varepsilon = 2$; (d) $\varepsilon = 2.5$ and $\alpha = 0.05$ in anomalous dispersion [25].

agreement with those obtained by Wang Xin et al [114].

1.2.7 Limits of the previous Regeneration mechanism

1R Regeneration

The principle of optical amplifiers is to use the phenomenon of stimulated emission to carry out the amplification process. However, this phenomenon of interaction between the matter and radiation is also accompanied by the phenomena of absorption and spontaneous emission. Part of the photons generated by spontaneous emission is guided and amplified. Therefore, the 1R regeneration allows to increase the transmission distance by compensating the losses of the optical fiber but causes the degradation of the signal with the addition of amplified spontaneous emission (ASE). The second stage of regeneration will therefore be necessary. It's here 2R regeneration, including reduction of intensity fluctuations and improvement of

extinction rate.

2R Regeneration

Although $2R$ regeneration reduces the intensity fluctuations on the symbols, it does not reduce the temporal jitter. On the contrary, she would tend to add. Indeed, the nonlinear gate transforms the intensity fluctuations into temporal jitter. To fight against this phenomenon, we must carry out a complete regeneration of the data corresponding to a $3R$ regeneration.

3R Regeneration

The regenerators when to them only modify the distribution of intensity ($2R$) and temporal fluctuations ($3R$). Therefore, regeneration is effective only when it is distributed over the during transmission, not upon receipt. Indeed, when regenerators are evenly distributed along the transmission, the signal degradations are periodically reduced. Thus, the degradations at the end of the signal transmission are limited, which leads to an improvement in the bit error rate compared to the transmission without regeneration.

Soliton amplification

Optical amplifiers, needed to restore the soliton energy, also add noise originating from spontaneous emission. The effect of spontaneous emission is to change randomly the parameters, at the output of each amplifier [115]. Amplitude fluctuations, as one might expect, degrade the SNR. However, for applications of solitons in optical communications, frequency fluctuations are of much more concern and noting that a change in the soliton frequency by d affects the speed at

which the soliton propagates through the fiber. Fluctuations in the arrival time of a soliton are referred to as the GHTJ [102]. Such a timing jitter limits the performance of long-haul systems, but it can be reduced in practice by using a variety of techniques [92, 103, 104]. These four regeneration mechanisms use regenerators. These make the transmission chain heavy and expensive.

Dispersion management

This regeneration technique, applied to the Airy pulse in order to increase its longevity in the fiber-optics link, is the first that does not require the presence of optical amplifiers. It highlights the intrinsic properties of the optical fiber such as dispersion and nonlinearity, thus making the transmission chain simple. Since DM scheme is based on the interaction between SOD and TOD, it is therefore impossible to apply this regeneration technique in zero-TOD systems such as FBGs, fibers made from silica, etc...

In the best of our knowledge, it still remained several paths both in the experimental and the theoretical aspects among which one can quote the following points :

- in the zero-TOD systems, what kind of the truncated Airy pulses regeneration could be implemented instead of using the interaction between GVD and TOD ?
- What is the influence of the CKN on this kind of regeneration ?
- Is there possible to make such regeneration with SFEAPs? if yes, within which conditions?
- What are the characteristics or efficient parameters to achieve optimally this kind of regeneration in fiber-optics links? The courses of this thesis goes in the direction to bring elements of answers to these raised questions.

1.2.8 Contributions on the truncated Airy pulses regeneration

Following this path of research, in this first part of our thesis, instead of using the interaction between GVD and TOD as in Refs. [25, 30], we conduct the regeneration of single FEAPs and SFEAPs in fiber links induced by the initial chirp called the chirp-dispersion management (CDM) technique. This technique of regeneration consists managing the product of $GVD \times chirp$ over each piece of fiber line in the case of zero-TOD systems, contrary to R. Driben and T. Meier [25]. Our contributions in this work are described as follows :

- Three models are developed: the first consists of alternation of the GVD with the chirp being constant, the second consists of the alternation of the chirp with a constant GVD, and the third consists of the alternation of both parameters.
- We show that only the first one allows to achieve a more stable regeneration of Airy pulses with an initial condition of $chirp \times GVD < 0$ corresponding to the A.I. mechanism.
- The beneficial parameter is found to be the initial chirp, while the temporal gap (only for SFEAPs) and the nonlinearity have deleterious impacts on this regeneration. We would like to remind the reader here that unlike the work done by R. Driben and T. Meier [25] who regenerated FEAP using the A.I. mechanism with $GVD \times TOD < 0$, we rather achieve the regeneration using the A.I. mechanism with $chirp \times GVD < 0$.
- Furthermore, contrary to Ref. [29], instead of achieving the evolution of SFEAPs within one continuous fiber, we proceed to the regeneration of SFEAPs in an optical system with several pieces of different fibers through the alternation of GVD.

1.3 Overview on SCG

1.3.1 Theoretical and physical descriptions

The supercontinuum generation (SCG) phenomenon is a well-known nonlinear process today since it has been observed in bulk glasses for 200-THz light pulses [2, 116]. The trend aroused has led on many works where the SCG has been extensively studied especially with the advent of the Photonic crystal fiber (PCFs) and tapered fibers (TFs) that overcame the limitations of the usual fibers because of their high malleable dispersive and nonlinear properties [1, 2, 6, 117, 118]. The possibility of designing the dispersive and nonlinear properties of these optical waveguides has made them as the best tools to realize the SCG process. To achieve the SCG, highly dispersive and nonlinear waveguides are required, it allows the injected optical pulses to excite these effects and therefore to undergo a large spectral broadening with the dramatic generation of side-components due to the transfer of energy from the central part of the spectrum to the pedestal part. Such extreme broadening can lead to a high temporal pulse compression as discussed by A. V. Gusakov et al [119], B. Schenkel et al [120]... The combination of dispersive effects with a multitude of nonlinear effects such as SPM, Cross-Phase Modulation (XPM), FWM, stimulated Raman scattering (SRS) ..., leads to generation of new frequencies within the pulse spectrum so that it extends over a frequency range exceeding 100 THz. The properties of the optical waveguide in which a launched pulse is propagating in order to lead to the SCG phenomenon are very important. Sure enough, both the linear properties as the dispersion and the nonlinear properties as the CKN are necessary for the SCG

efficient occurrence. We present basic descriptions of optical waveguides used for SCG.

- **Highly nonlinear optical waveguide**

A PCF is basically the best tool to create a good SCG process. It could be illustrated as shown in figure 1.18. The periodic nature of the air holes becomes important in the so-called *photonic bandgap* (PB) fibers in which the optical mode is confined to the core by periodic variations of the refractive index within the cladding. The core of such fibers often contains air to which light is confined by the PB [1]. This design allows to reach high values of nonlinearity when the air in the

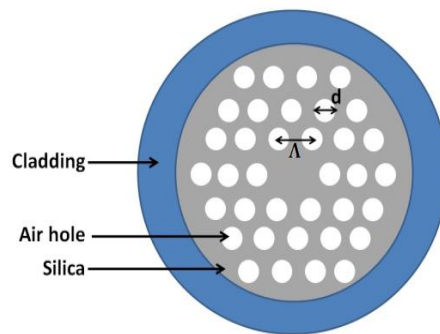


Figure 1.18: Diagram of a PCF or microstructured fiber. The parameters d and Λ represent the hole diameter and the pitch, respectively [121].

core is replaced with a suitable gas or liquid. Figure 1.19 shows some experimental PCFs. The main nonlinear mechanism of the pulse splitting achievement leading to the SCG process is the solitonic fission (SF)[121].

- **The SF mechanism**

The SCG occurs as a perturbation of HOS by HOD terms and high degree of nonlinearity of the medium. This implies that the SCG was firstly understood as a phenomenon which accompanies the solitons dynamics and so occurs in the anomalous dispersion regime of optical waveguide [130]. This HOS breaks into its

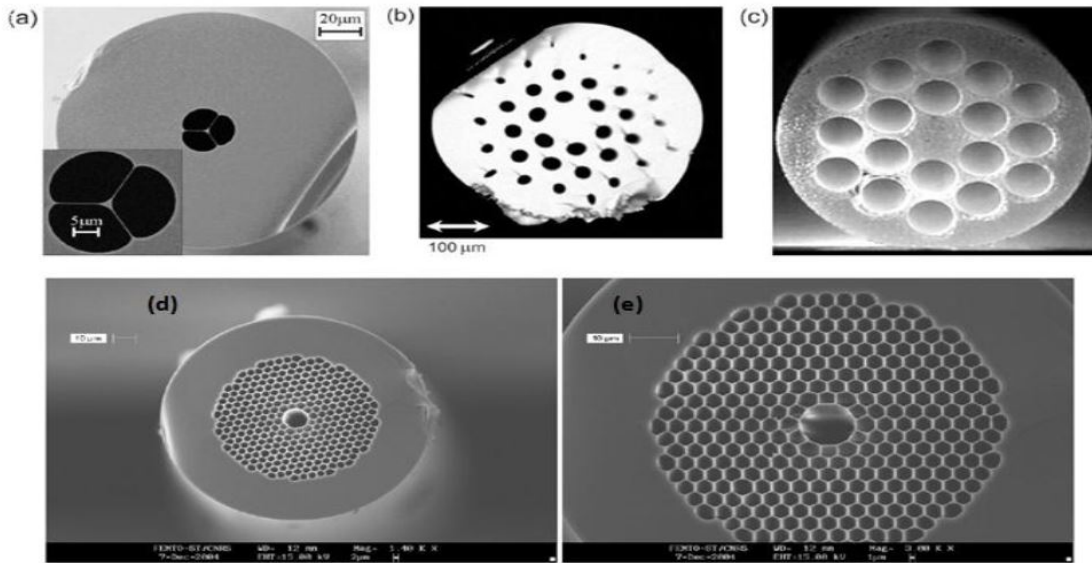


Figure 1.19: Some PCFs : Small core extruded PCF (*c*-2004 OSA, from Ebendorff-Heidepriem et al see [121, 127]), (b) Single mode tellurite PCF with extremely large mode area (*c*-2008 OSA, from Feng et al see [121, 128]), (c) Preform structure created by drilling (*c*-2004 IEEE, from Feng et al see [121, 129]), (d) a Hollow core PCF fabricated by Blazephotonics, image realized in the FEMTO-ST institute of the university of Franche-Comté, France (*c* – 2004 FEMTO-ST institute, from [130, 131]), (e) zoomed picture of (d)

fundamental components through the SF mechanism. Furthermore, the SF process appears at the start of HOS propagation in the medium, when the soliton spectrum extends. The Raman scattering or HOD can perturb the constituent fundamental solitons of the main soliton signal, leading them to move with different group velocities, and therefore to split apart.

The SF process can be investigated, by considering the propagation characteristics of an ideal HOS as the 3-OS drawn in figure 1.20. In this case, the injected 3-OS evolves periodically as illustrated in this figure. In the femtosecond regime, HOD and Raman scattering are the two most significant effects that can perturb such ideal periodic evolution and induce pulse splitting through SF [130]. The dominant effect depends on the input pulse duration. The Raman effect dominates generally for input pulses exceeding 200 fs while for pulses of duration less

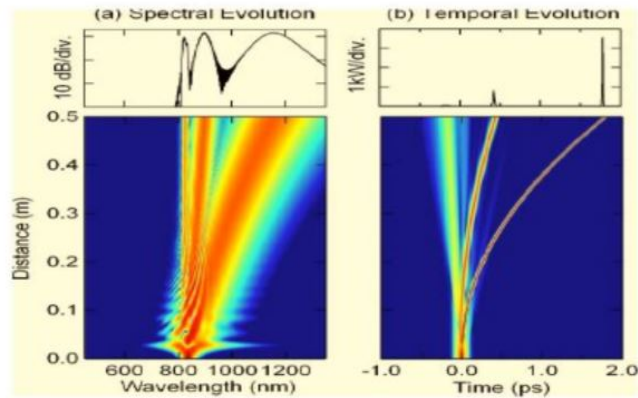


Figure 1.20: Illustration of the SF mechanism in the SCG phenomenon : results from numerical simulations showing (a) spectral and (b) temporal evolution for Raman induced fission of an incident 1.25 kW launched 3-OS. Top curves show the output profiles after 0.5 m propagation. (*c* -2006 APS, from [130])

than 20 fs, it is the HOD which dominates. So, for the two effects to operate in a balance manner in the SF process of the SCG, durations cover usually the intermediate range. The study of the SCG phenomenon through the SF mechanism has been extensively done this last decade [121,132-136]. Nearly, the whole aspects on SCG driven by SF were investigated in these works. Among these aspects, appear the emission and shedding of waves or radiations from the solitons which are themselves initially emitted from the SF mechanism. Figure 1.20 presents an illustration of the SF mechanism obtained by J. M. Dudley et al [130]. The SF mechanism in the temporal evolution of the 3-OS leads to a spectral broadening of the SCG. Some waves or radiations are emitted in both the time and the spectral domains. These features are briefly presented below.

- **Nonsolitonic radiation (NSR) or Cherenkov radiation, dispersive waves (DWs)**

The SCG phenomenon occurring in the SF mechanism is generally accompanied by the emission of waves such as the Raman solitons (RSs), and DWs... . The

RSs are obviously the sub-pulses stemming from the Raman induced SF while the DWs are the light shedding from the initial soliton in the right side of the time domain picture (see figure 1.21). The radiation assembling the DWs, is emitted at a frequency at which its phase velocity matches that of the soliton. This radiation is known to be the Cherenkov radiation or a NSR similarly to those emitted by charged particles in a bulk medium [1]. These DWs are naturally due to the dispersive properties of the optical waveguide. So, SCG-Based optical waveguides with strong chromatic dispersion profile (CDP) lead to strong DWs which however occur with the satisfaction of a PMC as extensively discussed in [1,137-140]:

$$\sum_{k=2}^{\infty} \frac{\beta_k}{(k!|\beta_2|t_0^{k-3})}(\omega_{DW} - \omega_S) = \frac{1}{2}(2N - 1)^2, \quad (1.25)$$

where ω_{DW} and ω_S are the carrier frequencies associated with the DW and the soliton, respectively. Another solitonic feature known as the MI has been found to conduct to the SCG phenomenon beyond the SF mechanism.

1.3.2 Improvement of the phenomenon: spectral bandwidth enhancement

After the discovery of the SCG process, many works were conducted to improve its efficiency in nonlinear optics in two aspects : the enhancement of the spectral bandwidth obtained and the achievement of its flatness inducing a spectral coherence.

- **Based on the waveguide properties**

The performing of the optical waveguide for the efficient achievement of the SCG phenomenon was the first approach developed [1, 2, 121, 130, 136]. The waveguides with a high degree of nonlinearity and strong Customer Data Platform

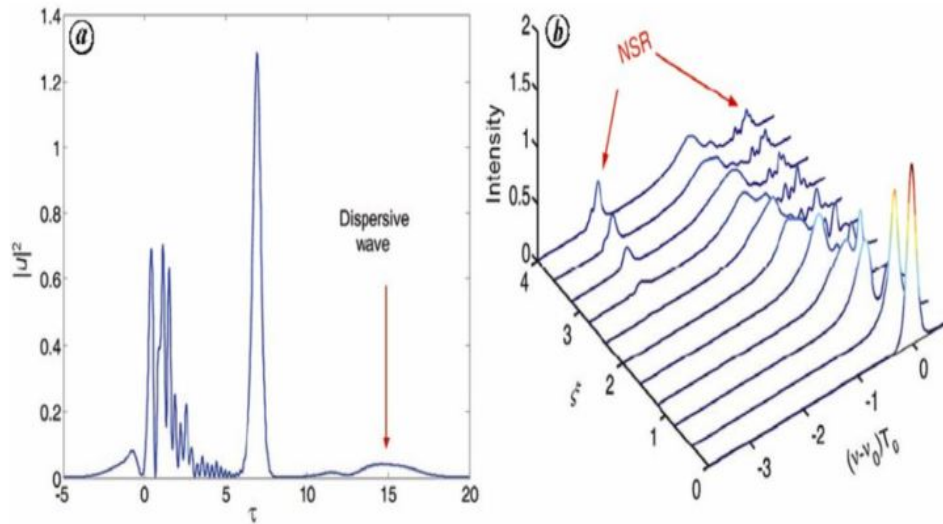


Figure 1.21: Illustration of the emission of DWs in a SCG process : (a) Low-amplitude pedestal in the form of DW, (b) NSR in spectral domain under two zero-dispersion conditions where FOD is dominant. (c – 2011 CURRENT SCIENCE, from [140])

(CDP) were investigated. The PCFs whose the possibility of designing the CDP and nonlinear properties has made them as the best tools to realize the SCG process. Designing characteristics of the PCFs as the effective core area, the ratio between the pitch and the hole diameter, the length ..., can properly enhance the nonlinearity and the ability of the waveguide to lead to ultra-large broadband spectra of SCG [1]. On the other hand, materials with large values of nonlinearity were also studied in order to use them in the classical PCFs instead of the basic silica material. Today, some other materials that provide large values of CKN coefficient are known and used in the place of silica. In this category of materials one can quote heavy-metal-doped oxide glasses, semiconductor materials as the silicon material, semiconductor doped glasses, polydiacetylene toluene sulfonate (PTS), chalcogenide glasses (As_2S_3 , As_2Se_3), tellurite glasses, fibers based on bismuth oxide ... [1, 121].

Table 1.1: Comparison of properties of some materials (c-2007 AP, from [1]); (c-2010 J. M. Dudley and R. Taylor, from [121]).

Material	SiO_2	Tellurite	Lead SiO_2	Bi_2O_3	As_2S_3	As_2Se_3	Si
$n_2^{(1)}$ ($\times 10^{-20} m^2W^{-1}$)	2.7 ⁽²⁾	25 ⁽³⁾	41 ⁽⁴⁾	32	~ 300	~ 1100	500 \sim 600
$\gamma^{(5)}$ ($W^{-1}m^{-1}$)	0.06	0.048	1.9	1.3	10	93.4	~ 100
$\alpha^{(6)}$ (dB/m)	0.001	-	0.3	2 \sim 3	5	60	25
TPA ⁽⁷⁾	-	-	-	-	yes	yes	yes

However, as seen in Tab. 1.1 some of these materials introduce other effects as nonlinear saturation, higher-order nonlinear effects, nonlinear absorptions It was therefore a challenge to manage the advantage taken on the high degree of nonlinearity against the deleterious ones raised simultaneously within the waveguide. In 2007 Yin and G. P. Agrawal studied the case of SOI-waveguides showing that they can be used to create SCG spectra extending over 400 nm by launching femtosecond pulses as HOSs through the SF mechanism [141]. The impact of absorption coefficients as the Two photon absorption (TPA) and the Free carrier absorption (FCA) was highlighted. Furthermore, they showed that the TPA reduces the spectral bandwidth of the SCG without an effect on its flatness. The free carriers generated during the SCG process were found to have a negligible impact on the pulse. So, neither the Stimulated Raman Scattering (SRS) nor FCA plays a significant role during the SCG process in SOI waveguides. Therefore, these ones were considered as other suitable tools to generate efficient SCG as confirmed by Wen et al in 2011, Castelló-Lurbe et al in 2012, and Cao et al in 2015. On the other hand, some kinds of PCFs that replace in the central core region rather a liquid were modeled [142-146]. The advantage to use a liquid material within the core region of the PCF consists to some special properties among which one

could have large nonlinearity, ultra-flattened dispersion, broadband single-mode guidance, high birefringence, very small effective areas etc. Such PCFs are called LCPCFs.

- **Based on the physical mechanisms**

Another approach consists to improve the efficiency of the SCG phenomenon by using the features of the physical mechanisms on which it is based. For example, in 2002 N. I. Nikolov et al [147] demonstrated the improving of the SCG phenomenon through the degenerate FWM. Several other works followed this approach as discussed in [121, 130, 136].

- **Based on the pulse characteristics**

1. *The peak power or energy*

Basically, the increase of the peak power enhances the Kerr effect [1, 148]. So, it improves the SCG phenomenon. However, there is a serious difficulty to use laser sources with high powers in practice. On the other hand, they are expensive. Furthermore, the heating due to the use of such lasers damages the waveguide. Therefore, this approach is not the best one to improve the efficiency of the SCG phenomenon. One should make the economy of energy. In this point of view, this approach is often avoided when possible. Other paths are explored in this case. The best method or approach to improve the SCG consists to do so without the need of high energies/powers ie an efficient achievement by reducing at the maximum the pulse energy.

2. *The pumping wavelength*

There is a great challenge to find the suitable laser source that emit light in the proper wavelength region for the achievement of the SCG process. Since the SF

mechanism drives the SCG phenomenon, the anomalous dispersion regime which is the fundamental field of the solitonic properties, is therefore more indicated for the obtaining of the broad spectra of SCG [130]. However, even the normal dispersion regime is suitable for the achievement of the SCG [149, 150]. Making a proper choice of the pumping wavelength is therefore relevant to the achievement of the SCG. In the normal dispersion regime, the interaction between the SPM and the normal GVD dominates the dynamics in the SCG. Bringing the pumping wavelength closer to the ZDW of the waveguide Chromatic dispersion profile (CDP) transfers the energy into the anomalous GVD regime.

3. *The pulse duration*

As observed in figure 1.22, J. M. Dudley et al [130] showed the dependence of the SCG phenomenon to the pulse duration. Reducing the pulse duration also decreases the spectral bandwidth and distorts its spectrum.

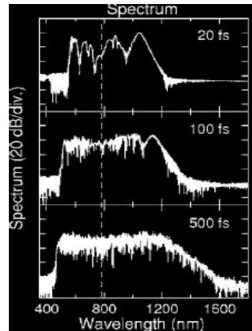


Figure 1.22: Influence of the SCG spectral bandwidth by the pulse width (*c* – 2006 APS, from [130])

4. *The pulse shape*

Considering the pulse shaping approach in the improvement of the SCG spectra, the overwhelming majority of prior studies utilized intense optical pulses with symmetric and compact temporal profiles such as Gaussian or hyperbolic secant pulses. There have been several reports on the optimization of SCG via pulse

shaping. However, the asymmetric profiles have also been investigated but more recently. Indeed, using the Airy pulses Ament et al [31], both experimentally and numerically, studied the quality of the SCG spectrum in terms of the interaction between the dominant peak and the oscillations tail through the soliton-dispersive-wave pairs features in a PCF. Moreover in 2012, D. Castelló-Lurbe et al [151](a) suggested that the preshaping of the input pulse with the correct skewness (in terms of asymmetry) compensates the deleterious effect of the FCA which was assumed to highly affect the trailing edge of the propagating pulse in silicon waveguides. Then, the SCG phenomenon in terms of spectral broadening was enhanced cause of this operation. More recently in 2014, the influence of steepness of pump temporal pulse profile on spectral flatness and SCG coherence in all-solid PCFs with flattened normal dispersion has been studied by Klimczak et al [151](b).

5. *The chirping process*

Considering the pulse chirping process, it has been shown earlier that the positive chirp increases the spectral bandwidth of the SCG [130, 152]. This effect is better than the one of the negative chirp as discussed in [152, 153]

• **Noise and coherence of SCG spectrum**

The SCG spectra are accompanied by noise induced by the multitude physical processes that intervene [1]. The sensitivity to noise of SCG in both SMF and PCF has been reported by a number of authors [130]. In fact achieving broadband spectra is not the only necessity, there is also the coherence which is important. A spectrum which is enough incoherent, is not useful in practical situations ie a spectrum which is highly distorted by noise does not serve in applications. So, it is necessary to obtain broadband spectra but they should be also the most

coherent as possible. One can appreciate the coherence of a SCG spectrum through the observation by considering its distortions or its flatness. Spectra which are more flattened, have a high probability to be more coherent than those which are highly distorted and less flattened. Rigorously, the spectral coherence of the SCG has been found by J. M. Dudley and S. Coen [154] to be measured through the modulus of the complex degree of first-order coherence which is defined at each wavelength in the SCG by:

$$|g_{12}^{(1)}(\lambda, t_1 - t_2)| = \left| \frac{\langle E_1^*(\lambda, t_1) E_2(\lambda, t_2) \rangle}{\langle |E_1(\lambda, t_1)| \rangle^2 \langle |E_2(\lambda, t_2)| \rangle^2} \right|. \quad (1.26)$$

Here the angular brackets denote an ensemble average over independently generated pairs of SCG spectra $[E_1(\lambda, t), E_2(\lambda, t)]$ obtained from a large number of simulations, and t is the time measured at the scale of the temporal resolution of the spectrometer used to resolve these spectra [1, 130, 154].

1.3.3 Applications of the SCG

The SCG phenomenon provides light sources with broad spectral coverage. It also provides spatially coherent radiation and can provide ultrashort pulses with large compression factors. The SCG can lead to the spectral versatility of lamp based sources with the advantages of laser radiation, including higher brightness for improved signal-to-noise measurements and ultrashort pulse operation. Using the SCG allows to avoid the complexity and costs associated with tunable visible laser systems that typically involve mode-locked lasers with second harmonic generation (SHG) or optical parametric generation [121]. The SCG phenomenon has several applications in nonlinear optics and other fields using the light. These applications

encompass domains like optical telecommunications, photonics, biophotonics For example, the SCG output could be used in optical telecommunications as a multichannel telecommunications source (SCG-Based WDM sources) [1]. In a 2000 experiment, the supercontinuum-based WDM technique was used to produce 1000 channels with 12.5-GHz channel spacing [117]. SCG can also be useful in applications as nonlinear spectroscopy, optical coherence tomography, optical frequency metrology, biophotonic microscopy ... [1, 121]. The figures 1.23 and 1.24 present some SCG-Based experiments in spectroscopy and in biophotonic microscopy, respectively [121]. In figure 1.24, the diagram presents a generalized schematic for multiphoton fluorescence microscopy with a SCG source, including an optional pulse compressor stage [121]. Further details and information about the description of the presented experiments and other applications of SCG can be found in [1, 121].

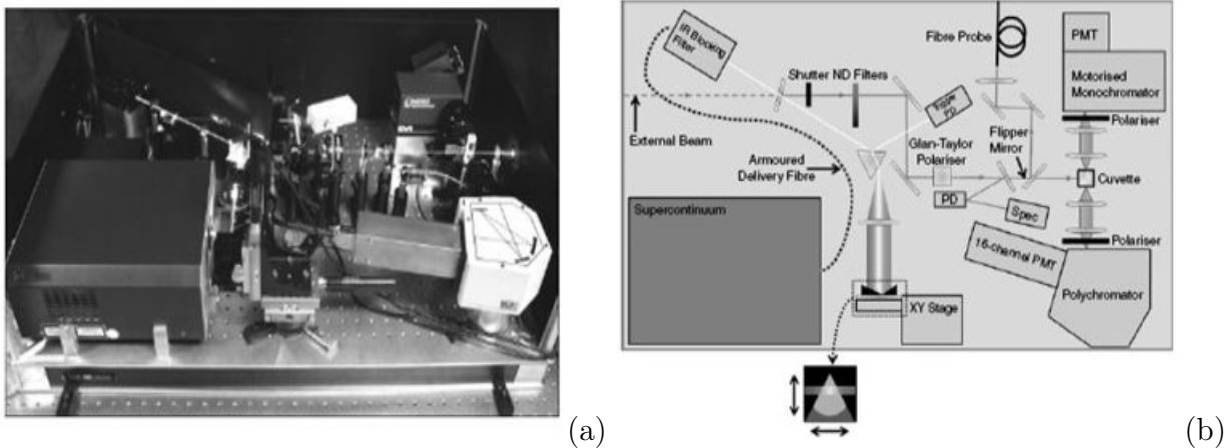


Figure 1.23: A SCG-Based experiment in spectroscopy :(a)- Photograph and (b)- experimental layout of a compact multidimensional spectrofluorometer based around a commercially available all-fibre SCG source (c-2010 J. Dudley and R. Taylor, from [121])

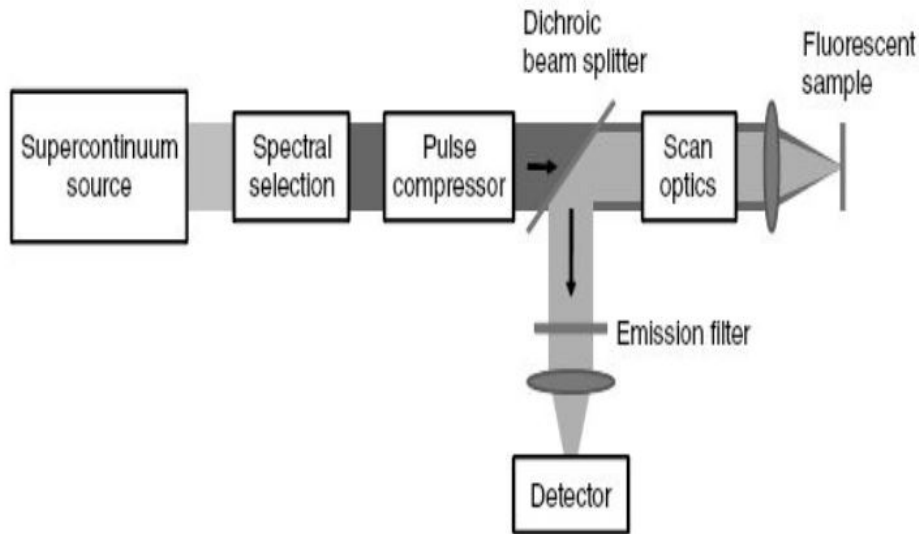


Figure 1.24: A SCG-Based experiment in biophotonic microscopy using a SCG source [121].

1.3.4 Limits of the previous works on SCG analysis

Regarding the two photons absorption (TPA) and the three photons absorption (3PA) processes, interest in these processes originates from the relevance of nonlinear photon absorption (NPA) in high-power laser technology as well as its role in many fundamental aspects of solid-state physics. Nonlinear absorption plays a crucial role in limiting the transparency of optical window materials and in causing laser-induced damage to optical components, particularly at short wavelengths [122-125]. NPA processes have been successfully used to produce population inversion in semiconductor laser materials [122]. For instance, the 3PA process has shown the potential for applications in optical limited fluorescence imaging and stimulated emission [123]. Moreover, the impact of the quintic Kerr nonlinearity (QKN) on the SCG has already been discussed in reference [125], in which Mandeng et al showed that the SCG spectra produced with a sech-type input profile were slightly compressed in the cooperative case, compared with the competi-

itive case. Also, in reference [5], Sharafali et al observed that the QKN increased the MI for cooperative nonlinearities, while it suppressed the MI for competitive nonlinearities.

In this second part of this thesis, we use the hypothesis of considering the high-order nonlinearity to be QKN, which has been neglected in the previous works mentioned above (except for [5, 125]). Indeed, all the previous works focused on the features of the obtained SCG spectra using only the cubic Kerr nonlinearity (CKN) term, which is, of course, the dominant one. For more insight, we choose to consider the impact of the QKN term by extending the Kerr nonlinearity to the fifth order, as done in references [5, 125, 126]. We suggest that the large value of nonlinearity provided by the materials allows this hypothesis to be understandable in the light of these works. Therefore, it is also interesting to observe that while TPA originates from the CKN, 3PA even originates from the QKN in a nonlinear material interacting with a luminous signal. Furthermore, considering the previous studies of Airy pulses in SCG investigations [28, 31] combined with the work done by M Diouf et al [40].

In our thesis, we conduct a numerical investigation that responds to the following interrogations:

- What is the impact of the QKN on MIR-SCG with a truncated Airy pulse?
- What are the NPA effects on this MIR-SCG, such as those of the TPA and the 3PA?
- Which features arise from the competitive and cooperative cases? Hence the interest of the second part for this thesis.
- One should note that Zhong et al [126] studied the properties of the temporal

evolution of truncated Airy pulses in a cubic-quintic optical system. Thus, before the present work, there was no study of MIR-SCG involving Airy pulses in such optical systems.

1.3.5 Contributions of SCG analysis

In the thesis, our contribution can be described as follows:

- the spectra at 20 dB-bandwidths could exceed approximately 97250 nm.

In the case in which the NPA parameters are not taken into account, only the cooperative QKN is beneficial for the MIR-SCG of the truncated Airy pulse within this waveguide.

- In the temporal domain, the emission of dispersive waves (DWs) is avoided by the presence of NPAs, while the cooperative nonlinearities allow this emission.

- Moreover, in the cooperative case, neglecting the 3PA and considering the cooperative QKN and TPA, we find an interesting spectral intensity (SI) of the SCG, compared with the competitive case.

- An interesting surprise concerns the 3PA, which appears to be a good tool for controlling the TPA. Considering, in particular, the competing nonlinearities, the 3PA enhances the SI of the MIR-SCG of the truncated Airy pulse compared to the single TPA case for larger wavelengths.

In the next section, we describe briefly the optical waveguides that are modeled in the different systems studied in the thesis.

1.4 Description of the optical waveguides studied in this thesis

1.4.1 Fiber-optics links

If the nonlinear effects in the optical fiber are considered as the factors of signal degradation in transmission systems, however, they can be controlled and used for optical regeneration. Devices based on the use of a nonlinearity in optical fiber (the Kerr effect in general) are very promising due to their near instantaneous response time (the Kerr effect response time is a few femtoseconds), and their wide spectral range of use. Moreover, with the development of microstructured fibers, the efficiency of nonlinear effects is greatly increased. Therefore, all-optical signal processing using the effects nonlinear in fiber is currently a very active area of research. However, their low integration capacity is the main drawback for their applications in optical transmission systems, in particular in Wavelength-division multiplexing (WDM) systems. A fiber-optic link (or fiber channel) is usually a part of an optical fiber communications system which provides a data connection between two points (point-to-point connection). It essentially consists of a data transmitter, a transmission fiber (in some cases with built-in fiber amplifiers), and a receiver. Even for very long transmission distances, extremely high data rates of many Gbit/s or even several Tbit/s can be achieved. The used components, which are mostly based on fiber optics, are explained in the following, beginning with a simple single-channel system. More sophisticated approaches are discussed thereafter.

A special kind of fiber-optic links is used for timing distribution and synchro-

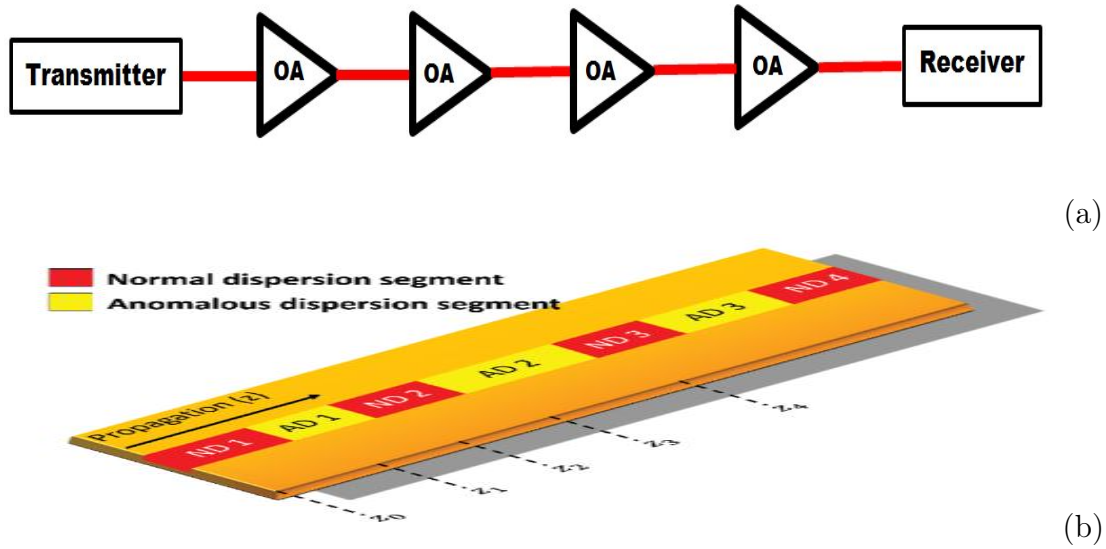


Figure 1.25: (a) - Schematic of a fiber-optic link, with a data transmitter, a long transmission fiber with several fiber amplifiers, and a receiver. The amplifiers can be supplemented with additional components for dispersion compensation or signal regeneration; (b) - Fiber-optic links [67].

nization.

Transmission Formats

In most cases, the data transmission is digital, making the system very versatile and relatively insensitive, e.g. to nonlinear distortions. There are various different modulation formats, i.e., different methods for encoding the information. For example, a simple non-return-to-zero (NRZ) format transmits subsequent bits by sending a high or low optical power value, with no gaps between the bits, and extra means for synchronization. In contrast, a return-to-zero (RZ) format is easily self-synchronizing by returning to a rest state after each bit, but it requires a higher optical transmission bandwidth for the same data rate. Apart from details of the equipment and the optical bandwidth required (related to the modulation efficiency), different transmission formats also differ in terms of their sensitivity

e.g. to noise influences and cross-talk.

Transmitter

The transmitter converts the electronic input signal into a modulated light beam. The information may be encoded e.g. via the optical power (intensity), optical phase or polarization; intensity modulation is most common. The optical wavelength is typically in one of the so-called *telecom windows*. A typical transmitter is based on a single-mode laser diode, which may either be directly modulated via its drive current, or with an external optical modulator (e.g. an electroabsorption or MZM). Direct modulation is the simpler option, and can work at data rates of 10 Gbit/s or even higher. However, the varying carrier density in the laser diode then leads to a varying instantaneous frequency and thus to signal distortions in the form of a chirp. Particularly for long transmission distances, this makes the signal more sensitive to the influence of chromatic dispersion. Therefore, external modulation is usually preferred for the combination of high data rates (e.g. 10 or 40 Gbit/s) with long transmission distances (many kilometers). The laser can then operate in continuous-wave mode, and signal distortions are minimized. For even higher single-channel data rates, time division multiplexing may be employed, where e.g. four channels with 40 Gbit/s are temporally interleaved to obtain a total rate of 160 Gbit/s. For high data rates with RZ formats, it can be advantageous to use a pulsed source (e.g. a mode-locked laser emitting soliton pulses (MLLESP)) combined with an intensity modulator. This reduces the bandwidth demands on the modulator, as it does not matter how the modulator's transmittance evolves between the pulses. For high data rates, the transmitter needs to meet a number of requirements. In particular, it is important to achieve a high

extinction ratio (low pedestal pulses), a low timing jitter, low intensity noise, and a precisely controlled clock rate. Of course, a data transmitter should operate stably and reliably with minimum operator intervention.

Transmission Fiber

The transmission fiber is usually a Single-Mode Fiber (SMF) in the case of medium or long-distance transmission, but can also be a multimode fiber for short distances. In the latter case, intermodal dispersion can limit the transmission distance or bit rate. Long-range broadband fiber channels can contain fiber amplifiers at certain points to prevent the power level from dropping to too low a level. Alternatively, it is possible to use a distributed amplifier, realized with the transmission fiber itself, by injecting an additional powerful pump beam (typically from the receiver end) which generates Raman gain. In addition, means for dispersion compensation (counteracting the effects of chromatic dispersion of the fiber) and for signal regeneration may be employed. The latter means that not only the power level but also the signal quality (e.g. pulse width and timing) is restored. This can be achieved either with purely optical signal processing, or by detecting the signal electronically, applying some optical signal processing, and resending the signal.

Bidirectional Transmission

So-called full duplex links provide a data connection in both directions. These may simply be based on separate optical fibers, or work with a single fiber. The latter can be realized e.g. by using fiber-optic beam splitters at each end to connect a transmitter and a receiver, which may preferably work at different wavelengths.

However, the need for bidirectional operation introduces various trade-offs, which in some cases (e.g. for very high data rates) make a system with two separate fibers preferable.

Multiplexing

A typical single-channel system for long-haul transmission has a transmission capacity of e.g. 2.5, 10 Gbit/s, 40 Gbit/s or even 160 Gbit/s. For higher data rates, several data channels can be multiplexed (combined), transmitted through the fiber, and separated again for detection. The most common technique is WDM technique. Here, different center wavelengths are assigned to different data channels. It is possible to combine even hundreds of channels in that way, but coarse WDM with a moderate number of channels is often preferred in order to keep the system simpler. The main challenges are to suppress channel cross-talk via nonlinearities, to balance the channel powers (e.g. with GFFA), and to simplify the systems.

Limitations via Noise and Cross-talk

Ultimately, the data transmission capacity of any system is limited by noise. In amplified optical systems, quantum noise e.g. in the form of spontaneous emission in fiber amplifiers is not avoidable. It can impact the system performance in different forms, such as timing jitter (Gordon-Haus jitter, particularly in soliton systems) or intensity noise affecting the photodetection. Apart from noise, certain systematic signal distortions can also limit the transmission distance or bit error rate. In particular, chromatic dispersion and nonlinearities of the transmission fiber can cause severe signal distortions. As an example, Fig. 1.26 shows a so-

called eye diagram. Here, the "eye" is wide open, so that the signal could still be well detected. For twice the fiber length (not shown here), this would be different.

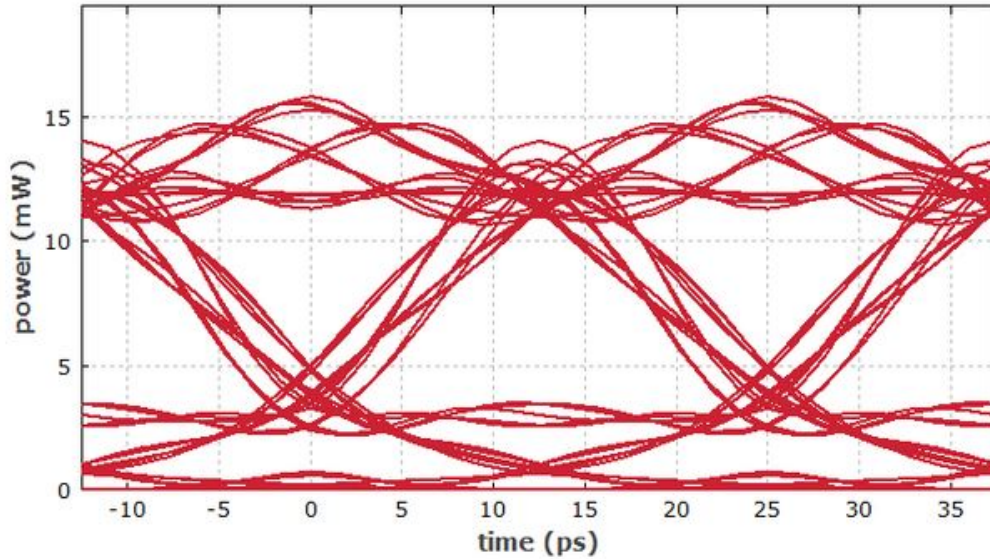


Figure 1.26: Eye diagram for the telecom signal after the fiber [67].

Note that the transmitter also has an important impact on signal detection issues. For example, a simple directly modulated transmitter may produce some unwanted frequency chirp, which increases the effect of chromatic dispersion in the transmission fiber and thus makes it more difficult to receive a clean signal after some propagation distance. A related and even more sophisticated topic is cross-talk between the different channels e.g. of a WDM system. In systems with constant channel spacing, the channels can also influence each other in the form that one channel is amplified at the expense of the power in another channel (case of FWM). The impact of such effects can depend strongly on the system architecture, including the transmitter type, modulation format, fiber parameters, detection techniques, etc. The modeling of these effects and the subsequent optimization of communication systems are complex tasks. Noise and related influences always cause some bit error rate, i.e., some portion of the transmitted

bits will not be correctly detected. Provided that the bit error rate is at a sufficiently low level, occasional bit errors can be detected with certain techniques and corrected (e.g. by resending of defective data packets). For increasing transmission distances and/or data rates, the bit error rate finally sets some limits. In that context, the bandwidth-distance product is often used in a comparison of different fiber-optic links.

Fiber-optic Links for Timing Distribution and Timing Synchronization

While most fiber-optic links are used for transmitting data, there are also similar systems for the distribution of ultra-precise timing signals. Even with quite simple technology, the ultra-precise pulse-to-pulse spacing of a mode-locked laser is quite well preserved even over a link length of tens of kilometers. Advanced technology can also largely suppress effects of varying group delays, e.g. as a result of temperature changes of the fiber. It has become possible, e.g., to synchronize laser oscillators with very high precision through such links.

1.4.2 Optical waveguide for SCG

Rib-like structure with chalcogenide glasses

The design of the studied $AsSe_2/As_2S_5 - ChRW$ is illustrated in Fig. 1.27 and corresponds to the one recently investigated in [38, 40]. It consists to a core composed of $AsSe_2$ glass while the cladding is composed of As_2S_5 . The $AsSe_2/As_2S_5 - ChRW's$ structure studied in this thesis is draw in Fig. 1.27.

The considered $AsSe_2/As_2S_5 - ChRW$ structure is filled in its upper cladding by air while As_2S_5 glass constitutes the lower one and $AsSe_2$ glass represents the

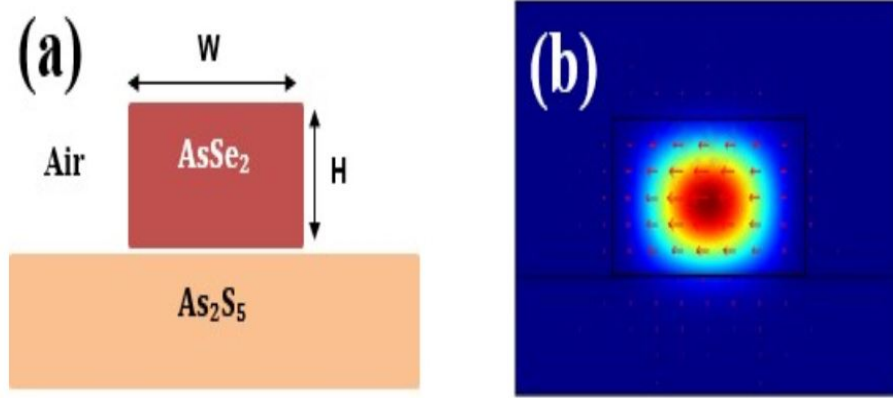
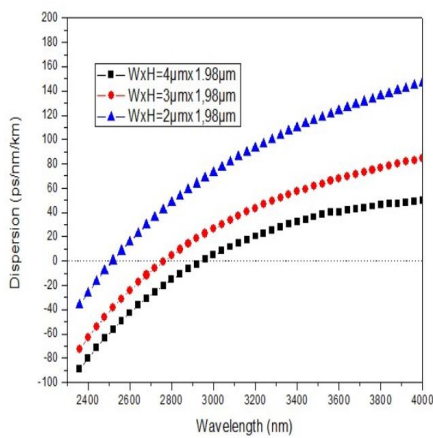


Figure 1.27: (a) and (b) are for the waveguide cross sections: (a)- Rib structure of the waveguide geometry: $H = 1.98\mu m$ and $W = 5\mu m$; (b) HE_{11} mode at the pumping wavelength $4\mu m$ [38, 40].

core of the structure. Using the full-vectorial finite element method (FVFEM) software, we draw the fundamental modes of field propagation within the optical waveguides that consists to the HE_{11} single mode when the pumping is done at the wavelength $4\mu m$ [38, 40]. This $AsSe_2/As_2S_5 - ChRW$ structure confines strongly (with its geometry) the fundamental mode especially when the height H is relevant [41].

Chromatic Dispersion Profiles of the $AsSe_2/As_2S_5 - ChRW$



(a)

Symbol	$AsSe_2/As_2S_5$ -PCF	$AsSe_2/As_2S_5$ -ChRW
β_0	$4.323866369 \times 10^6 m^{-1}$	$4.2204208841 \times 10^6 m^{-1}$
β_1	$9.6651 \times 10^9 s / m$	$9.7628 \times 10^9 s / m$
β_2	$-3.3375 \times 10^{-25} s^2 / m$	$-4.4942 \times 10^{-25} s^2 / m$
β_3	$4.0332 \times 10^{-39} s^3 / m$	$4.0876 \times 10^{-39} s^3 / m$
β_4	$-1.9392 \times 10^{-53} s^4 / m$	$-2.3331 \times 10^{-53} s^4 / m$
β_5	$1.1217 \times 10^{-67} s^5 / m$	$2.7364 \times 10^{-67} s^5 / m$
β_6	$-1.4933 \times 10^{-82} s^6 / m$	$-4.1439 \times 10^{-81} s^6 / m$
β_7	$-1.4293 \times 10^{-95} s^7 / m$	$6.2229 \times 10^{-95} s^7 / m$
β_8	$3.5791 \times 10^{-109} s^8 / m$	$-7.722 \times 10^{-109} s^8 / m$
β_9	$-4.774 \times 10^{-123} s^9 / m$	$6.6982 \times 10^{-123} s^9 / m$
β_{10}	$2.959 \times 10^{-137} s^{10} / m$	$-2.9742 \times 10^{-137} s^{10} / m$

(b)

Figure 1.28: (a)- Calculated CDPs of the HE_{11} mode for the considered $AsSe_2/As_2S_5 - ChRW$; (b)- Values of each order of the CDP [38, 40].

By carrying out the FEM to calculate the chromatic dispersion profiles (CDPs) of the considered structures, we obtained the Fig. 1.28. It appears that these two configurations have only one zero-dispersion wavelength (ZDW). Expecting an efficient SCG achievement within the studied structures, we have chosen to pump in the ADR so that the extreme spectral broadening is driven by the SF mechanism accompanied by some DWs emission [2, 92, 121, 130, 136, 141]. For the PCF, the configuration with $\Lambda = 2.5\mu m$, $d = 0.6\mu m$ and $ZDW = 3.3\mu m$, represents a good candidate for ultra-broadband MIR-SCG at the pumping wavelength $4\mu m$. Concerning the rib structure, the ZDW is around $3\mu m$, $W = 5\mu m$, $H = 1.98\mu m$ and the pumping wavelength is also $4\mu m$. We focus on the effects of quintic nonlinearity and the associated nonlinear absorption using the spectra for long wavelengths, assuming that for short wavelengths around the pumping wavelength, there are no large differences between the different cases.

1.5 Conclusion

In summary we have presented in this chapter, a brief overview on regeneration mechanism through its physical descriptions, fiber optic transmission system, transmitter and receiver, transmission channel, optical pulse, regeneration technique based on optical fiber, limits in the theoretical analyses and the highlights of our contribution in this field of research. Considering the SCG phenomenon, we have done a brief presentation, highlighting its physical description and other features raised during its achievement. We have also presented the paths of our contribution on the SCG analysis. The different waveguides studied in the thesis have been described.

2.1 Introduction

This chapter presents the different methods used to obtain the results of the thesis. We start in section 2.2 by the modeling of our systems that are described in general through the NLSE in silica fibers. In this section, we derive the considered NLSE from the Maxwell's equations of electromagnetism. In section 2.3, the analytical and numerical treatments of CDM technique are showed. In this section, we presents the analytical treatment of CDM, the diagram of the numerical algorithm or set-up schemes to applied CDM scheme and the SSFM. We describe in section 2.4 the analytical and numerical treatments of SCG while a conclusion is done in the last section of the chapter.

2.2 Propagation modeling: the NLSE

Beyond the experimental study, the theoretical one consists to model rather analytically this pulse propagation by a fundamental equation which simulates the dynamics within an optical waveguide. This fundamental equation well-known and widely used in different forms according to the study, is the NLSE. It has been earlier derived by A. Hasegawa and F. Tappert [118] for optical fibers, from

the Maxwell's equations of electromagnetism [2, 8]:

$$\nabla \cdot \mathbf{E} = 0 \quad (2.1)$$

$$\nabla \wedge \mathbf{E} = -\frac{\partial \mathbf{B}}{\partial t} \quad (2.2)$$

$$\nabla \cdot \mathbf{B} = 0 \quad (2.3)$$

$$\nabla \wedge \mathbf{B} = \frac{1}{c^2} \frac{\partial \mathbf{E}}{\partial t} + \mu_0 \frac{\partial \mathbf{P}}{\partial t} \quad (2.4)$$

where \mathbf{E} , \mathbf{B} , ε_0 , c , μ_0 and \mathbf{P} are the electric field vector, the magnetic flux density vector, the vacuum electric permittivity, the speed of light in the vacuum, the vacuum magnetic permeability and the induced electric polarization, respectively with $\varepsilon_0 \mu_0 c^2 = 1$. In this form, these equations belong to the specific case where one applies the following physical assumptions:

✦ in a medium as the silica which constitutes essentially the optical fibers, there is no free charges, so the electric charge density ρ_f and the current density vector \mathbf{J} are equal to zero.

✦ This medium is nonmagnetic, therefore the induced magnetic polarization \mathbf{M} is null.

The medium of optical fibers allows to use the relation that relates \mathbf{P} and \mathbf{E} far from the resonances [92]. Combining Eq. (2.2) and Eq. (2.4) and eliminating \mathbf{B} in favor of \mathbf{E} and \mathbf{P} we obtain:

$$\nabla \wedge \nabla \wedge \mathbf{E} = -\left(\frac{1}{c^2} \frac{\partial^2 \mathbf{E}}{\partial t^2} + \mu_0 \frac{\partial^2 \mathbf{P}}{\partial t^2} \right) \quad (2.5)$$

The relation between \mathbf{P} and \mathbf{E} is nonlinear as written below [1]:

$$\begin{aligned} \mathbf{P}(\mathbf{r}, t) = & \varepsilon_0 \left(\int_{-\infty}^t \chi^{(1)}(t-t') \cdot \mathbf{E}(\mathbf{r}, t') dt' \right) + \\ & \varepsilon_0 \left(\int_{-\infty}^t dt_1 \int_{-\infty}^t dt_2 \times \chi^{(2)}(t-t_1, t-t_2) : \mathbf{E}(\mathbf{r}, t_1) \mathbf{E}(\mathbf{r}, t_2) \right) + \\ & \varepsilon_0 \left(\int_{-\infty}^t dt_1 \int_{-\infty}^t dt_2 \int_{-\infty}^t dt_3 \times \chi^{(3)}(t-t_1, t-t_2, t-t_3) : \mathbf{E}(\mathbf{r}, t_1) \mathbf{E}(\mathbf{r}, t_2) \mathbf{E}(\mathbf{r}, t_3) + \dots \right) \end{aligned} \quad (2.6)$$

where $\chi^{(k)}$ is the k -th order susceptibility. It is generally a tensor of rank $k+1$. The linear susceptibility $\chi^{(1)}$ representing the most important parameter of $\mathbf{P}(\mathbf{r}, t)$, acts in the system through the refractive index n and the attenuation coefficient α mentioned earlier. Since the silica of optical fibers is a symmetric molecule, the second-order susceptibility $\chi^{(2)}$ generally responsible for nonlinear effects as SHG and sum-frequency generation vanishes in this medium. The development of \mathbf{P} should go further beyond the third-order susceptibility $\chi^{(3)}$ (presence of the suspension points in Eq. (2.6)) for highly nonlinear media, however for convenience to reach the cubic NLSE we should stop the development until order three. Reaching this order is necessary for analysis of short (picosecond domain) and ultra-short pulses (femtosecond and sub-femtosecond domains) propagation including the most nonlinear effects in optical fibers. The tensorial products $\langle \cdot \rangle$, $\langle : \rangle$ and $\langle : : \rangle$ correspond to $\chi^{(1)}$, $\chi^{(2)}$ and $\chi^{(3)}$ related to the electric field components $\mathbf{E}(\mathbf{r}, t')$, $\mathbf{E}(\mathbf{r}, t_1) \mathbf{E}(\mathbf{r}, t_2)$ and $\mathbf{E}(\mathbf{r}, t_1) \mathbf{E}(\mathbf{r}, t_2) \mathbf{E}(\mathbf{r}, t_3)$, respectively. The medium response being assumed to be local, usually one should emit several hypotheses that permit to simplify the modeling :

✦ The nonlinear part of \mathbf{P} should be considered as a small perturbation,

✦ in a scalar analysis of the pulse propagation, the polarization state should be maintained regular along the fiber length,

✠ the light injected should be considered almost monochromatic : this assumption is satisfied for short and ultra-short pulses,

✠ the envelope of the electromagnetic field should vary slowly approximately : it is the well-known and famous slowly varying envelope approximation (SVEA) [92].

Let us use the following form of the electrical field $\mathbf{E}(\mathbf{r}, t)$ that models the dynamics into a glass fiber including all kinds of optical fibers :

$$\mathbf{E}(\mathbf{r}, t) = \frac{1}{2} [E(\mathbf{r}, t) \exp(-i\omega_0 t) + c \cdot c] \tilde{x} \quad (2.7)$$

where $E(\mathbf{r}, t)$, \tilde{x} and $c \cdot c$ represent the slowly varying function of time, the polarization unit vector and the complex conjugated part of \mathbf{E} . Similarly, one can also write the vector \mathbf{P} :

$$\mathbf{P}(\mathbf{r}, t) = \frac{1}{2} [P(\mathbf{r}, t) \exp(-i\omega_0 t) + c \cdot c] \tilde{x} \quad (2.8)$$

Taking into account Eqs. (2.6), (2.7) and (2.8), this vector can be re-expressed explicitly by the susceptibility coefficients as follows :

$$\begin{aligned} P(r, t) = & \varepsilon_0 \left(\int_{-\infty}^t \chi_{xx}^{(1)}(t-t') E(r, t') \exp[-i\omega_0(t-t')] dt' \right. \\ & \left. + \frac{3\varepsilon_0}{4} \chi_{xxxx}^{(3)} E(r, t) \int_{-\infty}^t R(t-t_1) E^*(\mathbf{r}, t_1) E(\mathbf{r}, t_1) dt_1 \right) \end{aligned} \quad (2.9)$$

where the intensity-dependent nonlinear effects associated to third-order susceptibility have been included using [92, 155]:

$$\chi^{(3)}(t-t_1, t-t_2, t-t_3) = \chi^{(3)} R(t-t_1) \delta(t_1-t_2) \delta(t_1-t_3), \quad (2.10)$$

with $R(t)$ being the nonlinear Raman response function normalized to one because it must be zero when $t_1 > t$ with respect to the causality. The subscripts <

$xx >$ for $\chi^{(1)}$ and $< xxx >$ for $\chi^{(3)}$ in Eq. (2.9), represent the single polarization following the $x - axis$ assuming that we focus only on the scalar case in which the modal birefringence (that includes the y-axis) has been neglected [1, 92]. For pulse width $T > 1ps$, one should make some approximations on Eq. (2.9) that eliminate the delayed Raman response and consider the medium to have instantaneous nonlinear response. Therefore, we distinguish the two cases:

1. *the local instantaneous medium*

the relation (2.9) becomes :

$$\mathbf{P}(\mathbf{r}, t) = \varepsilon_0 \left(\chi_{xx}^{(1)} + \frac{3}{4} \chi_{xxxx}^{(3)} |E(\mathbf{r}, t)|^2 \right) \mathbf{E}(\mathbf{r}, t). \quad (2.11)$$

Introducing Eq.(2.11) into Eq.(2.5) and taking the Fourier transform of the resulting equation leads to the following form well-known as the Helmholtz equation satisfied by the scalar field \tilde{E} :

$$\nabla^2 \tilde{E} + \left(\frac{\omega}{c} \right)^2 \left(1 + \tilde{\chi}_{xx}^{(1)} + \frac{3\varepsilon_0}{4} \chi_{xxxx}^{(3)} F \left[|E(\mathbf{r}, t)|^2 \right] \right) \tilde{E} = 0 \quad (2.12)$$

where $F[\]$ and \tilde{E} are the Fourier transform operator and the Fourier transform of E respectively. The operator $F[\]$ is defined as :

$$F[u(t)] = \tilde{u}(\omega) = \int_{-\infty}^{+\infty} u(t') \exp(i\omega t') dt', \quad (2.13)$$

If we set that $q(\omega) = 1 + \tilde{\chi}_{xx}^{(1)} + \frac{3\varepsilon_0}{4} \chi_{xxxx}^{(3)} F \left[|E(\mathbf{r}, t)|^2 \right]$ and introduce two parameters \tilde{n} , \tilde{a} as $q(\omega) = \left(\tilde{n} + \frac{i\tilde{a}c}{2\omega} \right)^2$, we normally arrive to the nonlinear-index coefficient n_2 and the *TPA* coefficient a_2 as :

$$n_2 = \frac{3}{8n} \text{Re}(\chi_{xxxx}^{(3)}), \alpha_2 = \frac{3\omega_0}{4nc} \text{Im}(\chi_{xxxx}^{(3)}). \quad (2.14)$$

To obtain Eq. (2.14), it is necessary to set that

$$\tilde{n} = n + n_2|E|^2, \tilde{\alpha} = \alpha + \alpha_2|E|^2.$$

The coefficient n is the linear index and α represents the linear loss parameter. Since $\chi_{xxxx}^{(3)}$ is complex, its real and imaginary parts are represented respectively by $\text{Re}(\chi_{xxxx}^{(3)})$ and $\text{Im}(\chi_{xxxx}^{(3)})$. As n_2 and α_2 link with $\chi_{xxxx}^{(3)}$, n and α are found to link with $\chi_{xx}^{(1)}$ as following :

$$n = 1 + \frac{1}{2} \text{Re}(\tilde{\chi}_{xx}^{(1)}), \alpha = \frac{\omega}{nc} \text{Im}(\tilde{\chi}_{xx}^{(1)}), \quad (2.15)$$

Generally, α_2 vanishes for silica that is why it is neglected in optical fibers. However, it is not the case for silicon waveguides and chalcogenide glasses. The Helmholtz equation above, can be satisfactorily solved by using the method of separation of variables in which we assume the solution of form :

$$\tilde{E}(\mathbf{r}, \omega - \omega_0) = F(x, y) \tilde{u}(z, \omega - \omega_0) \exp(i\beta_0 z), \quad (2.16)$$

where $\tilde{E}(\mathbf{r}, \omega - \omega_0)$, $F(x, y)$, $\tilde{u}(z, \omega - \omega_0)$, β_0 and z are the Fourier transform of the optical field (of an envelope pulse whose frequency components ω are defined around a central one ω_0), the transversal distribution function, the Fourier transform of the slowly varying amplitude function, the wave number, the axial variable which defines the propagation distance of the pulse within the waveguide.

Using Eq. (2.16) in Eq. (2.12) leads to the system :

$$\frac{\partial^2 F(x, y)}{\partial x^2} + \frac{\partial^2 F(x, y)}{\partial y^2} + \left[q(\omega) \left(\frac{\omega_0}{c} \right)^2 - \tilde{\beta}^2 \right] F(x, y) = 0 \quad (2.17)$$

$$2i\beta_0 \frac{\partial \tilde{u}}{\partial z} + (\tilde{\beta}^2 - \beta_0^2) \tilde{u} = 0 \quad (2.18)$$

The relation (2.17) is the eigenvalue equation of the optical waveguide modes which involves the transversal distribution of the field $F(x, y)$. Solving this equation by using for example the first-order perturbation theory [155, 156], leads to the definition of the modal field distribution [1, 92]. For optical fibers, there are two kinds of modes : EH_{mn} and HE_{mn} . These modes are similar to the transverse-electric (TE) and transverse-magnetic (TM) modes of planar waveguides such as SOI-waveguides for $m = 0$. The case of SMFs is described by the fundamental mode in which $m = 1$ and $n = 1$. It allows to approximate the function $F(x, y)$ by a Gaussian distribution form as $\sim \exp[-(x^2 + y^2)/\omega^2]$, where w is the width parameter defined in ref.[1, 92, 155, 156].

On the other hand, the dielectric constant $q(\omega)$ and the wave number $\tilde{\beta}$ could be nearly identified respectively by :

$$q(\omega) \approx n^2 + 2n\Delta n \quad (2.19)$$

and

$$\tilde{\beta}(\omega) \approx \beta(\omega) + \Delta\beta(\omega), \quad (2.20)$$

where the perturbations Δn and $\Delta\beta(\omega)$ are themselves defined respectively

as :

$$\Delta n = n_2|u|^2 + \frac{ic\tilde{\alpha}}{2\omega_0} \quad (2.21)$$

and

$$\Delta\beta(\omega) = \frac{\omega^2 n(\omega)}{c^2 \beta(\omega)} \frac{\int \int_{-\infty}^{+\infty} \Delta n |F(x, y)|^2 dx dy}{\int \int_{-\infty}^{+\infty} |F(x, y)|^2 dx dy} \quad (2.22)$$

Let us approximate the term $\tilde{\beta}^2 - \beta_0^2$ of Eq. (2.18) by $2\beta_0(\tilde{\beta} - \beta_0)$ and take the relation (2.20), we obtain the following modified form of Eq. (2.18):

$$i \frac{\partial \tilde{u}}{\partial z} + i(\beta(\omega) - \beta_0 + \Delta\beta_0)\tilde{u} = 0 \quad (2.23)$$

with $\Delta\beta_0$ being an approximation of $\Delta\beta(\omega)$ as its first term in a Taylor series. It is described as follows :

$$\Delta\beta \simeq \frac{\omega n_2}{c} \frac{\int \int_{-\infty}^{+\infty} |F(x, y)|^4 dx dy}{(\int \int_{-\infty}^{+\infty} |F(x, y)|^2 dx dy)^2} |u|^2 + i \frac{\tilde{\alpha}}{2}. \quad (2.24)$$

It is observed in Eq. (2.24) the CKN $\gamma(\omega_0)$ and the effective mode area A_{eff} parameters defined respectively as :

$$\gamma(\omega_0) = \frac{\omega_0 n_2}{c A_{eff}} \quad (2.25)$$

and

$$A_{eff} = \frac{(\int \int_{-\infty}^{+\infty} |F(x, y)|^2 dx dy)^2}{\int \int_{-\infty}^{+\infty} |F(x, y)|^4 dx dy} \quad (2.26)$$

The interaction between the electromagnetic field and the bound electrons of a dielectric leads generally to dependence on the optical frequency ω .

This property refers to the chromatic dispersion which manifests through

the frequency dependence of the refractive index $n(\omega)$. The CDP of an optical waveguide is usually approximated by expanding the mode-propagation constant $\beta(\omega)$ in a Taylor series around the pump frequency ω_0 as :

$$\beta(\omega) = n(\omega) \frac{\omega}{c} = \beta_0 + \sum_{k=1}^M \frac{(\omega - \omega_0)^k}{k!} \beta_k \quad (2.27)$$

where $\beta_k = (d^k \beta(\omega) / d\omega^k)_{\omega=\omega_0}$ is k^{th} order of the CDP. Physically, the orders 1, 2, 3, 4, ... represent the group velocity, the *GVD*, the *TOD*, the *FOD* Inserting Eqs. (2.24), (2.25), (2.26) and (2.27) in the reciprocal Fourier transform of Eq. (2.23) yields:

$$i \frac{\partial u}{\partial z} + \sum_{k=1}^M \frac{(i)^k \beta_k}{k!} \frac{\partial^k u}{\partial t^k} + \gamma(\omega_0) |u|^2 u + \frac{i\alpha}{2} u = 0, \quad (2.28)$$

where the term $\omega - \omega_0$ of Eq. (2.27) has been replaced in the time-domain by the differential operator $i(\partial/\partial t)$ [92]. The integer $M (\geq 2)$ represents the last order reached in the CDP of the optical waveguide. Equation (2.28) is the so-called NLSE of a local instantaneous medium. The nonlinear term associated to $\gamma(\omega_0)$ corresponds to the SPM or Kerr effect. It is a manifestation of intensity dependence of the refractive index in the nonlinear optical waveguide and generally it is responsible to the spectral broadening of optical pulses. When more than one pulse is launched within the optical waveguide as done in WDM systems, the dynamic is described by coupled equations whose the number corresponds to the number of launched pulses. In this specific case, each sub-NLSE of the system is described by a similar version of Eq. (2.28) with additional terms linked to the coupling between the propagating waves.

This nonlinear coupling through the CKN parameter is the so-called XPM effect. This phenomenon does not include an energy transfer between the interacting fields. Physically, XPM occurs because the effective refractive index seen by an optical pulse in a nonlinear optical waveguide depends not only on the intensity of this pulse but also on the intensity of other copropagating pulses. Making the transformation of the well-known retarded frame of time τ , assuming a reference frame moving with the pulse at $1/\beta_1$ as $\tau = t - \beta_1 z$, we obtain the following simplified form of Eq. (2.28):

$$i \frac{\partial u}{\partial z} + \sum_{k=2}^M \frac{(i)^k \beta_k}{k!} \frac{\partial^k u}{\partial \tau^k} + \gamma(\omega_0) |u|^2 u + \frac{i\alpha}{2} u = 0, \quad (2.29)$$

2. The local non-instantaneous medium

In this case, we use completely Eq. (2.9). It corresponds to the higher-order nonlinear systems since it includes the delayed response (stemming from the molecular vibrations : Raman effect) of the medium which must be added when ultra-short pulses are studied. Indeed in this specific case, the pulse spectra are wide $> 0.1\text{Thz}$ and it leads the Raman gain to increase the intensity of the low-frequency components of the propagating optical field through an energy transfer from the high-frequency components of the same pulse : it is the description of the intra-pulse Raman scattering (IPRS) phenomenon. Considering Eq. (2.10) with (2.9) leads to a modified form of Eq. (2.12) [1, 92, 157]:

$$\begin{aligned} \nabla^2 \tilde{E} + n^2(\omega) \frac{\omega_0^2}{c^2} \tilde{E} = & -i \frac{\omega_0}{c} - \chi_{xxxx}^3 \frac{\omega_0^2}{c^2} \int_{-\infty}^{\infty} \int_{-\infty}^{\infty} \tilde{R}(\omega_1 - \omega_2) \\ & \times \tilde{E}(\omega_1, z) \tilde{E}^*(\omega_2, z) \tilde{E}(\omega - \omega_1 + \omega_2, z) d\omega_1 d\omega_2 \end{aligned} \quad (2.30)$$

where \tilde{R} is the Fourier transform of $R(t)$. From Eq. (2.23) to (2.28) a similar process could be done in the actual case of (2.30). However a Taylor series expansion of $\gamma(\omega)$ as done for $\beta(\omega)$ in Eq. (2.30), should be included in the development (at least until to the first order of the expansion). The form of the obtained NLSE is well-known as the GNLSE [1, 92, 157, 158]:

$$i \frac{\partial u}{\partial z} + \sum_{k=2}^M \frac{(i)^k \beta_k}{k!} \frac{\partial^k u}{\partial \tau^k} + \gamma \left(1 + \frac{1}{\omega_0} \frac{\partial}{\partial \tau} \right) \times \left(u(z, \tau) \int_{-\infty}^{\tau} R(\tau - \tau') |u(z, \tau')|^2 \right) + \frac{i\alpha}{2} u = 0, \quad (2.31)$$

The term with ω_0 is associated to the self-steepening (SS) effect. The SS phenomenon stems from the intensity dependence of the group velocity and leads to an asymmetry in the SPM-broadened spectra of ultrashort pulses [1, 92]. It creates an optical shock which is similar to the development of an acoustic shock on the leading edge of a sound wave [159]. The integral and the function $R(t)$ correspond to the delayed Raman response (DRR) that includes the IPRS and the SRS. The scattering effects implicate that the optical fields transfer part of their energy to the nonlinear medium.

In silica fibers and more generally, $R(t) = (1 - f_R)\delta(t) + f_R h_R(t)$, where the first term governs the nearly instantaneous electronic response and $h_R(t)$ is the Raman response function [92, 141]. $h_{R(t)}$ is defined as [92, 129, 131, 137, 138]: $h_R(t) = (f_a + f_c)h_a(t) + f_b h_b(t)$ with $h_a(t) = (\tau_1^2 + \tau_2^2)/(\tau_1 \tau_2) \exp(-t/\tau_2) \sin(t/\tau_1)$ and $h_b(t) = (2\tau_3 - t)/(\tau_3^2) \exp(-t/\tau_3)$. The values of the coefficients are given as $f_a = 0.75$, $f_b = 0.21$ and $f_c = 0.04$ that quantify the relative contributions of the isotropic and the anisotropic parts of the Raman response. Considering

the characteristic times τ_1 , τ_2 and τ_3 , their values are generally taken as 12, 32, and 96 fs, respectively [132-135]. The Raman scattering includes optical phonons in the interaction between the propagating field and the nonlinear medium. In a quantum-mechanical view, the photon of the optical field is annihilated to create a photon at a lower frequency (the Stokes component), a photon at a longer frequency (the ASC) and a phonon allowing the conservation of the energy and the momentum. Beyond the energy transfer between the optical field and the medium, their impact depends on their nature. For instance talking about the IPRS, one observes a large temporal shift of the pulse position and a RIFS in the pulse spectrum toward the longer wavelengths [1, 92]. On the other hand, the SRS exhibiting a threshold-like behavior, can transfer energy from one channel to the neighboring channels in a multichannel lightwave system like multiplexing systems. So it is an issue for these systems while in other cases it can be useful. For example allowing the fabrication of broadband Raman amplifiers and tunable Raman lasers. On the other hand, for some fibers materials as chalcogenide or some liquidcore filled fibers the CKN coefficient exhibits a nonlinear saturation as $\gamma = \gamma_0(1 + I|u|^2)$ with $I = 1/P_s$. The saturation power P_s is the threshold power at which the CKN starts to saturate. An approximation of this CKN leads generally to the so-called cubic-quintic NLSE and then septic, neptic ... according to the degree of this approximation.

Both of these two cases (local instantaneous and non-instantaneous cases) are those which interest our study in the thesis. We do not investigate the nonlocal NLSE widely used in the case of spatial beams of planar waveguides

or waveguides lattices [92].

2.3 Analytical and numerical treatments of the CDM

2.3.1 Analytical treatment of CDM

Linear propagation of truncated Airy pulses

Here, the optical system is designed by a segmented line of several pieces of equal length connected to each other by links including chirping components. Each piece of fiber is a SMF that can be modeled analytically by the cubic normalized dimensionless linear Schrodinger equation (CNDLSE):

$$i\frac{\partial U}{\partial \xi} - \frac{s}{2}\frac{\partial^2 U}{\partial \tau^2} = 0, \quad (2.32)$$

where the dimensionless quantities U , ξ , τ , s are the slowly varying amplitude of the envelope of the electrical field, the propagation distance, the retarded frame of time, the GVD sign respectively. The GVD sign s denotes normal ($s = 1$) and anomalous ($s = -1$) normalized dispersion regime as $s = \beta_2/|\beta_2| = \pm 1$ with β_2 being the physical GVD coefficient. The input profile of the normalized FEAP is given by $U(0, \tau) = A_i(\tau)\exp(a\tau)$ [27, 28, 51]. with $A_i(\tau)$ and a being the Airy function and the truncation coefficient, respectively. The truncation coefficient or decay factor a ($0 < a < 1$) is a quantity to ensure containment of the infinite Airy tail and can thus enable the physical realization of such pulses[51]. In this work, the value of a is 0.05. In practice, an Airy pulse can be produced by adding a cubic phase to a Gaussian spectrum [31]. The chirping process applied on the pulse is modeled analytically by adding to the profile the term " $\exp(-iC\tau^2/2)$ "

with C being the chirp parameter [26, 27, 51, 92]. So, the input profile becomes $U(0, \tau) = A_i(\tau) \exp(a\tau) \exp(-iC\tau^2/2)$. Our analysis is conducted through both the linear and the nonlinear regimes of propagation. In the whole work, the discussion is focused on the product $s \times C$ which is relevant in the development of the CDM technique. Indeed, the propagation depends on the sign of this product highlighting the GVD sign s and the chirp C . Thus, the CDM technique includes periodic fiber sections with alternation of an interaction between the GVD (s) and the chirp (C) in each piece of fiber.

Equation 2.32 is readily solved by use of the Fourier-transform method. The general solution of this equation is giving by:

$$U(\xi, \tau) = \frac{1}{2\pi} \int_{-\infty}^{+\infty} \tilde{U}(0, \omega) \exp\left(i\frac{s\omega^2\xi}{2}\right) \exp(-i\omega\tau) d\omega, \quad (2.33)$$

where $\tilde{U}(0, \omega)$ is the Fourier transform of the incident field at $\xi = 0$ and is obtained by using

$$\tilde{U}(0, \omega) = \int_{-\infty}^{+\infty} U(0, \tau) \exp(i\omega\tau) d\tau.$$

For the chirped Airy pulse $U(\xi = 0, \tau) = A_i(\tau) \exp(a\tau) \exp(-iC\tau^2/2)$, its Fourier spectrum is given by:

$$\begin{aligned} \tilde{U}(0, \omega) = & \sqrt{\frac{2\pi}{iC}} A_i \left(\frac{\omega + ia}{C} - \frac{1}{4C^2} \right) \exp \left[\frac{a}{2C^2} (2C\omega - 1) \right] \\ & \times \exp \left[-i \left(\frac{\omega^2}{2C} + \frac{\omega}{2C^2} - \frac{1}{12C^3} - \frac{a^2}{2C} \right) \right] \end{aligned} \quad (2.34)$$

Equation 2.34 shows the Fourier spectrum of chirped Airy pulse exhibits Airy distribution as well. For the linear propagation at $\xi \neq 0$, the single FEAP

(SFEAP) within the optical system gets the following analytical expression obtained similarly to that of ref. [27] but re-adapted for our situation:

$$|U(\xi, \tau)| = \left| \frac{1}{\sqrt{\theta}} A_i \left(\frac{\tau}{\theta} - \frac{\xi^2}{4\theta^2} + i \frac{a\xi s}{\theta} \right) \times \exp \left(\frac{a\tau}{\theta} - \frac{a\xi^2}{2\theta^2} \right) \right|, \quad (2.35)$$

with $\theta = 1 - sC\xi$. We remind once again here that the regeneration done in this work, is a forced regeneration. It means that Eq. 2.35 just describes the evolution of the pulse over one piece of fiber. At the end of this piece, we forced the signal to undergo other propagation conditions within the next piece. Thus, even if the signal depletes in one piece, it will be regenerated reversely in the next piece.

Furthermore, considering the linear propagation of the SFEAPs within our optical system at ξ , we take the symmetric Airy pulses with an initial chirp is taken into consideration:

$$U(\xi = 0, \tau) = [\Phi(\tau_B - \tau) + \Phi(\tau_B + \tau)] \exp \left(-i \frac{C\tau^2}{2} \right), \quad (2.36)$$

where $\Phi(\xi = 0, \tau) = A_i(\tau) \exp(a\tau)$ represents finite energy Airy pulse[29]. a is the truncated coefficient, $\tau_B > 0$ defines the normalized temporal relative positions of the dominant peaks of the SFEAPs and C represents the initial chirps.

Substituting Eq. 2.36 into Eq. 2.33, the evolution of symmetric Airy pulses can be approximately described by:

$$\begin{aligned} |U(\xi, \tau)| = & \left| \frac{1}{\sqrt{\theta}} A_i \left(\frac{\tau_B + \tau - sC\tau_B\xi}{\theta} - \frac{\xi^2}{4\theta^2} + i s \frac{a\xi}{\theta} \right) \right. \\ & \times \exp \left[\frac{a(\tau_B + \tau - sC\tau_B\xi)}{\theta} - \frac{a\xi^2}{2\theta^2} \right] + \frac{1}{\sqrt{\theta}} A_i \left(\frac{\tau_B - \tau - sC\tau_B\xi}{\theta} - \frac{\xi^2}{4\theta^2} + i s \frac{a\xi}{\theta} \right) \\ & \left. \times \exp \left[\frac{a(\tau_B - \tau - sC\tau_B\xi)}{\theta} - \frac{a\xi^2}{2\theta^2} \right] \right|. \end{aligned} \quad (2.37)$$

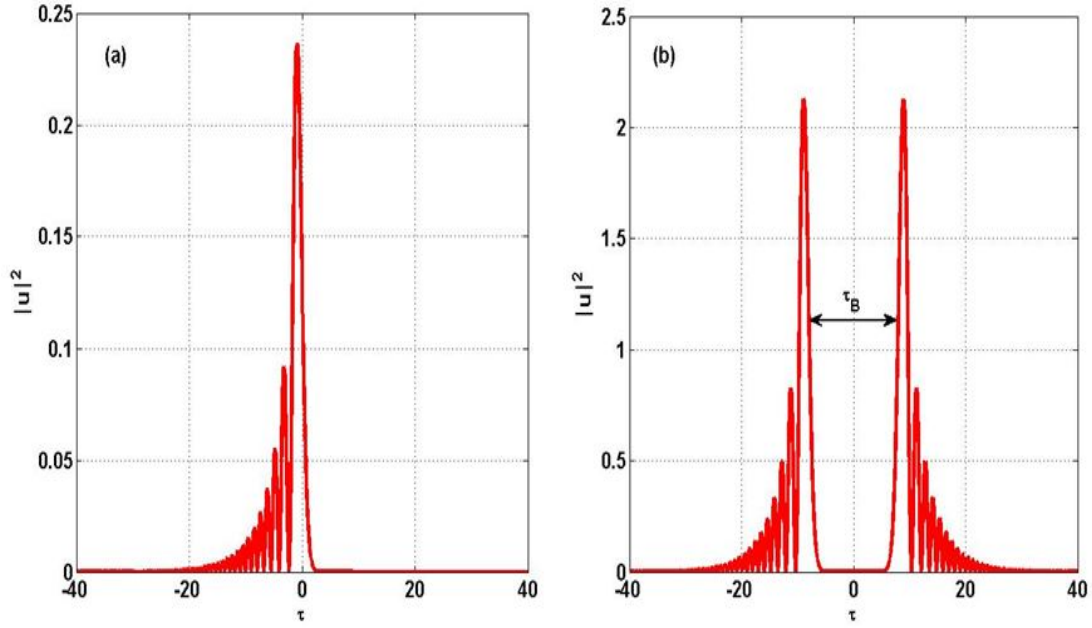


Figure 2.1: Plot asymmetric (a) and symmetric (b) Airy pulse. $\tau_B = 8$, $P_0 = 9$, $|C|=0.5$.

As expected the resulting amplitude distribution is the result of the interference of the two waves. In nonlinear regime, the analysis conducted through numerical simulations using the well-known split-step Fourier method (SSFM)[1, 16, 29, 92].

Nonlinear propagation of truncated Airy pulses

In this subsection, we study the nonlinear dynamic of chirped Airy pulses in fiber links. The equation reflecting this dynamic is given by the nonlinear Schrodinger equation (NLSE).

$$i \frac{\partial U}{\partial \xi} - \frac{s}{2} \frac{\partial^2 U}{\partial \tau^2} + N^2 |U|^2 U = 0, \quad (2.38)$$

Here the parameter $N = \sqrt{\gamma \tau_0^2 P_0 / |\beta_2|}$, represents the strength of the Kerr nonlinearity, where P_0 and γ are the input peak and de nonlinear coefficient respectively. It must be pointed out that, for Airy pulse with multipeak structure, the width of the main lobe of Airy pulse τ_0 is usually used as a temporal scale[16].

In this case, the analysis is conducted through numerical simulations using the well-known SSFM [1, 16, 29, 92]. In the next subsection, we show three diagrams of models describing the numerical algorithms and the expected experimental set-up schemes of the studied system.

2.3.2 Diagrams of the numerical algorithms/set-up schemes

The following diagrams are given in order to give to the reader a suitable comprehension of the algorithms used in our numerical simulations. Furthermore, these diagrams also suggest ideas for achieving experimental set-up for the considered algorithms. Thus, the related description indicates basically how the experimental process could be conducted.

✠ *First model: Fixed chirp and alternation of GVD only*

For instance, we have the following diagram : first avoid, the pulse is generated from a laser source and passes through a pulse-shaper that forms a Gaussian profile on which is applied a cubic phase to produce a FEAP [9, 31].

Then, the FEAP passes through a chirping device to chirp the signal with a value of C . Once it is chirped, the signal is injected within the first piece f_1 of fiber having a sign of the GVD s_1 . At the end of this piece, one alternates the sign of the GVD $s_2 = -s_1$ by splicing f_1 to a second piece of fiber f_2 (with s_2 as GVD). Thus, the output signal U_1 from f_1 is injected within f_2 . At the end of this piece, one alternates once again the sign of the GVD $s_3 = -s_2 = s_1$ by splicing f_2 to a third piece of fiber f_3 (with $s_3 = s_1$ as GVD).

Thus, the output signal U_2 from f_2 is injected within f_3 and so on for the next sections or pieces of the fiber line realizing so an optical system with fiber links

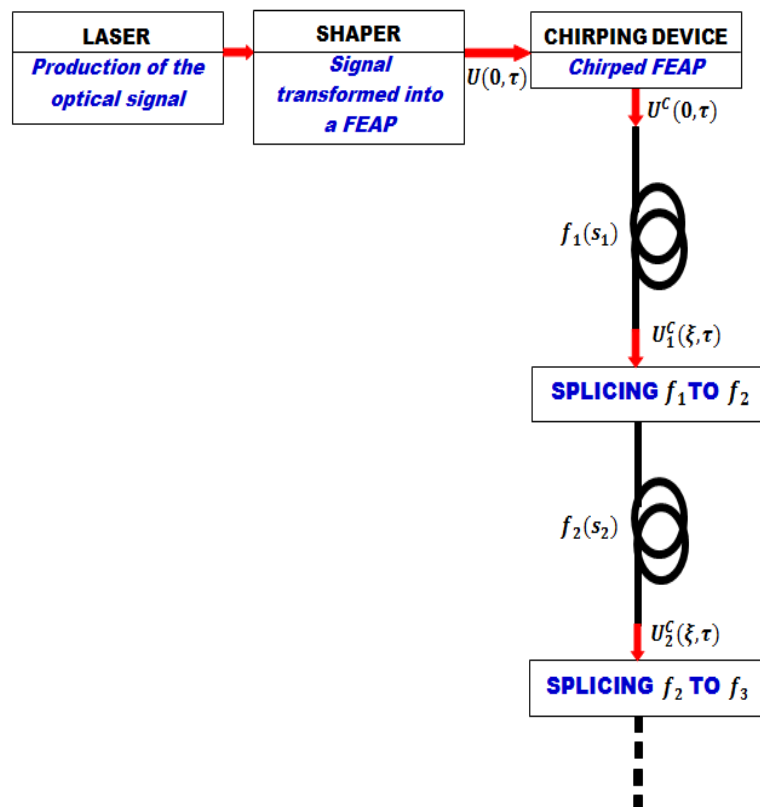


Figure 2.2: Diagram of the numerical algorithm or the set-up scheme for the first case : constant initial chirp with alternation of the GVD by piece of fiber.

that can be similar to that of ref. [25] in which the TOD replaces the chirp C .

✠ *Second model: Fixed GVD and alternation of chirp*

To draw this case, we have for instance the second diagram in Fig. 2.3 below: the scheme consists to a pulse that is generated from a laser source and shaped after within a pulse-shaper into the FEAP profile $U(0, \tau)$. Then, the chirp is added on

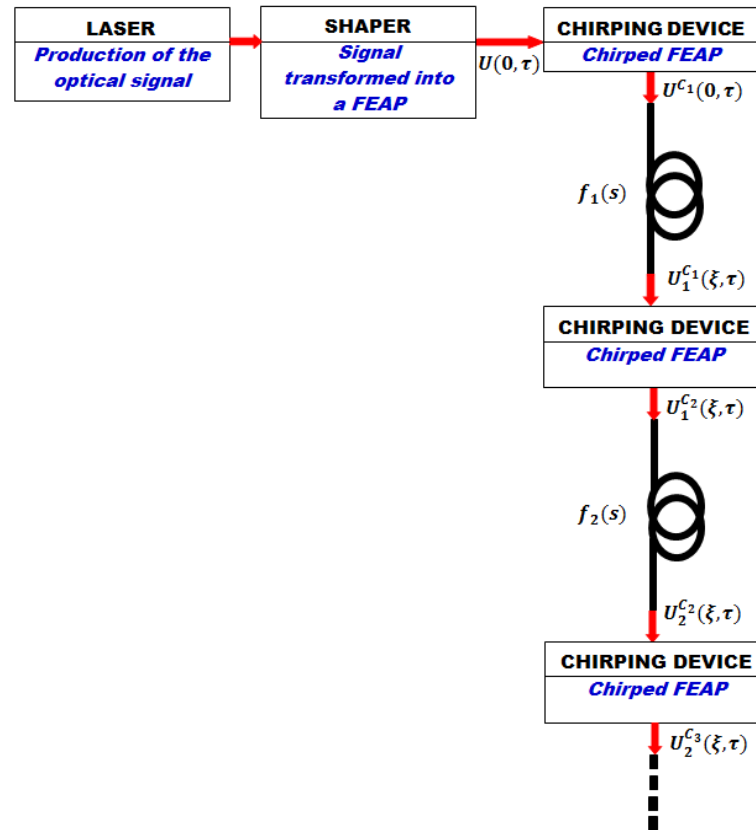


Figure 2.3: Diagram of the numerical algorithm or the set-up scheme for the second case : constant GVD sign with alternation of the initial chirp by piece of fiber.

the input field with an initial value C_1 leading to an input chirped pulse $U^{C_1}(0, \tau)$. Once it is obtained, this input chirped pulse is injected into the first section of fiber line (f_1) under a GVD sign s . After a second chirping (C_2), the propagating field $U_1^{C_1}(\xi, \tau)$ interacts with the same sign of GVD (s) within (f_2) becoming so an output field $U_2^{C_2}(\xi, \tau)$ ready to be injected into the next section of fiber line

(f_3) and so on. The characteristic of this system falls on the invariance of GVD sign interacting with the alternation of the chirp by fiber sections. Experimentally, it could be achieved by just putting a chirping device between each section of the fiber line and replacing the same SMF after, periodically.

✠ *Third model: Alternation of both the GVD and the chirp ($s \times C < 0$ or $s \times C > 0$)*

For this model, we force the system to produce a combination $s \times C < 0$ or $s \times C > 0$ on each section of the fiber line however, by alternating the signs of these parameters.

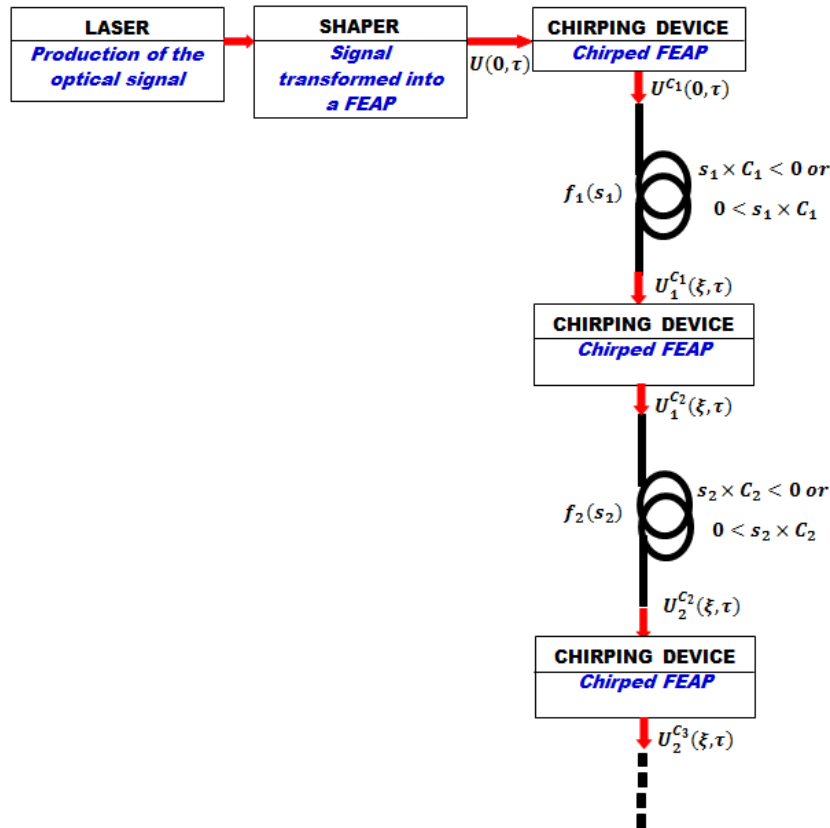


Figure 2.4: Diagram of the numerical algorithm or the set-up scheme for the third case : both the GVD and the chirp signs are alternated by piece of fiber in order to have whether $s \times C < 0$ or $s \times C > 0$.

It is therefore, a combination of both the two previous models into one. Thus,

we obtain the figure 2.4 showing the related diagram. The chirping device is added at the end of each different section of fiber line which is also alternated in order to change both the chirp and the GVD but under the condition of having whether $s \times C < 0$ or $s \times C > 0$. Therefore for instance, within the first piece f_1 we have s_1 and C_1 , concerning the second piece f_2 , one gets $s_2 = -s_1$ and $C_2 = -C_1$, while through the third one it yields $s_3 = -s_2 = s_1$ and $C_3 = -C_2 = C_1$, for the i^{th} piece of fiber f_i it gives $s_i = -s_{i-1}$ and $C_i = -C_{i-1}$ and so on.

The whole suggested diagrams above, describe what we call in this work the CDM technique for the regeneration of the FEAP in fiber optics links. In order to conduct this study numerically, we choose to employ the well-known numerical method such as the SSFM with specific modifications within the MATLAB numerical code that include the related changes for each piece of the fiber line.

2.3.3 Numerical treatments of CDM technique

To understand the philosophy behind the split-step Fourier method, it is useful to write Eq. 2.38 formally in the form

$$\frac{\partial U}{\partial \xi} = [\widehat{D} + \widehat{N}] U, \quad (2.39)$$

where \widehat{D} is a differential operator that accounts for dispersion within a linear medium and \widehat{N} is a nonlinear operator that governs the effect of fiber-optics link nonlinearities on pulse propagation. These operators are given by:

$$\widehat{D} = \frac{-is}{2} \frac{\partial^2}{\partial \tau^2} \quad (2.40)$$

$$\widehat{N} = iN^2|U|^2. \quad (2.41)$$

In general, dispersion and nonlinearity act together along the length of the fiber. The SSFM obtains an approximate solution by assuming that in propagating the optical field over a small distance h , the dispersive and nonlinear effects can be assumed to act independently. More specifically, propagation from ξ to $\xi + h$ is carried out in two steps. In the first step, the nonlinearity acts alone, and $\widehat{D} = 0$ in Eq. 2.38. In the second step, dispersion acts alone, and $\widehat{N} = 0$ in Eq. 2.38. Mathematically,

$$U(\xi + h, \tau) \approx \exp(h\widehat{D})\exp(h\widehat{N})U(\xi, \tau). \quad (2.42)$$

The exponential operator $\exp(h\widehat{D})$ can be evaluated in the Fourier domain using the prescription

$$\exp(h\widehat{D})H(\xi, \tau) = F_T^{-1}\exp[h\widehat{D}(-i\omega)]F_TH(\xi, \tau), \quad (2.43)$$

where F_T denotes de Fourier-transform operator, $\widehat{D}(-i\omega)$ is obtained from Eq. 2.39 by replacing the operator $\partial/\partial\tau$ by $-i\omega$, and ω is the frequency in the Fourier domain. As $\widehat{D}(i\omega)$ is just a number in the Fourier space, the evaluation of Eq. 2.42 is straightforward. The use of the Fast FT (FFT) algorithm [1, 160] makes numerical evaluation of Eq. 2.42 relatively fast. It is for this reason that the SSFM can be faster by up to two orders of magnitude compared with most finite-difference schemes (FDS)[1, 161].

To estimate the accuracy of the SSFM, we note that a formally exact solution of Eq. 2.39 is given by

$$U(\xi + h, \tau) = \exp(h(\widehat{D} + \widehat{N}))U(\xi, \tau). \quad (2.44)$$

The accuracy of SSFM can be improved by adopting a different procedure to propagate the optical pulse over one segment from ξ to $\xi + h$. In this procedure

Eq. 2.42 is replaced by:

$$U(\xi + h, \tau) \approx \exp\left(\frac{h}{2}\widehat{D}\right) \exp\left(\int_{\xi}^{\xi+h} \widehat{N}(\xi')d\xi'\right) \exp\left(\frac{h}{2}\widehat{D}\right) U(\xi, \tau) \quad (2.45)$$

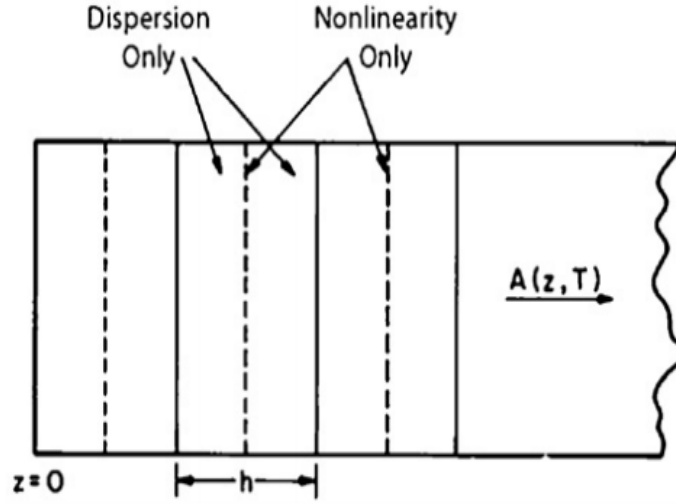


Figure 2.5: Schematic illustration of the symmetrized split-step Fourier method used de numerical simulations. Fiber-optics link is divided into a large number of segments of width h . Within a segment, the effect of nonlinearity is included at the midplane shown by a dashed line [1, 92].

The main difference is that the effect of nonlinearity is included in the middle of the segment rather than at the segment boundary. Because of the symmetric form of the exponential operators in Eq. 2.45, this scheme is known as the symmetrized SSFM [1,160-162]. The integral in the middle exponential is useful to include the ξ dependence of the nonlinear operator \widehat{N} . If the step size h is small enough, it can be approximated by $\exp(h\widehat{N})$, similar to Eq. 2.43.

The accuracy of the SSFM can be further improved by evaluating the integral in Eq. 2.43 more accurately than approximating it by $h\widehat{N}(\xi)$. A simple approach is to employ the trapezoidal rule and approximate the integral by[163]

$$\int_{\xi}^{\xi+h} \widehat{N}(\xi')d\xi' \approx \frac{h}{2}[\widehat{N}(\xi) + \widehat{N}(\xi + h)], \quad (2.46)$$

However, the implementation of Eq. 2.46 is not simple because $\widehat{N}(\xi + h)$ is unknown at the midsegment located at $\xi + \frac{h}{2}$. It is necessary to follow an iterative procedure that is initiated by replacing $h\widehat{N}(\xi + h)$ by $h\widehat{N}(\xi)$. Eq. 2.45 is then used to estimate $U(\xi + h, \tau)$ which in turn is used to calculate the new value of $\widehat{N}(\xi + h)$. Although the iteration procedure is time-consuming, it can still reduce the overall computing time if the step size h can be increased because of the improved accuracy of the numerical algorithm. Two iterations are generally enough in practice.

The implementation of the split-step Fourier method is relatively straightforward. As shown in this Figure, the fiber length is divided into a large number of segments that need not be spaced equally. The optical pulse is propagated from segment to segment using the prescription of Eq. 2.45. More specifically, the optical field $U(\xi, \tau)$ is first propagated for a distance $\frac{h}{2}$ with dispersion only using the FFT algorithm and Eq. 2.43. At the midplane $\xi + \frac{h}{2}$, the field is multiplied by a nonlinear term that represents the effect of nonlinearity over the whole segment length h . Finally, the field is propagated for the remaining distance $\frac{h}{2}$ with dispersion only to obtain $U(\xi + h, \tau)$. In effect, the nonlinearity is assumed to be lumped at the midplane of each segment (dashed lines in Figure ??).

In practice, the SSFM can be made to run faster by noting that the application of Eq. 2.45, over M successive steps results in the following expression:

$$U(L, \tau) \approx e^{-\frac{h}{2}\widehat{D}} \left(\prod_{m=1}^M e^{h\widehat{D}} e^{h\widehat{N}} \right) e^{\frac{h}{2}\widehat{D}} U(0, \tau), \quad (2.47)$$

where $L = Mh$ is the total fiber-links length and the integral in Eq.2.46 was approximated with $h\widehat{N}$. Thus, except for the first and last dispersive steps, all

intermediate steps can be carried over the whole segment length h . This feature reduces the required number of FFTs roughly by a factor of 2 and speeds up the numerical code by the same factor.

The SSFM has been applied to a wide variety of optical problems including wave propagation in atmosphere[164], graded-index fibers[165], semi-conductor lasers[166], unstable resonators[167], and waveguide couplers[168]. It is referred to as the beam-propagation method when applied to the propagation of CW optical beams in nonlinear media when dispersion is replaced by diffraction [165-169]. For the specific case of pulse propagation in optical fibers, the SSFM was first applied in 1973 [118]. Since then, this method has been used extensively for studying various nonlinear effects in optical fibers [170], mainly because of its fast execution compared with most finite-difference schemes [171]. Although the method is relatively straightforward to implement, it requires that step sizes in ξ and τ be selected carefully to maintain the required accuracy [172]. The optimum choice of step sizes depends on the complexity of the problem, and a few guidelines are available [173-176]. The use of FFT imposes periodic boundary conditions whenever the split-step Fourier method is employed. This is acceptable in practice if the temporal window used for simulations is made much wider than the pulse width. Typically, the window size is chosen to be 10-20 times the pulse width. In some problems, a part of the pulse energy may spread so rapidly that it may be difficult to prevent it from hitting the window boundary. This can lead to numerical instabilities as the energy reaching one edge of the window automatically re-enters from the other edge. It is common to use an "*absorbing window*" in which the radiation reaching window edges is artificially absorbed even though

such an implementation does not preserve the pulse energy. In general, the SSFM is a powerful tool provided care is taken to ensure that it is used properly. Several generalizations of this method have been developed that retain the basic idea behind the split-step technique but employ an expansion other than the Fourier series; examples include splines and wavelets[177].

2.4 Analytical and numerical treatments of SCG

2.4.1 Analytical modeling and data conditions

The analytical modeling of non-ideal chalcogenide glasses should normally include NPA processes [178]. Normally, such highly nonlinear materials are analytically modeled with a saturable nonlinearity, which is often approximated by the cubic-quintic form. Indeed, the considered approximation consists into a combination of self-focusing cubic and self-defocusing quintic terms, which correspond respectively to real parts of the cubic ($\chi^{(3)}$) and quintic ($\chi^{(5)}$) susceptibilities [178]. In addition, imaginary parts of $\chi^{(3)}$ and $\chi^{(5)}$ represent the TPA and 3PA effects, respectively [1, 178]. For our AsSe₂/As₂S₅-ChRW structure contrarily to ref. [40], we set the hypothesis of its high nonlinearity leading the waveguide to be modeled by a cubic-quintic NLSE (CQNLSE) whose CDP values are defined in the table II of ref. [38, 40]. This CQNLSE includes the Kerr nonlinearity or self-phase modulation (SPM), the self-steepening (SS : optical shock), the SRS and nonlinear photon absorption (NPA) effect both for the cubic and the quintic orders as [28, 179]:

$$\begin{aligned}
& i \frac{\partial U(z, t)}{\partial z} + \sum_{k=2}^{k=10} \frac{i^k \beta_k \partial^k U(z, t)}{\partial t^k} = -i \frac{\alpha}{2} U(z, t) \\
& -\gamma_1 \left(1 + \delta_1 \frac{\partial}{\partial t} \right) \left[U(z, t) \int_{-\infty}^{+\infty} R(t') |U(z, t - t')|^2 dt' \right] \\
& -\gamma_2 \left(1 + \delta_2 \frac{\partial}{\partial t} \right) \left[U(z, t) \int_{-\infty}^{+\infty} R(t') |U(z, t - t')|^4 dt' \right],
\end{aligned} \tag{2.48}$$

where $U(z, t)$, z , t , β_k , α , γ_1 , δ_1 , and $R(t')$ are respectively the electrical field amplitude, the distance of propagation, the retarded frame of time, the CDP coefficient of k^{-th} order, the linear loss, the parameter of cubic nonlinearity that includes the CKN and the TPA effect, cubic SS (CSS), and the Raman response function [32]. In addition, the parameters γ_2 , δ_2 account respectively for the quintic nonlinearity (that includes the QKN and the 3PA effect) and the quintic SS (QSS). While all the parameters are defined as in ref. [38], we have exceptionally γ_1 , δ_1 , γ_2 , and δ_2 which are defined as follows [28]:

$$\begin{aligned}
\gamma_1 &= \gamma + i \frac{\alpha_2}{2A_{eff}} \\
\delta_1 &= -\frac{i}{\omega_0} \\
\gamma_2 &= \pm \frac{\gamma_1}{P_0} \\
\delta_2 &= \delta_1,
\end{aligned} \tag{2.49}$$

where the TPA value of the combined material $\text{AsSe}_2/\text{As}_2\text{S}_5$ is given by $\alpha_2 = 2.5 \times 10^{-12} \text{W}^{-1} \cdot \text{m}$ [38, 40]. The CKN coefficient is defined as [39]:

$$\gamma = \frac{n_2 \omega_0}{c A_{eff}}, \tag{2.50}$$

with $n_2 = 1.1 \times 10^{-17} \text{W}^{-1} \text{m}^2$ and c being the nonlinear refractive index and

the speed of light in the vacuum respectively. The nonlinear coefficient is evaluated $\gamma = 1.76W^{-1}.m^{-1}$ and the effective mode area $A_{eff} = 9.92\mu m^2$. The function $R(t)$ is the Raman response usually modeled as [39, 92, 121, 180] by

$$R(t) = (1 - f_R)\delta(t) + f_R h_R(t), \quad (2.51)$$

where $f_R = 0.148$ [39], $\delta(t)$ and $h_R(t)$ are the fractional contribution of the delayed Raman response to the nonlinear polarization, the Dirac function and the Raman response function responsible for the Raman gain, respectively. This last function is described as:

$$h_R(t) = \frac{\tau_1^2 + \tau_2^2}{\tau_1\tau_2} \exp\left(-\frac{t}{\tau_2}\right) \sin\left(\frac{t}{\tau_1}\right) \quad (2.52)$$

with $\tau_1 = 15.34fs$ and $\tau_2 = 106.1fs$ [40, 180], corresponding, respectively, to the inverse of the phonon oscillation frequency and the bandwidth of the Raman gain spectrum. The pumping is done at $\lambda_0 = 4\mu m$ with an unchirped input pulse having a FEAP profile. The peak power of the pulse P_0 is $10 kW$ in order to excite the high-order nonlinear terms. The timewidth is $t_0 = 50fs$ while the maximum distance of propagation through the considered waveguide is $L = 15cm$. The input profile is given as $U(z, t) = (P_0)^{1/2} Ai(t/t_0) \exp(at/t_0)$ [28] with $Ai(t/t_0)$ and a being the Airy function and the truncation coefficient, respectively. The truncation coefficient or decay factor a ($0 < a < 1$) is a quantity to ensure containment of the infinite Airy tail and can thus enable the physical realization of such pulses [8-13,15,22,182,183]. In practice, an Airy pulse can be produced by adding a cubic phase to a Gaussian spectrum [8, 31]. By using of the Fourier Transform (FT) of equation Eq. 2.48, we obtain:

$$\begin{aligned}
\frac{\partial \tilde{U}(z, \omega)}{\partial z} - \sum_{k=2}^{k=10} \frac{i^{2k+1} \beta_k}{k!} (\omega - \omega_0)^k \tilde{U}(z, \omega) = -\frac{\alpha}{2} \tilde{U}(z, \omega) + \\
i\gamma_1 F \left[\left(1 + \delta_1 \frac{\partial}{\partial t} \right) U(z, t) \int_{-\infty}^{+\infty} R(t') |U(z, t - t')|^2 dt' \right] \\
+ i\gamma_2 F \left[\left(1 + \delta_2 \frac{\partial}{\partial t} \right) U(z, t) \int_{-\infty}^{+\infty} R(t') |U(z, t - t')|^4 dt' \right],
\end{aligned} \tag{2.53}$$

where $\tilde{U}(z, \omega)$ represent the FT of the envelope $U(z, t)$. From the definition of the convolution integral, we can write:

$$\begin{aligned}
F \left[\left(1 + \delta_1 \frac{\partial}{\partial t} \right) U(z, t) \int_{-\infty}^{+\infty} R(t') |U(z, t - t')|^2 dt' \right] = \\
i\delta_1 \omega F \left(U(z, t) \int_{-\infty}^{+\infty} R(t') |U(z, t - t')|^2 dt' \right) \\
F \left[\left(1 + \delta_2 \frac{\partial}{\partial t} \right) U(z, t) \int_{-\infty}^{+\infty} R(t') |U(z, t - t')|^4 dt' \right] = \\
i\delta_2 \omega F \left(U(z, t) \int_{-\infty}^{+\infty} R(t') |U(z, t - t')|^4 dt' \right)
\end{aligned} \tag{2.54}$$

Eq. 2.53 becomes:

$$\begin{aligned}
\frac{\partial \tilde{U}(z, \omega)}{\partial z} - \sum_{k=2}^{k=10} \frac{i^{2k+1} \beta_k}{k!} (\omega - \omega_0)^k \tilde{U}(z, \omega) + \frac{\alpha}{2} \tilde{U}(z, \omega) = \\
-\gamma_1 \delta_1 \omega F \left[U(z, t) \int_{-\infty}^{+\infty} R(t') |U(z, t - t')|^2 dt' \right] \\
-\gamma_2 \delta_2 \omega F \left[U(z, t) \int_{-\infty}^{+\infty} R(t') |U(z, t - t')|^4 dt' \right].
\end{aligned} \tag{2.55}$$

We introduce the following change of function :

$$\tilde{U}'(z, \omega) = \tilde{U}(z, \omega) \exp[-\hat{L}(\omega)z], \tag{2.56}$$

with $\widehat{L}(\omega)$ being the linear operator, given by $\widehat{L}(\omega) = -\left(\frac{\alpha}{2}\right) + i\beta(\omega)$ and $\beta(\omega)$ is defined as:

$$\beta(\omega) = \sum_{k=2}^{k=10} \frac{(-1)^{k+1}}{k!} \beta_k (\omega - \omega_0)^k. \quad (2.57)$$

Replacing Eq. 2.56 and Eq. 2.57 into Eq. 2.55 leads to the form used in our simulations as follows:

$$\begin{aligned} \frac{\partial \widetilde{U}'(z, \omega)}{\partial z} = & -\gamma_1 \delta_1 \omega \exp[-\widehat{L}(\omega)] F \left[U(z, t) \int_{-\infty}^{+\infty} R(t') |U(z, t - t')|^2 dt' \right] \\ & -\gamma_2 \delta_2 \omega \exp[-\widehat{L}(\omega)] F \left[U(z, t) \int_{-\infty}^{+\infty} R(t') |U(z, t - t')|^4 dt' \right], \end{aligned} \quad (2.58)$$

. The CDP being an important part in the SCG, we have chosen to stop up to $M = 10$ (assuming that the orders beyond ten have a negligible influence on the results). For the numerical simulations, we modify the trial MATLAB code provided by J. C. Travers et al in [121] assuming Eq. 2.58 given above.

2.4.2 Description of the numerical code used and the simulation conditions

Our results were obtained using the MATLAB polyspace R20193.0 software run on a quad-core (Intel Pentium Gold G5500 CPU @3.80 GHz) computer. The numerical code used is the one kindly provided in [121, 136] by J. C. Travers, M. H. Frosz, and J. M. Dudley. We have modified the command lines according to the specificities of our work as follows:

Modifications within the M-file "gnlse.m"

We modify the argument of the M-file by introducing two parameters, *gamma1* for CKN and *gamma2* for QKN as (line 1):

```
function [Z, AT, AW, W] = gnlse(T, A, w0, gamma1, gamma2, betas, loss, ...
fr, RT, flength, nsaves)
```

In the code, we introduce the shock, we write:

```
gamma1 = gamma1/w0;
gamma2 = gamma2/w0;
```

Then, the modification of the function called $R = rhs(z, AW)$: yields:

```
function R = rhs(z, AW)
AT = fft(AW.*exp(L*z));
IT1 = abs(AT).^2;
IT2 = IT1.^2;
if (length(RT) == 1) || (abs(fr) < eps)
M1 = ifft(AT.*IT1);
M2 = ifft(AT.*IT2);
else
RS1 = dT*fr*fft(ifft(IT1).*RW);
RS2 = dT*fr*fft(ifft(IT2).*RW);
M1 = ifft(AT.*((1-fr).*IT1+RS1));
```

```

M2 = ifft(AT .* ((1 - fr) .* IT2 + RS2));
end

R1 = 1i * gamma1 * W .* M1 .* exp(-L * z);
R2 = 1i * gamma2 * W .* M2 .* exp(-L * z);
R = R1 + R2;
end

```

Modifications within the M-file "*code.m*"

For the parameters linked to the nonlinearity, we have:

```

CKN = 1.76;
a2 = 2.55e - 12;
Aeff = 9.92e - 12;
TPA = (0.5i * a2/Aeff);
gamma1 = CKN + TPA;
QKN = CKN/power;
ThPA = TPA/power;
gamma2 = s * (QKN + ThPA);

```

The call of the "*gnlse.m*" M-file is performed as follows:

```

[Z, AT, AW, W] = gnlse(T, A, w0, gamma1, gamma2, betas, loss, ... fr, RT,
flength, nsaves)

```

With all these modifications to the MATLAB code provided in [136], we obtain the results discussed in the next chapter.

2.5 Conclusion

At the end of this chapter, the different analytical and numerical models were presented. Considering the regeneration phenomenon, the FT has been described analytically assuming both the linear and the nonlinear cases of regeneration. Taking into account the SCG analyses, we have firstly investigated the system modeled by the CQNLSE and we have described its numerical algorithm scheme. We present in the last chapter of this thesis the numerical results obtained.

3.1 Introduction

This chapter presents the main results obtained in the thesis. The second section shows those of the linear regeneration of truncated Airy pulse in fiber-optics links obtained numerically through the CDM technique while section 3.3 concerns the nonlinear regeneration based on both the single and the symmetric FEAPs. In section 3.4, we highlight and discuss on the CDM technique applied on FEAPs and in section 3.5 MIR-SCG phenomenon of truncated Airy pulses in a cubic-quintic $AsSe_2/As_2S_5$ is investigated while a conclusion is done in the last section of the chapter.

3.2 On the linear CDM inducing regeneration of truncated Airy pulses in fiber-optics links

We start studying the linear optical system by setting $N = 0$.

3.2.1 Constant positive (respectively negative) initial chirp with alternation of the GVD

Here, we observe the periodic evolution of the FEAP showing the appearance of the FEAP regeneration. We notice that the choice of an initial combination concerning the GVD and chirp signs, is relevant for this regeneration. Indeed, the cases in which we start with the A.I. mechanism $s \times C < 0$ (see Fig.3.1(a.1) and Fig.3.1(a.2)), are similar to the figures 1(a) et 1(b) obtained by R. Driben and T. Meier [25], while the cases in which one starts with $s \times C > 0$ (see Fig. 3.1(b.1) and 3.1(b.2)), are more similar to the zero-TOD case of Ref. [25]. In Figs. 3.1(a.1) and 3.1(a.2), the FEAP regeneration is well developed and one obtains an A.I. mechanism within each piece of the system showing the relevance of this process in the regeneration. Starting with the positive product $s \times C > 0$, yields the worst result of [25] in which the GVD seems to act alone without the TOD. Furthermore as discussed in ref. [25], the most interesting cases fall on those in which the A.I. mechanism is observed periodically within the optical systems following each piece of fiber as seen in Figs. 3.1(a.1) and 3.1(a.2). It means that, in the CDM technique concerning the first model of Fig. 2.2, starting with the A.I mechanism condition $s \times C < 0$ is well indicated to perform the FEAP regeneration compared with the initial condition of $s \times C > 0$. A confirmation of this feature is raised when we compare the maximum intensity of the dominant peak in Figs. 3.1(a.2) and 3.1(b.2) versus ξ . Particularly in these 2D-plots, one sees that the maximum intensity $\max|U|^2$ of Fig. 3.1(a.2) belongs to the dimensionless interval [0.4;0.6] while the one of Fig. 3.1(b.2) belongs to [0.2;0.3]. Choosing to start with the A.I. mechanism $s \times C < 0$ (Figs. 3.1(a.1) and 3.1(a.2)) is definitely the best case.

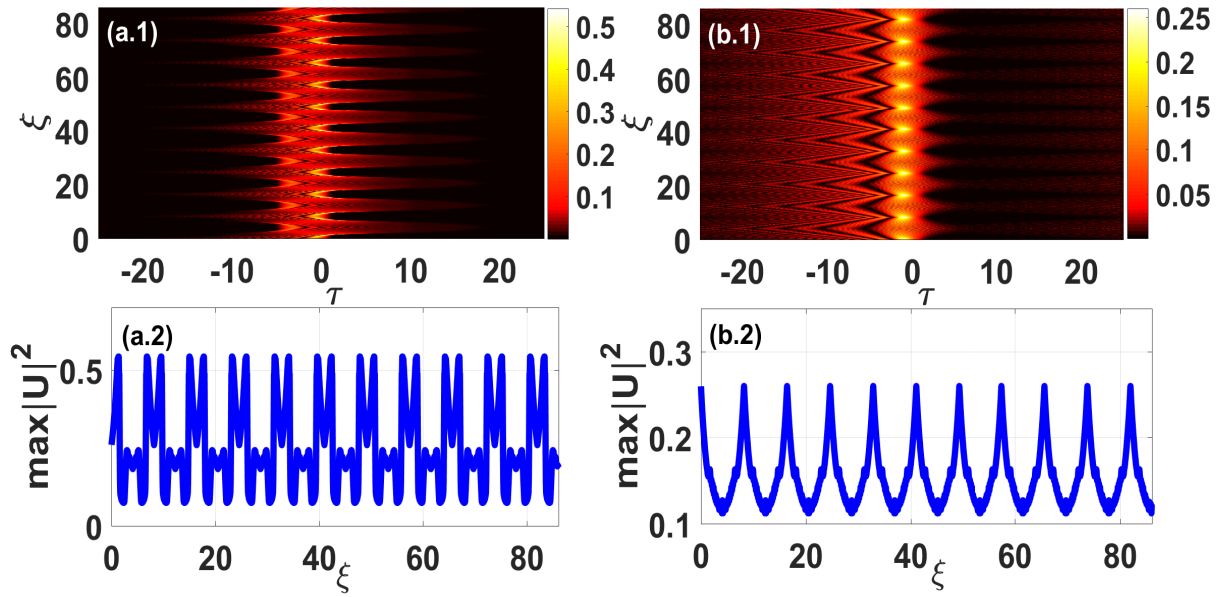


Figure 3.1: $|C| = 0.5$, $|s| = 1$ and $a = 0.05$; (a.1) and (b.1) for 3D-contour plots of the FEAP propagation within the fiber links in the first model of Fig. 2.2; (a.2) and (b.2) for 2D-plots of $\max|U|^2$ versus ξ ; The initial conditions are described as: (a.1) and (a.2) starting with the A.I. mechanism $s \times C < 0$; (b.1) and (b.2) starting with $s \times C > 0$.

3.2.2 Constant GVD (normal or anomalous dispersion) with alternation of chirp

We show here, the FEAP regeneration when we choose to fix the GVD regime through the system while the chirp is alternated as discussed in the second model of Fig. 2.3. The first observation is the poor quality or design of the FEAP regeneration. Indeed, the regeneration is noised and more irregular than in the first model of Fig. 3.1. It means that, in the CDM technique concerning the second model of Fig. 2.3, fixing the GVD such as using the same type of fiber while the chirping devices are implemented at the input of each fiber piece in the whole system C_1, C_2, C_3, \dots until the end of the fiber links, will have a deleterious effect on the regeneration design compared with the first model. This observation is confirmed in Figs. 3.2(a.2) and 3.2(b.2) with the maximum intensity $\max|U|^2$

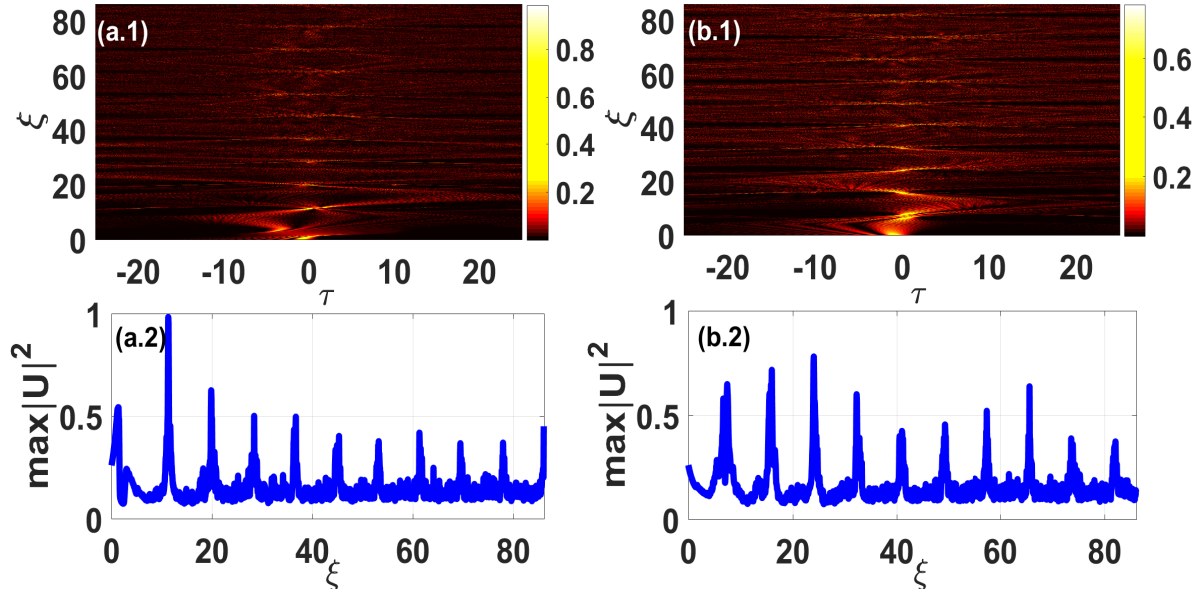


Figure 3.2: The conditions are the same as in Fig. 3.1 however this simulation corresponds to the second model of Fig. 2.3 : s is constant while C alternates. The initial condition : (a.1) and (a.2) for the A.I. mechanism $s \times C < 0$; (b.1) and (b.2) for $s \times C > 0$.

versus ξ . As shown in Fig. 3.2, whatever the initial conditions used, the evolution of the intensity of the dominant peak remains periodically noised suggesting that this option of regeneration is less interesting than the previous one.

3.2.3 Alternation of both the GVD and the initial chirp

In this case, we combine the two previous models into one by alternating the GVD and the initial chirp on each fiber piece as described in the third model of Fig. 2.4. We obtain this result. As depicted in this figure, the FEAP regeneration is completely destroyed. This feature is more pronounced in the case having the initial condition $s \times C > 0$ (see Figs. 3.3(b.1) and 3.3(b.2)) compared with the case starting with the A.I. mechanism $s \times C < 0$ (see Figs. 3.3(a.1) and 3.3(a.2)). The successive alternation of the two parameters in each piece of the system is certainly the main cause of this pulse regeneration destruction.

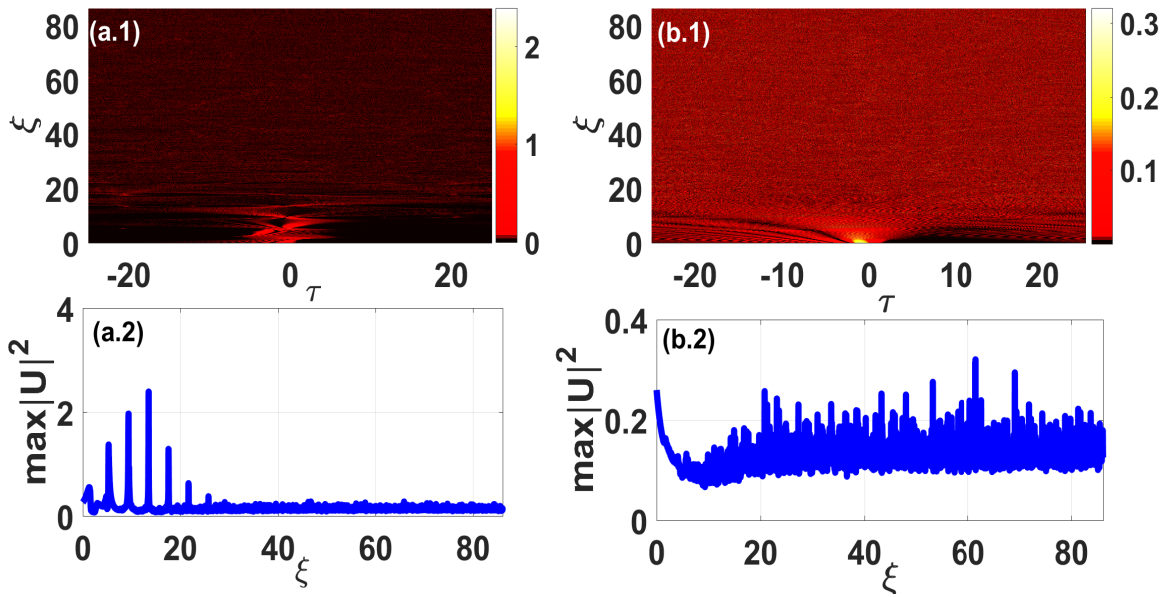


Figure 3.3: The conditions are the same as in Fig. 3.1 however this simulation corresponds to the third model of Fig. 2.4 : both s and C alternate. The initial condition : (a.1) and (a.2) for the A.I. mechanism $s \times C < 0$; (b.1) and (b.2) for $s \times C > 0$.

At the end of this numerical analysis of the three mentioned models of Figs. 2.2, 2.3 and 2.4 with their corresponding regenerations in Figs. 3.1-3.3, we can conclude that the best model to conduct the achievement of the FEAP regeneration in fiber links based on the CDM technique, consists to the case in which the initial chirp is maintained constant with a periodical alternation of the GVD regime while the initial condition should be the achievement of the A.I. mechanism with $s \times C < 0$ giving nearly a similar result to that of ref. [25]. Using this configuration, we proceed to the study of chirp influence on the regeneration in the next subsection.

3.2.4 Effect of the initial chirp on the FEAP regeneration in the linear system

Here, we study the effect of initial chirp on the regeneration in order to show how the chirp affects its quality. The first observation done in Fig. 3.4, concerns the

design obtained on the 3D – *contour* plots of the FEAP propagation.

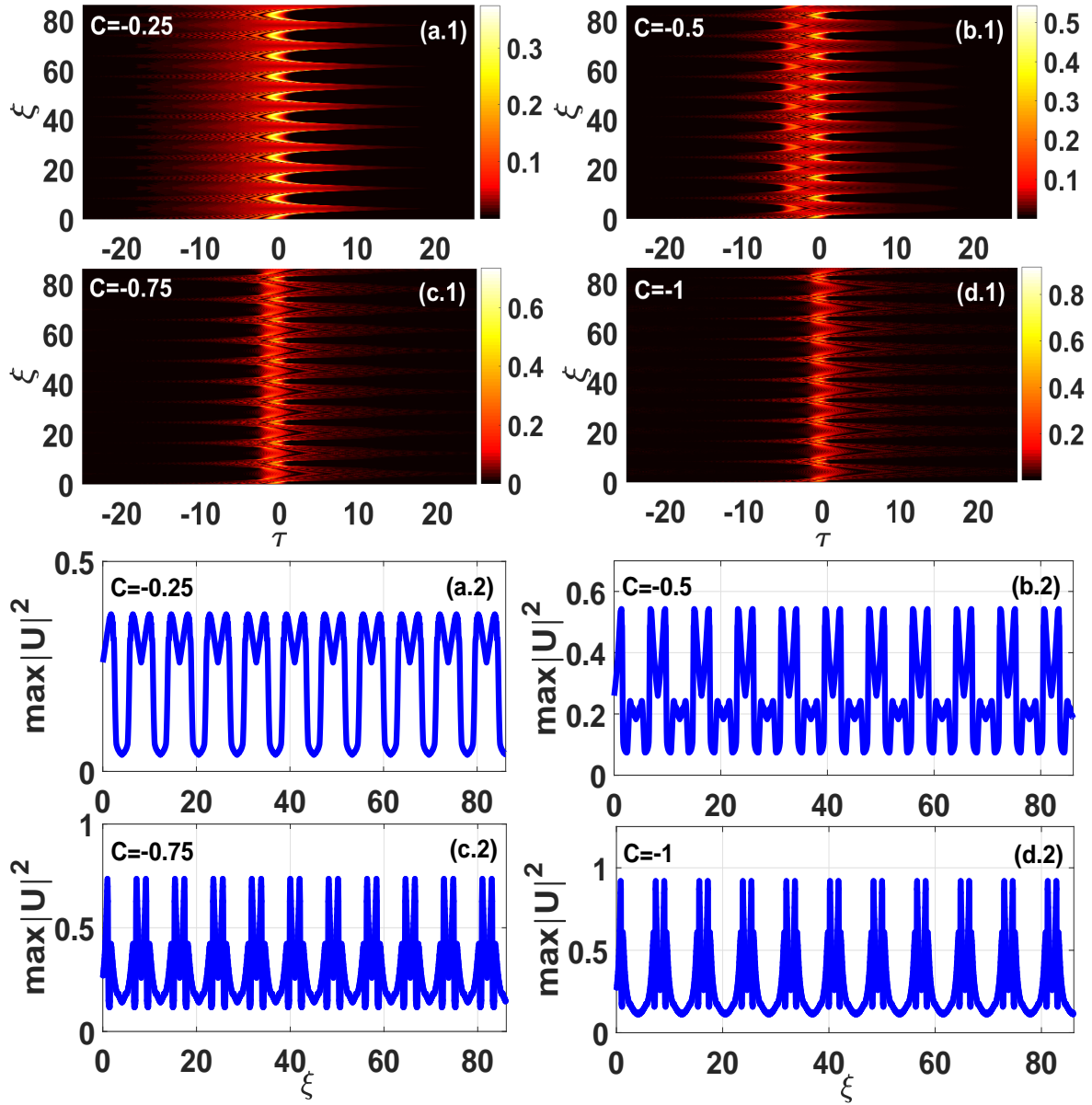


Figure 3.4: Effect of initial chirp (change of the initial value of $C \in \{-0.25; -0.5; -0.75; -1\}$): (a.1) to (d.1) for 3D-contour plots of the FEAP propagation within the first model of Figs. 2.2 with the initial condition of the A.I. mechanism $s \times C < 0$ as $s = 1$ and $C < 0$; (a.2) to (d.2) for the 2D-plots of the $\max|U|^2$ versus ξ .

Indeed, the regeneration becomes more refined as the initial chirp value changes for example from -0.25 to -1 starting with normal GVD ($s = 1$). This result can also be obtained if we start with $C \in [0.25; 1]$ and the anomalous GVD ($s = -1$). The 2D-plots of the dominant peak maximum intensity $\max|U|^2$ versus ξ obtained

in Figs. 3.4(a.2), 3.4(b.2), 3.4(c.2) and 3.4(d.2) show that, the increase of the absolute value of chirp $|C|$ also enhances $\max|U|^2$. It means that, the regeneration is performed with the increase of the absolute value of the initial chirp. However, as the chirp also introduces a certain perturbation of the signal during its propagation, this increase cannot be undefined. In this subsection, we address this point to frame an optimal value range for the chirp. In the next subsection, we conduct the numerical analysis on the regeneration of the twins Airy pulses namely the SFEAPs described by Eq. 2.36. Reminding that the temporal gap τ_B is relevant in the propagation of SFEAPs as discussed in ref. [29], we choose consequently to investigate the impact of τ_B on their regeneration.

3.2.5 Effect of the temporal gap τ_B on the regeneration of SFEAPs in the linear system

In this part, contrary to S. Xiaohui et al. [29] who studied the propagation of chirped SFEAPs in a SMF, we choose to investigate the regeneration of SFEAPs in fiber links with the CDM technique. More specifically, we analyze in this subsection the effect of the temporal gap τ_B on their regeneration in fiber links through the first and best model of the CDM technique mentioned in Figs. 2.2, 3.1(a.1) and 3.1(a.2). We start in Fig. 3.5 with $C = -0.5$ showing the contour plots from the value $\tau_B = 1$ to $\tau_B = 7.5$. The SFEAPs regeneration is well obtained with an influence on the maximum intensity of the dominant peaks. Furthermore, having a look on the 2D-plots of Fig. in 3.5(a.2) to 3.5(d.2), indicates that more τ_B is small, more $\max|U|^2$ of the SFEAPs is strong. These observations suggest that the increase of τ_B is not beneficial for the regeneration. On contrary, it can be

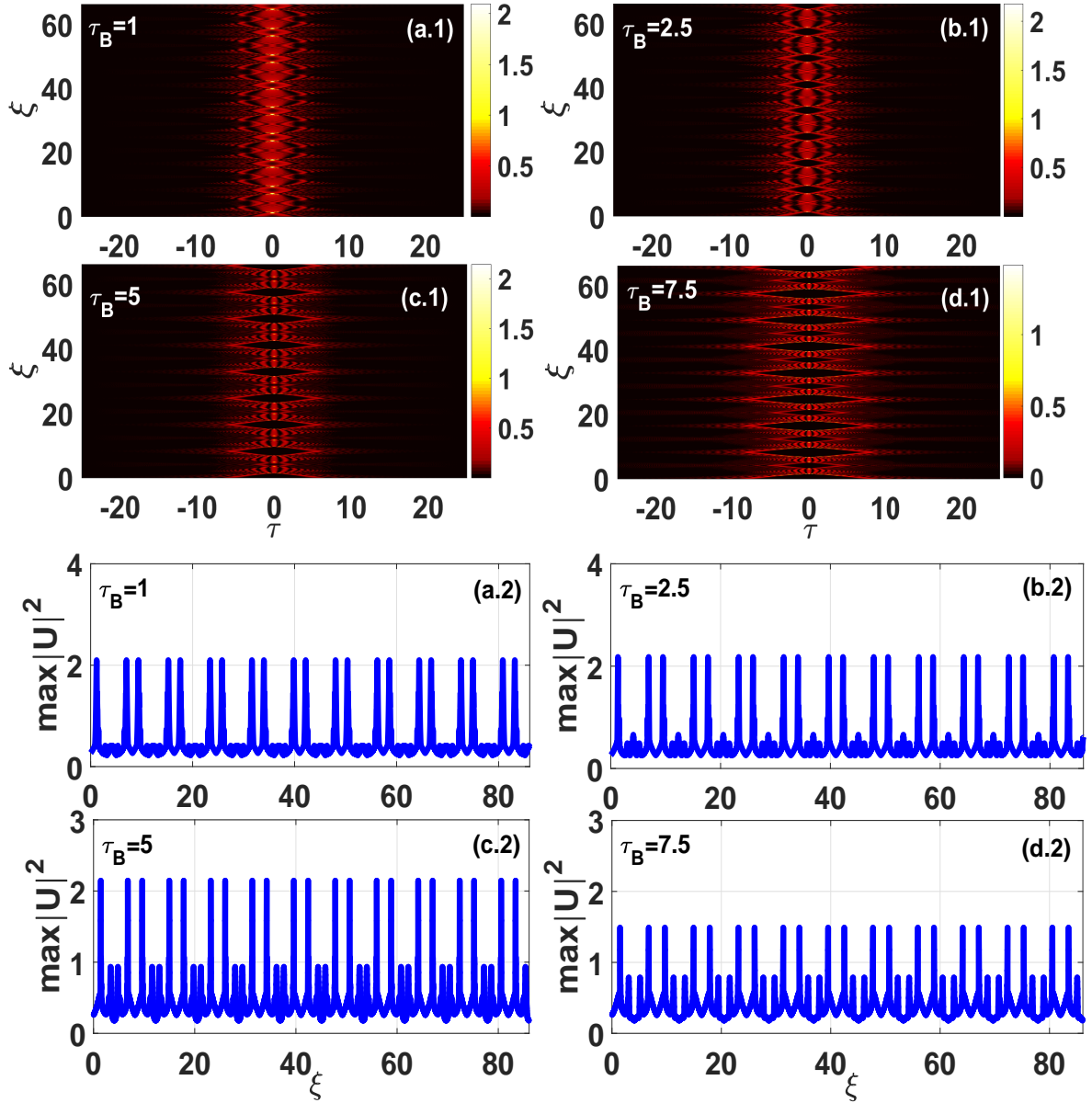


Figure 3.5: Effect of τ_B on the regeneration of SFEAPs (change of the value of $\tau_B \in \{1; 2.5; 5; 7.5\}$) : (a.1) to (d.1) for 3D-contour plots of the SFEAPs under the configuration of Figs. 2.2, 3.1(a.1) and 3.1(a.2) with the initial condition of A.I. mechanism $s \times C < 0$ and $C = -0.5$; (a.2) to (d.2) for 2D-plots of $\max|U|^2$ versus ξ .

detrimental.

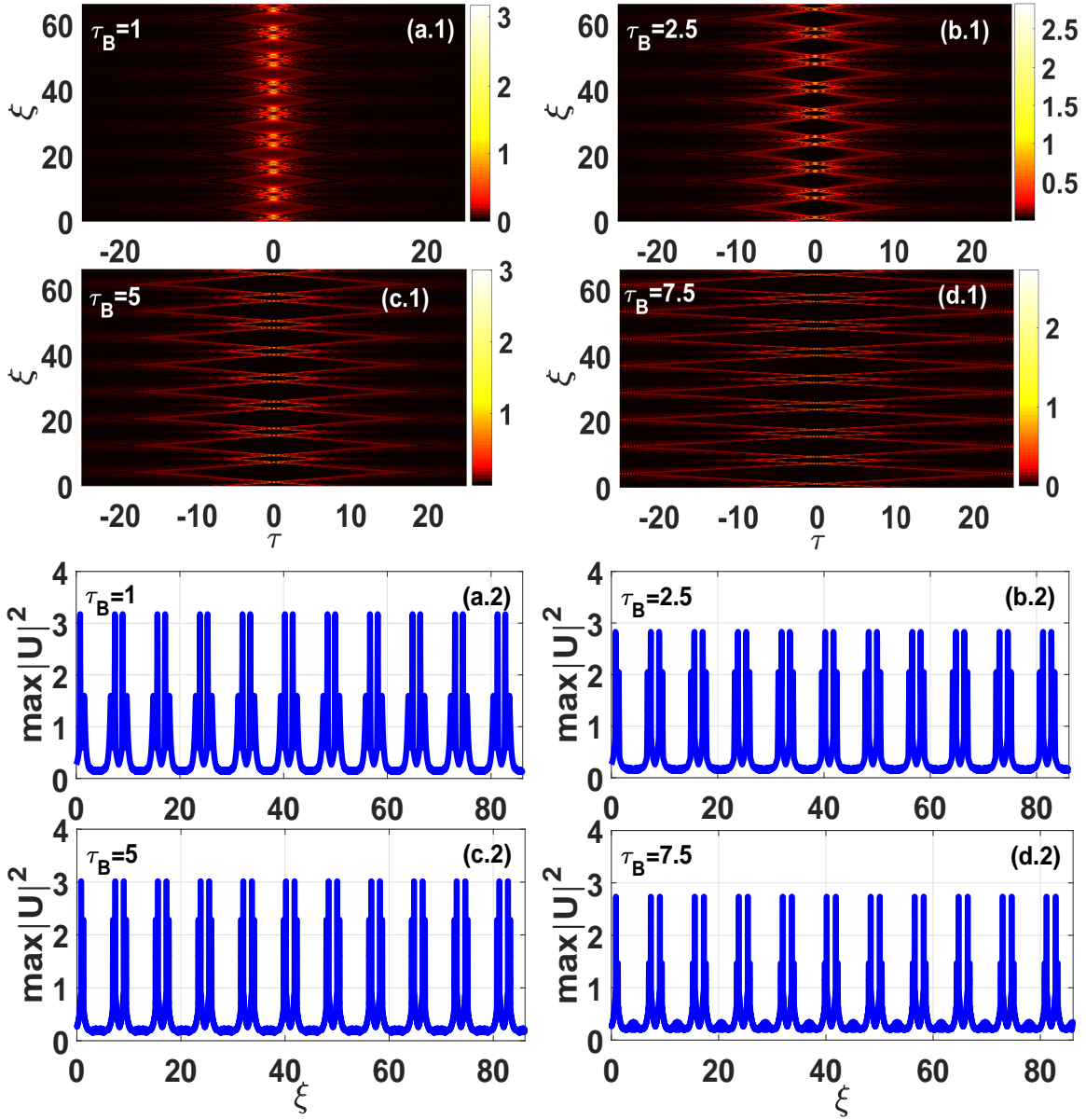


Figure 3.6: Same conditions as in Fig. 3.5 but with $C = -1$.

To counteract the deleterious effect related to the increase of τ_B , one can increase the absolute value $|C|$ of the chirp as done in Fig. 3.6 ($C = -1$). It is observed that the increase of $|C|$ really competes the increase of τ_B . Indeed, from $\tau_B = 1$ to $\tau_B = 7.5$ with $C = -1$, the signal energy (linked to $|U|^2$) also increases compared with Fig. 3.5. Nonetheless, we always observe that the increase of τ decreases the $\max|U|^2$ (see Figs. 3.6(a.2) to 3.6(d.2)).

3.3 On the nonlinear CDM inducing regeneration of truncated Airy pulses in fiber-optics links

We present here the numerical analysis of the propagation of a chirped FEAP in the regeneration process considering the effect of the Kerr nonlinearity ($N \neq 0$).

3.3.1 Effect of the nonlinearity on the regeneration of a FEAP

We realize the regeneration of the FEAP in the nonlinear system using obviously the best model which the first one discussed in Figs. 2.2, 3.1, 3.4, 3.5 and 3.6 with the initial condition of the A.I. mechanism $s \times C < 0$. The main feature and observation in Fig. 3.7 is the deterioration of the system performance induced by the nonlinearity. Indeed, as the nonlinearity increases from $N = 1$ Fig. 3.7(a.1) to $N = 4$ Fig. 3.7(d.1), one observes the increase of distortions in the regeneration process. One should notice that this result is in agreement with that of **R. Driben and T. Meier [25]**.

Moreover in ref. [25], the nonlinearity interacts with the regeneration induced by the DM technique between the GVD and the TOD through the A.I mechanism. Nonetheless in Fig. 3.7, the initial chirp replaces the TOD. Thus, we demonstrate here that one obtains the same result as in ref. [25], but rather using the CDM technique instead of the GVD-TOD DM technique. Another observation from Fig. 3.7, concerns the $2D - plots$ drawn in (a.2) to (d.2). Indeed, with $N = 1$, $\max|U|^2$ increases periodically following ξ (see Fig. 3.7(a.2)). However, in Figs. 3.7(b.2), 3.7(c.2) and 3.7(d.2) after an increase over a very short distance, $\max|U|^2$ starts to decrease following ξ compared with 3.7(a.2). In addition, we can also observe that more N is great, more the plot of $\max|U|^2$ versus ξ is noised. Fig.3.7 just

differs from Figs. 3.4(d.1) and 3.4(d.2) by $N \neq 0$. When the comparison is done, it yields that with $N = 0$ result of Figs. 3.4(d.1) and 3.4(d.2) is stable while results in Fig. 3.7 with $N \neq 0$ are unstable. It is therefore obvious to note the detrimental effect for the increase of nonlinearity on the FEAP regeneration. It is also interesting to have a look about the effect of the nonlinearity on the CDM-regeneration of SFEAPs in fiber-optics links.

3.3.2 Effect of the nonlinearity on the regeneration of strongly SFEAPs

The parameters are similar to those of Fig. 3.7 with $\tau_B = 1$. So, the results obtained here are to be compared with those of Figs. 3.6(a.1) and 3.6(a.2). As discussed above for the FEAP, the increase of N produces a noised regeneration even for the SFEAPs.

Comparing Fig. 3.8 with Figs. 3.6(a.1) and 3.6(a.2), shows the nonlinearity as a cause of a noise within the regeneration.

3.4 Highlights and discussion on the CDM technique applied on FEAPs

3.4.1 Among the three models discussed, what is the best?

By recapitulating all that was said above, we underline the best result obtained for the FEAP regeneration in the linear system is the one of Figs. 3.1(a.1) and 3.1(a.2). It corresponds to the first model of Fig. 2.2 in which the initial chirping is done at the beginning of the propagation while the GVD sign alternates from

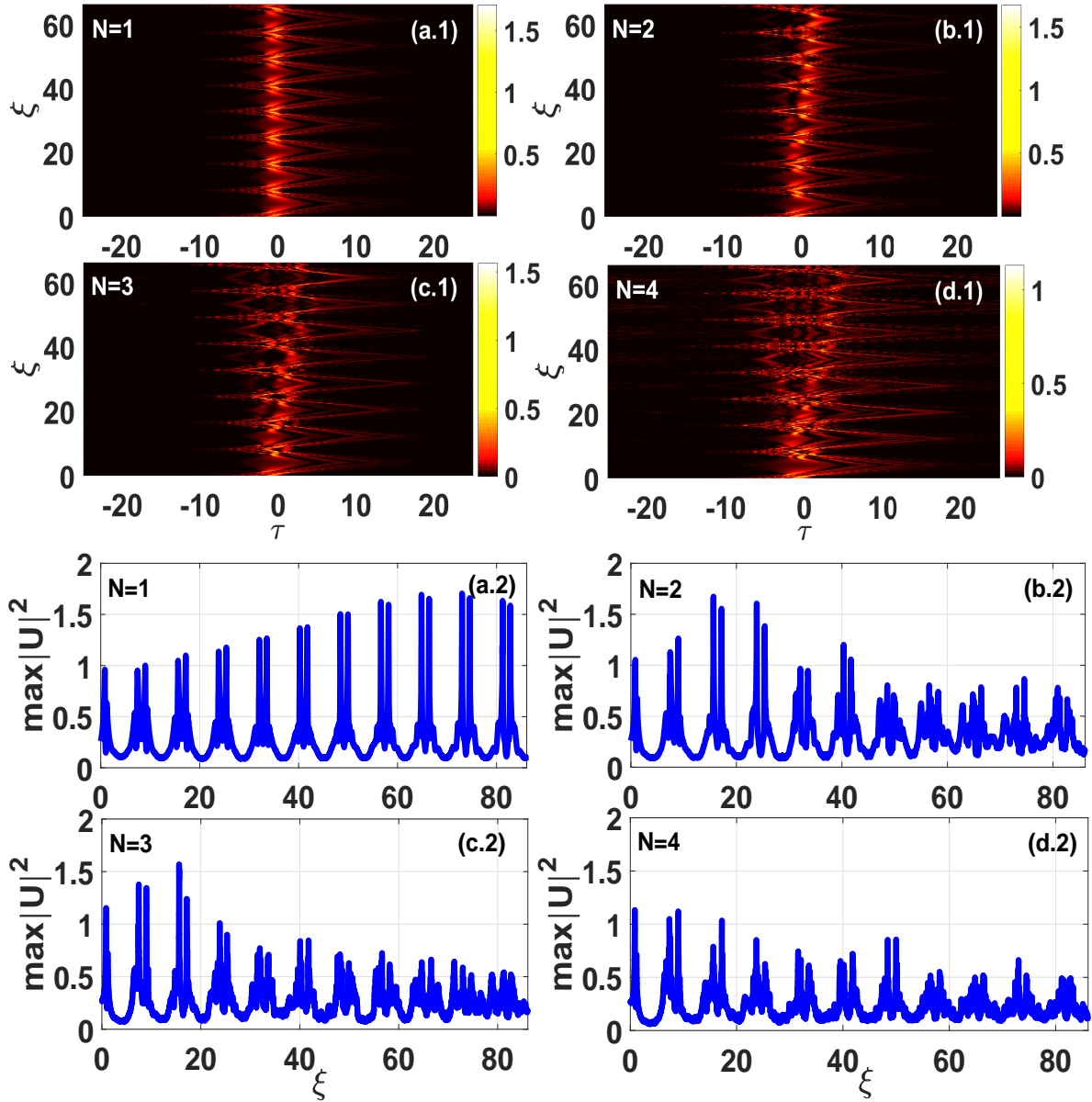


Figure 3.7: Effect of N on the FEAP propagation (change of $N \in \{1; 2; 3; 4\}$): (a.1) to (d.1) for 3D-contour plots of the FEAP under the configuration of Figs. 2.2, 3.1(a.1) and 3.1(a.2) with the initial condition of A.I. mechanism $s \times C < 0$ and $C = -1$; (a.2) to (d.2) for 2D-plots of $\max|U|^2$ versus ξ .

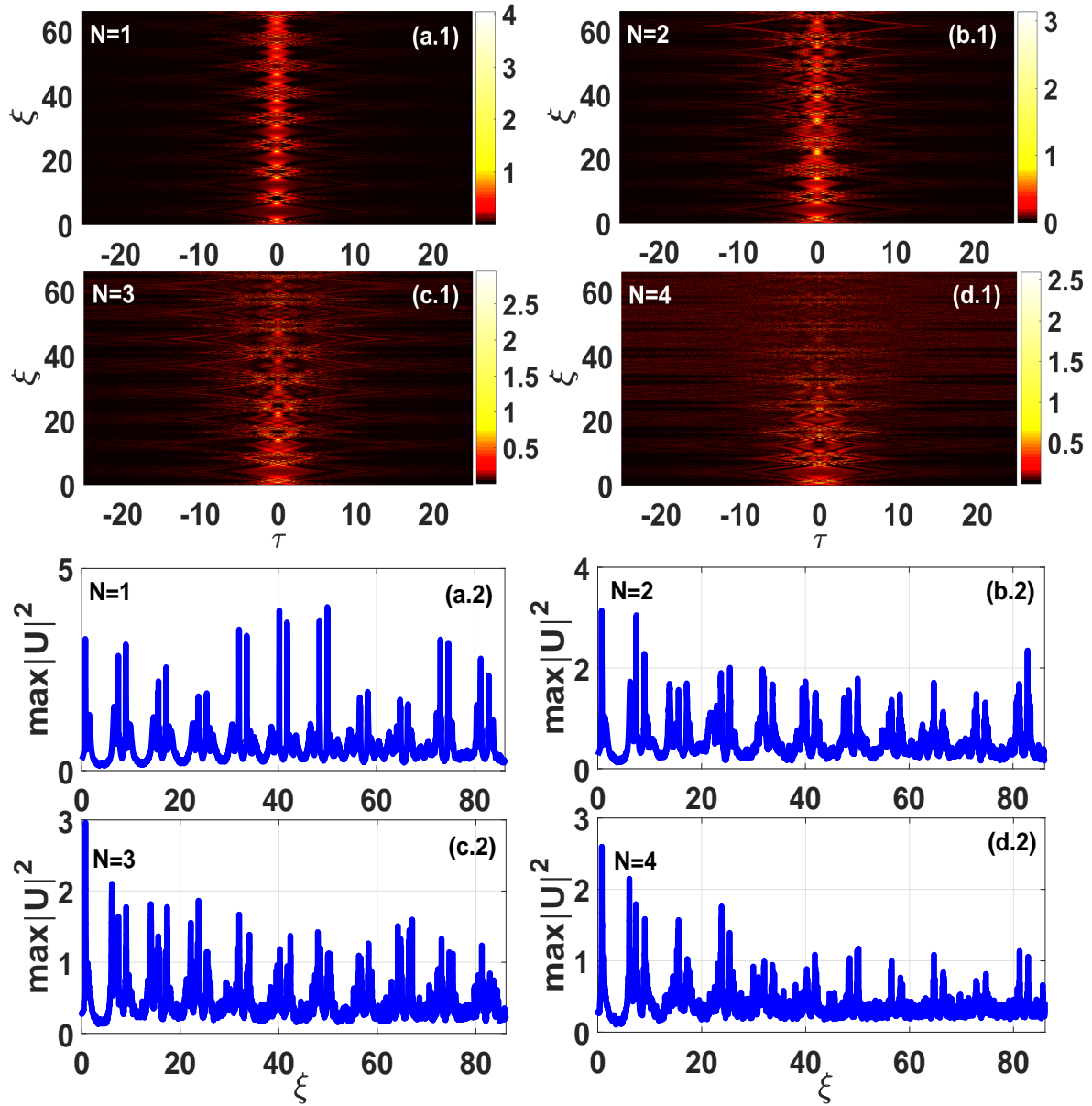


Figure 3.8: Effect of N on the SFEAPs regeneration (change of $N \in \{1; 2; 3; 4\}$): (a.1) to (d.1) for 3D-contour plots of the SFEAPs under the configuration of Fig. 3.7 with the initial condition of A.I. mechanism $s \times C < 0$ and $C = -1$; (a.2) to (d.2) for 2D-plots of $\max|U|^2$ versus ξ .

one piece of fiber to another. For instance, we zoom in the regeneration done in Fig. 3.1 by highlighting what happen within the first three pieces of fiber $f_{i=1..3}$ as depicted in Fig. 3.9.

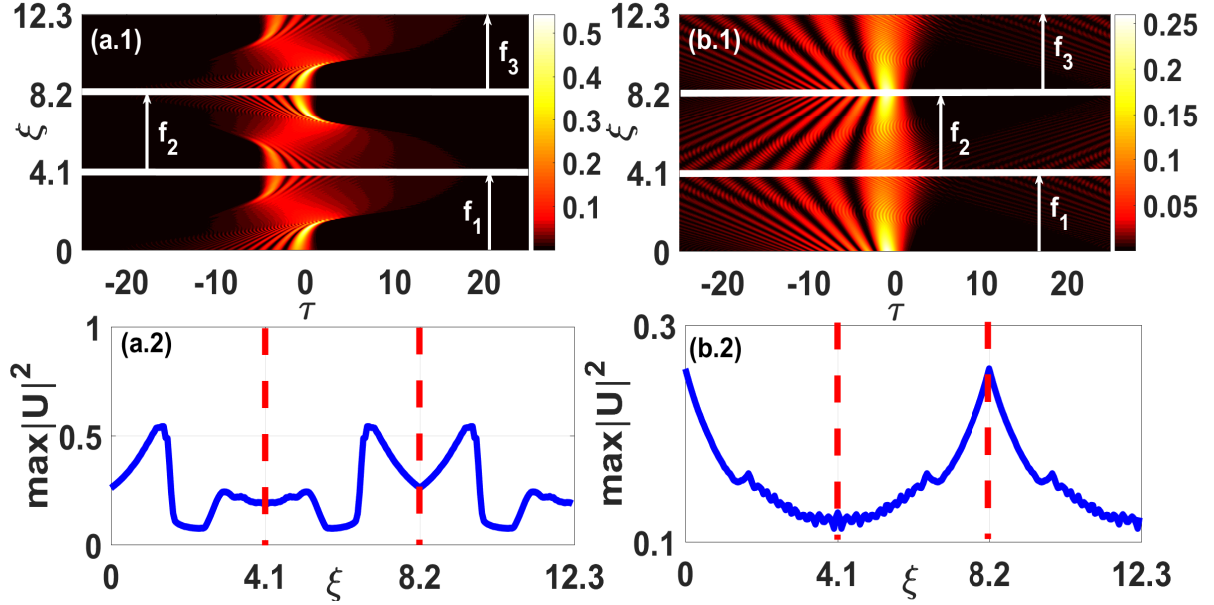


Figure 3.9: Zoom on the FEAP propagation through the first three pieces ($f_{i=1..3}$) of optical system described by the first model of Fig. 3.1. The initial condition : (a.1) and (a.2) for the A.I. mechanism $s \times C < 0$, (b.1) and (b.2) for $s \times C > 0$.

As shown in this figure, for the first case in which the initial condition is the A.I. mechanism $s \times C < 0$ corresponding to Figs. 3.9(a.1) and 3.9(a.2), the regeneration is more efficient than that of the initial condition $s \times C > 0$ in 3.9(b.1) and 3.9(b.2) as already discussed in Fig. 3.1. With this zoomed picture, we notice effectively that the best case implies the achievement of the A.I. mechanism in each piece of fiber : for instance in f_1 we observe an A.I. mechanism (see 3.9(a.1)), the reverse A.I. mechanism in f_2 while it still reverses in f_3 and so on. To explain how it works, we suggest that when the pulse is chirped initially by C oppositely with s , we get the first A.I. mechanism because the condition $s \times C < 0$ is already satisfied in f_1 . The pulse develops its own chirp C' during the propagation within

f_1 , so that when the GVD sign changes in f_2 , this intrinsic chirp C' matches once again with this novel GVD according to the A.I. condition and the process starts all over again within f_3 and so on. The opposite happens in Fig. 3.9(b.1) in which we start with $s \times C > 0$. This condition indicates that both the chirp and the GVD cooperate to disperse the FEAP in the opposite direction of the conventional acceleration as shown in f_1 while the reverse happens in f_2 and after once again in $f_3 \dots$. In short, the best model is the first model of Fig. 3.1 with the initial condition of the A.I. mechanism which is also realized on each piece of fiber over the whole optical system. The distance between the red vertical dashed lines in the $2D$ – *plots* of Figs. 3.9(a.2) and 3.9(b.2), represent the length of each piece of fiber as highlighted in the $3D$ – *contour* plots of Figs. 3.9(a.1) and 3.9(b.1). The figure 3.9(a.2) correspond to 3.9(a.1) and 3.9(b.2) to 3.9(b.1).

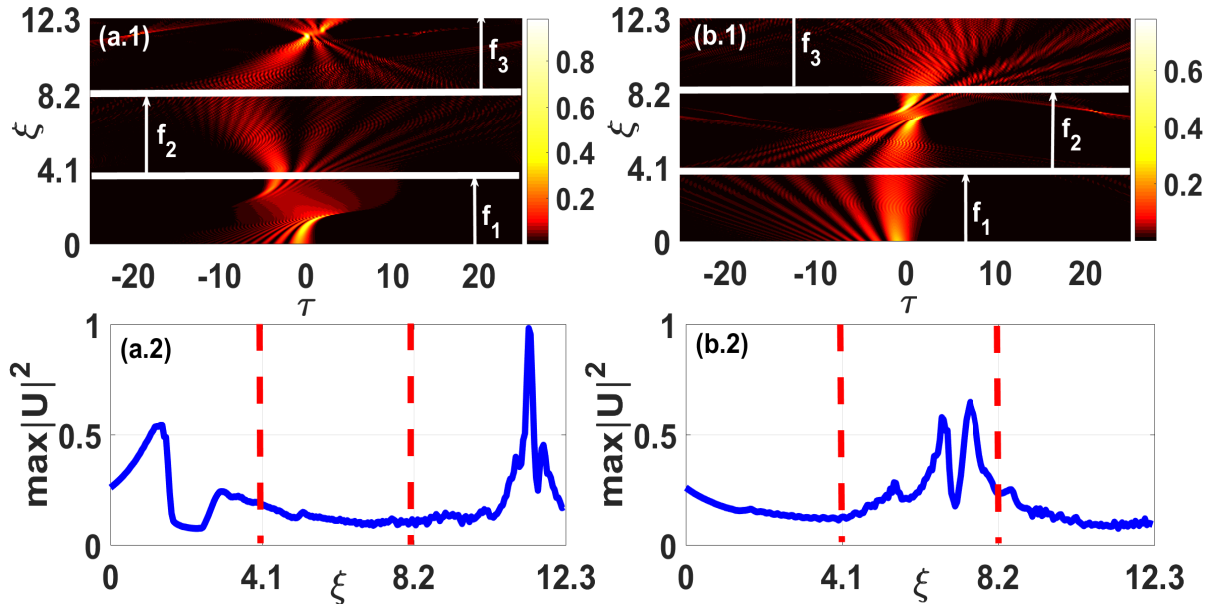


Figure 3.10: Zoom on the FEAP propagation through the first three pieces ($f_{i=1..3}$) of optical system described by the second model of Fig. 3.2. The initial condition : (a.1) and (a.2) for the A.I. mechanism $s \times C < 0$, (b.1) and (b.2) for $s \times C > 0$.

In Fig. 3.10, we present the zoom of Fig. 3.2 in the same way as above but

for the second model. While the A.I. mechanism starts in Fig. 3.10(a.1) and 3.10(a.2) within f_1 , the next pieces of fiber $f_{i=2,3}$ distorts completely the signal demonstrating that this model is not well indicated to regenerate the FEAP. The result becomes worst in Fig. 3.10(b.1) and 3.10(b.2) with the initial condition $s \times C > 0$.

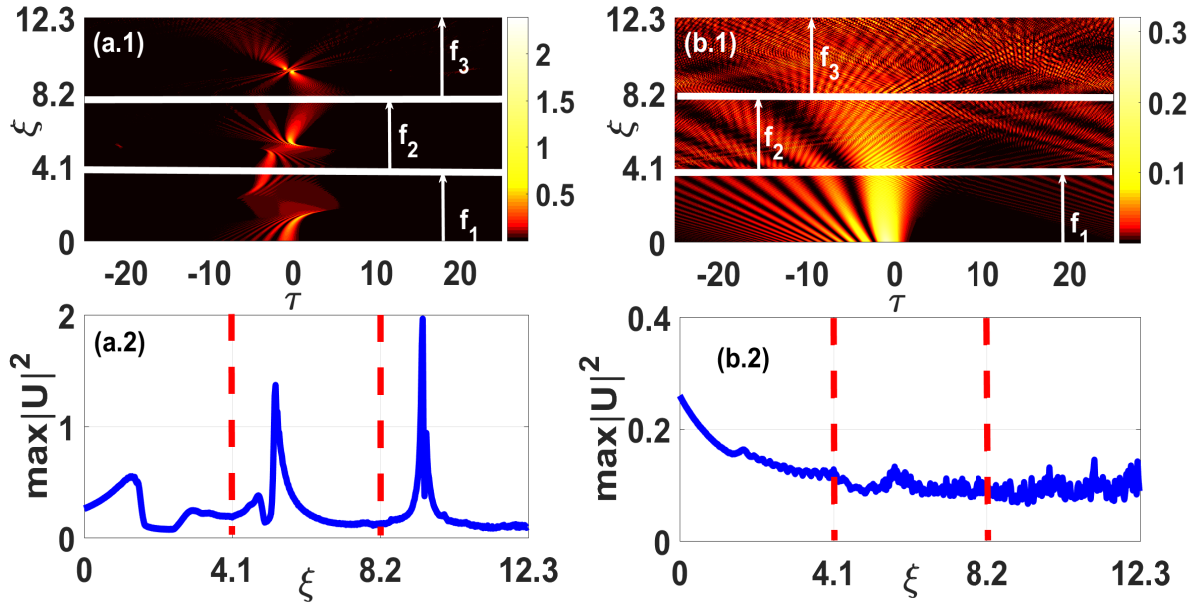


Figure 3.11: Zoom on the FEAP propagation through the first three pieces ($f_{i=1..3}$) of optical system described by the third model of Fig. 3.3. The initial condition : (a.1) and (a.2) for the A.I. mechanism $s \times C < 0$, (b.1) and (b.2) for $s \times C > 0$.

We also zoom in the noised regeneration of Fig. 3.3 in Fig. 3.11 in the same way as in Figs. 3.9 and 3.10. Considering Figs. 3.1-3.3 and 3.9-3.11, we suggest that the noise originates from : (i) the alternation of the initial chirp by the introduction of the chirping device at the end of each piece of fiber (result from the second model: see Figs. 3.2 and 3.10), (ii) using the initial condition $s \times C > 0$ that allows a cooperation of these parameters to disperse the FEAP (see Figs. 3.2(b.1), 3.2(b.2), 3.10(b.1), 3.10(b.2), 3.11(b.1) and 3.11(b.2)), (iii) a combination of (i) and (ii) as done in the third model (see Figs. 3.3 and 3.11), (iv) the increase of

the nonlinearity (see Figs. 3.7 and 3.8).

3.4.2 Is there an optimal value of the chirp? what about the temporal gap ?

After the result obtained in Fig. 3.4, we found that the increase of the absolute value $|C|$ of initial chirp also increases the maximum intensity of the main lobe (see Figs. 3.4(a.2) to 3.4(d.2)). Furthermore, in the linear system if we note the maximum values reached in the $2D$ -plot of $I_{max} = \max|U|^2$ versus ξ , we generate another $2D$ -plot showing I_{max} versus $|C|$ in Fig. 3.12(a).

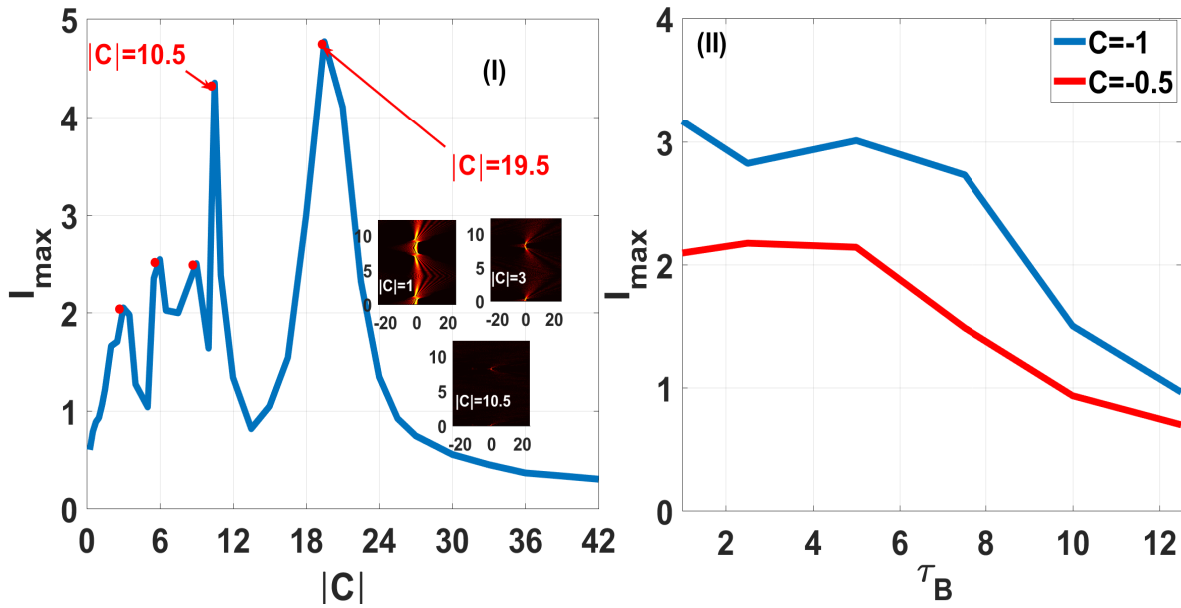


Figure 3.12: (a) Plot of $I_{max} = f(|C|)$ in the case of FEAP following Fig. 3.4; (b) Plot of $I_{max} = f(\tau_B)$ in the case of SFEAPs following Figs. 3.5 and 3.6.

We do the same thing with τ_B in Fig. 3.12(b). Figure 3.12(a) shows how the chirp really influences the intensity in the regeneration while Fig. 3.12(a) highlights the influence of the increase of τ_B . In Fig. 3.12(a), we retain some remarkable values for $|C|$ displayed with red points as $|C| \in \{3; 6; 9; 10.5; 19.5\}$. We note however that the more $|C|$ also increases the more the regeneration loses in quality

despite the increase in intensity. This observation could be done with the insets pictures in Fig. 3.12(a) where the regeneration is well designed for $|C| = 1$ than the other values (3 and 10.5). For instance, $|C| = 3$ yields a better regeneration quality than 10.5. The physical reason explaining this feature falls on the nature of the chirp which is basically a perturbation. The regeneration obtained with $|C| = 1$ is also better in quality than that of $|C| = 3$ while in intensity this last value enhances more the regeneration than $|C| = 1$. So, increasing the initial chirp also increases the perturbation of the signal that could become more and more unstable. Thus, $|C|_{opt}$ should include not only the increase of the intensity but also a good quality of regeneration. Therefore, we suggest that values of $|C|$ should belong to $[1; 3]$ (see the insets pictures in Fig. 3.12(a) where the regeneration is well designed for $|C| = 1$ than the other values). In Fig. 3.12(b), it is confirmed that the increase of τ_B is deleterious for the regeneration. At the end of this work, we suggest that to achieve efficiently the regeneration of FEAP through the CDM technique, it is necessary to fulfill only the following points: (a) choose the best model, which is the first one (see Fig. 2.2); (b) use the initial condition of the A.I. mechanism; (c) in the nonlinear context, the value of N should be small; (d) the absolute initial value of the chirp should be a little high but not too high to avoid chirping dominating and destroying the quality of the regeneration [see the inset pictures in Fig. 3.12(a)] (we have chosen to manage $|C| \in [1; 3]$), and (e) for SFEAPs, use a small value of τ_B .

3.5 On the SCG of truncated Airy pulses in a cubic-quintic $\text{AsSe}_2/\text{As}_2\text{S}_5$ optical waveguide with rib-like structure

3.5.1 Numerical results

The simulations of Eq. 2.58 with the modified M-files of the MATLAB code yields the results of this work. In Fig. 3.13, we have the contour plots showing the propagation of the signal within the waveguide for different cases. For instance

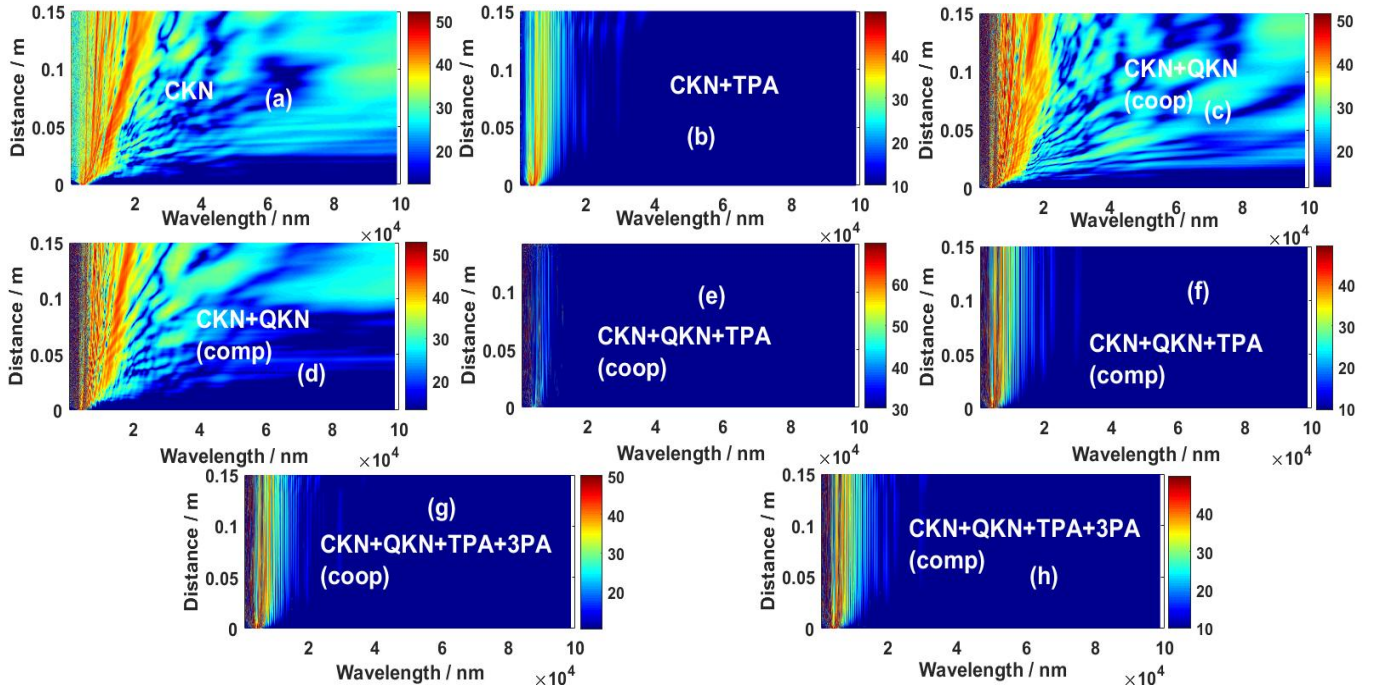


Figure 3.13: Contour plots of SCG Airy pulse spectral propagation for a 50fs input pulse with 10kW peak power at a central wavelength of $4\mu\text{m}$ along 15cm long $\text{AsSe}_2/\text{As}_2\text{S}_5$ - ChRW: (a)- Single CKN, (b)- CKN+TPA, (c)- CKN+QKN in case of cooperating nonlinearities ($\gamma_1\gamma_2 > 0$), (d)- CKN+QKN in case of competing nonlinearities ($\gamma_1\gamma_2 < 0$), (e)- CKN+QKN+TPA in case of cooperating nonlinearities, (f)- CKN+QKN+3PA in case of competing nonlinearities, (g)- CKN+QKN+TPA+3PA in case of cooperating nonlinearities, (h)- CKN+QKN+TPA+3PA in case of competing nonlinearities.

in Fig. 3.13(a), we have the single CKN case in which all the other parameters are set zero (TPA, QKN, and 3PA). We notice that this nonlinearity generates an explosive spectrum with this peak power of $P_0 = 10\text{kW}$ in the MIR region

beyond 97250 *nm* of bandwidth. This result with a FEAP is widely relevant compared with those of refs. [31]. We also notice that the drastic spectral explosion (beyond 97250 *nm*) appears with the action of the CKN which manifests itself approximately at the propagation distance $L_{3NL} \sim 24$ *mm*. Obviously with the effect of the TPA, we obtain the figure 3.13(b) in which the spectrum is drastically reduced both in intensity and in bandwidth.

This result is in agreement with those of previous works [184-186]. Removing the TPA and considering the QKN only with a zero 3PA, for the cooperating case of nonlinearities $\gamma_1 \times \gamma_2 > 0$, we observe a distinct slight improvement of the SCG spectrum (see Fig. 3.13(c)). That is an expected result because CKN and QKN cooperate together to allow the spectral broadening. That happens soon approximately with the propagation distance $L_{3NL+5NL} \sim 0.16$ *mm*. On contrary in Fig. 3.13(d), the competing case $\gamma_1 \times \gamma_2 < 0$ reduces slightly the spectrum and makes it to explode late comparatively to the cooperating case. This result also suggests an expected feature in which the competition of nonlinearities is a serious handicap for the SCG. Indeed, the QKN γ_2 competes against the CKN γ_1 : when the CKN leads to spectral broadening while QKN hinders this effect. The approximate distance when it explodes is $L_{3NL-5NL} \sim 34$ *mm*. One can also observe the deleterious effect of the TPA combined with the QKN in Figs. 3.13(e) and 3.13(f). Furthermore, the main feature observed in these pictures concerns the spectral intensity (SI). In fact, the TPA reduces the intensity. This effect is more important when the competition is considered (see the power colourbar of Fig. 3.13(f)) than that of the cooperation (see the power colourbar of Fig. 3.13(e)). When the 3PA is taken into account in Figs. 3.13(g) and 3.13(h), a similar

manifestation is also observed : the 3PA also reduces the SI (see the colourbars of these pictures). However, the effect of the 3PA differs for each case according to the combination of the nonlinearities.

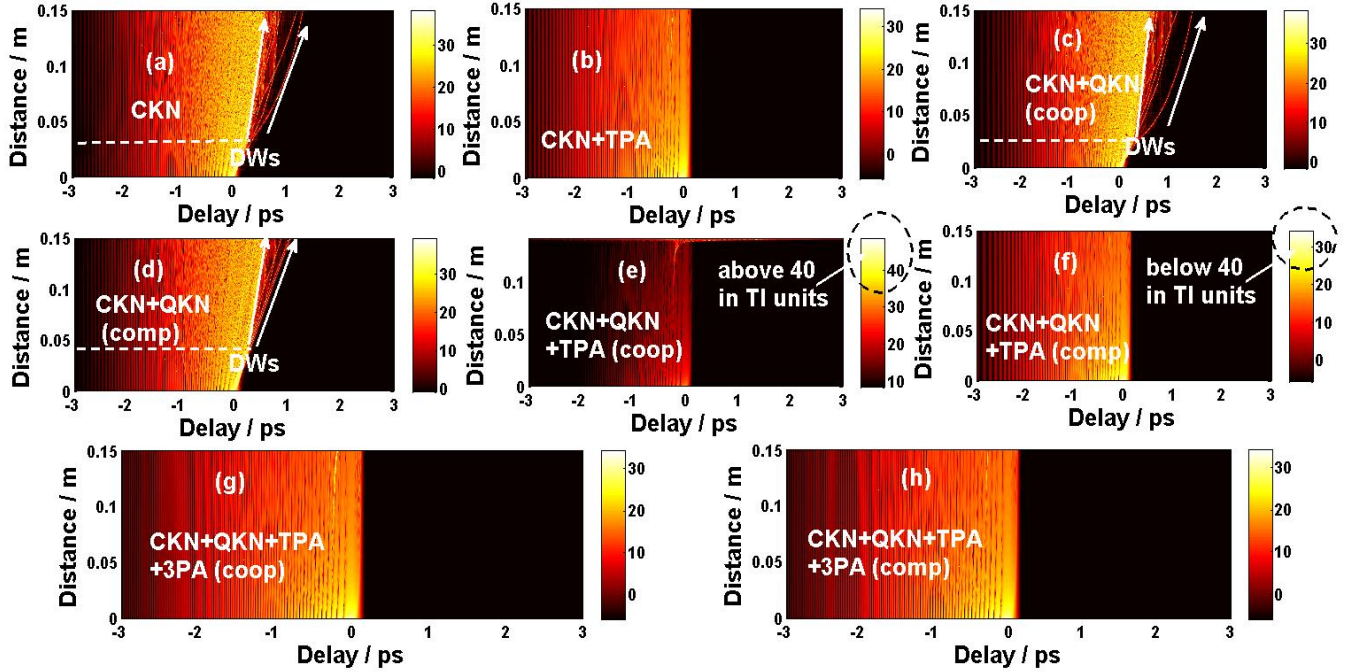


Figure 3.14: Contour plots of SCG Airy pulse temporal propagation for the different cases of Fig. 3.13.

We show in Fig. 3.14 the temporal propagation of the truncated Airy pulse for the different cases depicted in Fig. 1. As observed in this figure, there are some DWs shed from the pulse during its propagation only for the cases in which the nonlinear absorptions are not taken into account (see Figs. 3.14(a), 3.14(c) and 3.14(d)). Indeed, the nonlinearity combined with the dispersion of the waveguide yields the emission of these DWs with different magnitude [140]. For instance, the DWs emission is more drastic in the cooperating case (see Fig. 3.14(c)) than that of the single CKN case (see Fig. 3.14(a)), the competing case being the last (see Fig. 3.14(d)). This result demonstrates that the increase of nonlinearity brought by the cooperation of CKN and QKN (see Fig. 3.14(c)) also performs the DWs emission than in the single CKN case (see Fig. 3.14(a)). Consequently, the

competition between the CKN and the QKN, diminishes the nonlinearity and the DWs emission. This mechanism appears for the single CKN case around 26 *mm* (see Fig. 3.14(a)) while in the cooperating nonlinearities case it appears around 24 *mm* (see Fig. 3.14(c)). In the last case of competing nonlinearities, we find about 49 *mm* (see Fig. 3.14(d)). It is therefore obvious that the nonlinearity is a catalyst for the emission of DWs as discussed previously in ref. [140]. Another observation done in this picture, consists into the interaction between the TPA and the QKN shown in Figs. 3.14(e) and 3.14(f). When we consider the colourbars of these two cases, we notice that the cooperating nonlinearities case has a temporal intensity (TI) above about 40 units (see the black dashed circle) while in the competing nonlinearities case, we have a TI below 40 units. That is an expected result in agreement with the effect of nonlinearity. The main impact of nonlinear absorptions (both the TPA and the 3PA) in this temporal propagation of Fig. 3.14, consists to avoid the DWs emission as seen in Figs. 3.14(b), 3.14(e), 3.14(f), 3.14(g) and 3.14(h).

To address more insights about the features obtained in Figs. 3.13, and 3.14 we plot in Fig. 3.15, the output spectra at the final propagation distance $L = 15$ cm, for each case. Thus, the TPA effect with the single CKN is shown in Fig. 3.15(a), while the combination of nonlinearities is addressed in Fig. 3.15(b). The effect of TPA combined with the QKN is observed in Fig. 3.15(c). We compare in Fig. 3.15(d) the manifestations of the 3PA in the cooperating or competing nonlinearities. Moreover, the highlight of the impact of TPA compared with the 3PA is drawn in Figs. 3.15(e) and 3.15(f). As discussed in Fig. 3.13, we see that the TPA reduces the spectral intensity (SI) (see Fig. 3.15(a)): it is an expected re-

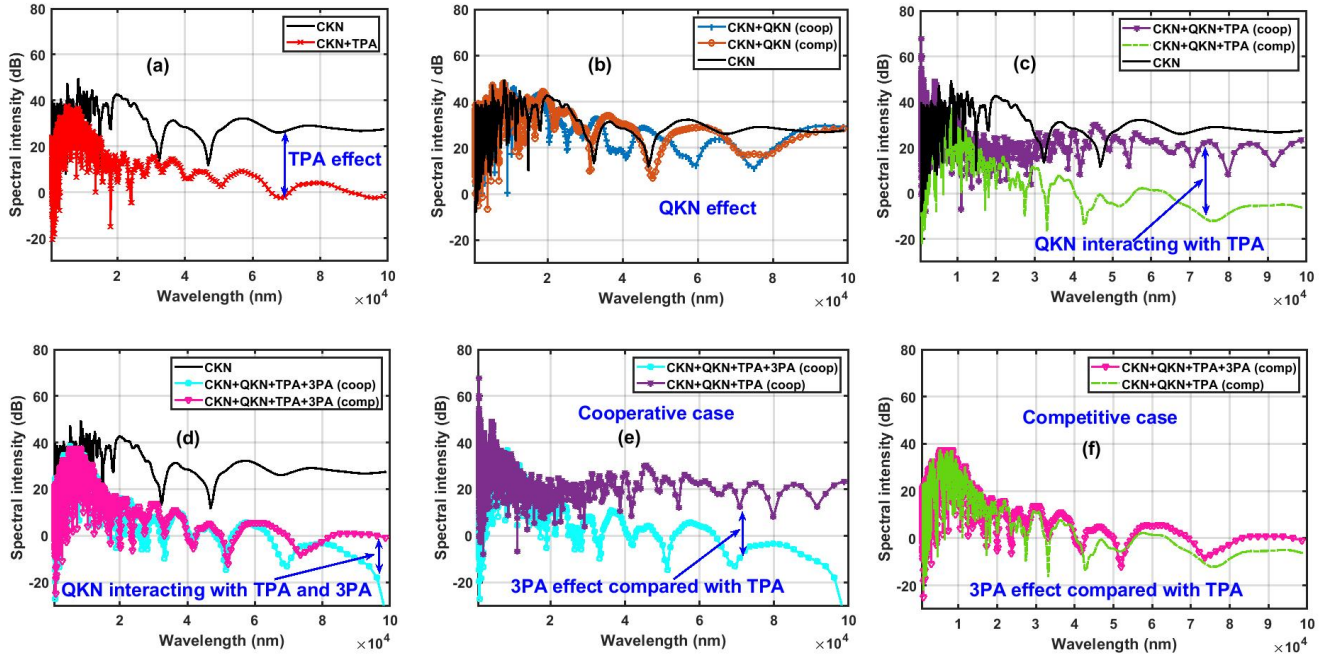


Figure 3.15: SCG spectra for the FEAP in the anomalous GVD regime for different cases mentioned above. $L = 15\text{cm}$, $a = 0.05$, $t = 50\text{fs}$, $P = 10\text{KW}$.

sult already discussed in refs. [179, 187, 188]. Nonetheless, the interaction between the TPA and the combination of the nonlinearities shown in Fig. 3.13(c), demonstrates the specific effects of the studied cases : the cooperating nonlinearities (see the purple curve of Fig. 3.13(c)) and the competing nonlinearities (see the green dashed curve of Fig. 3.13(c)). In fact, we can see that the SI is more reduced in the case of competing nonlinearities (see the green dashed curve of Fig. 3.13(c)) than that of cooperating nonlinearities (see the purple curve of Fig. 3.13(c)). On the other hand, when the consideration of the 3PA is done in Fig. 3.13(d), we observe a surprising result : the 3PA weakly affects the competing case than that of the cooperating case. Indeed, it is notorious to note the reduction of the SI brought by the 3PA following the TPA however differently with the combination of the nonlinearities. The cooperating case undergoes more the reduction mostly at the high wavelengths around $8 \times 10^4\text{nm}$ than in the case of competing nonlinearities.

To compare how the TPA reduces the SI of the SCG and the action of the $3PA$, it is depicted in Fig. 3.13(e) the cooperating case. The TPA and $3PA$ merge their strength to reduce the intensity of the SCG (see the cyan curve in Fig. 3.13(e)). On contrary, considering the case of competing nonlinearities in Fig. 3.13(f), the $3PA$ appears to enhance rather the SI while the single TPA rather reduces it.

3.5.2 Discussion

As we have observed the different spectral outputs above, we notice that the main discrepancies appear in the high wavelengths of the MIR-region.

Interaction between the CKN and the QKN

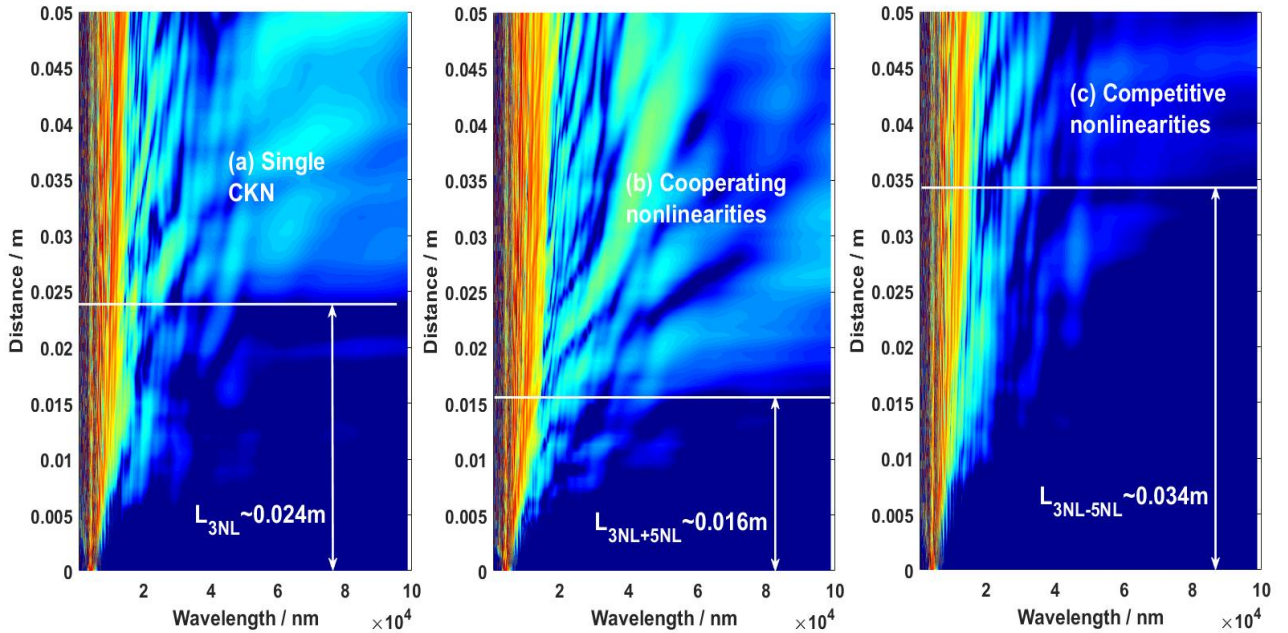


Figure 3.16: Highlight on the spectral propagation distance $L = 0.05m$ of the effect of QKN in the MIR-SCG of FEAP within the considered optical waveguide: (a) for the single CKN, (b) for the case of $\gamma_1\gamma_2 > 0$, (c) for the case of $\gamma_1\gamma_2 < 0$.

We show in Fig. 3.16, the highlight of the effect of the QKN on the MIR-SCG

of the FEAP pump within the considered optical waveguide. Indeed, considering the propagation distance of $L = 0.05m$, we can see that the drastic broadening that leads the pulse to explode over the whole bandwidth between 750 nm and 10^5 nm , does not appear at the same distance. For instance, for the case of the single CKN, it appears approximately around 0.024 m , in the case of cooperating nonlinearities ($\gamma_1\gamma_2 > 0$), it appears around 0.016 m approximately. For the last case of competing nonlinearities ($\gamma_1\gamma_2 < 0$), it appears only around 0.034 m approximately. This can be explained by the intrinsic action of the QKN : when it is positive, the QKN cooperates with the CKN in order to broaden the spectrum of the SCG and the nonlinearity of the medium is sufficiently high to have the appearance of the explosion very sooner than that of the single CKN. However, when the QKN is negative, the nonlinearity becomes smaller and the spectral explosion over the whole bandwidth between 750 nm and 10^5 nm arrives later in the propagation because the nonlinearity acts more weakly than both of the two previous cases. Therefore, in the case where the NPA parameters (TPA and 3PA) are not taken into account, only the cooperating QKN ($\gamma_1\gamma_2 > 0$) is beneficial for the MIR-SCG of the FEAP within this waveguide.

Interaction between the TPA and the combination of the nonlinearities

The figure 3.17 demonstrates that the competition between the two nonlinearities is very detrimental for the MIR-SCG of the FEAP for the great wavelengths because of the discrepancy between the red curve and the green dashed curve. One can note here that the cooperation ($\gamma_1\gamma_2 > 0$) enhances rather the SI of the SCG and thwarts the deleterious effect of the TPA. Thus, considering the cooperating QKN with the TPA when the 3PA is neglected, is also interesting

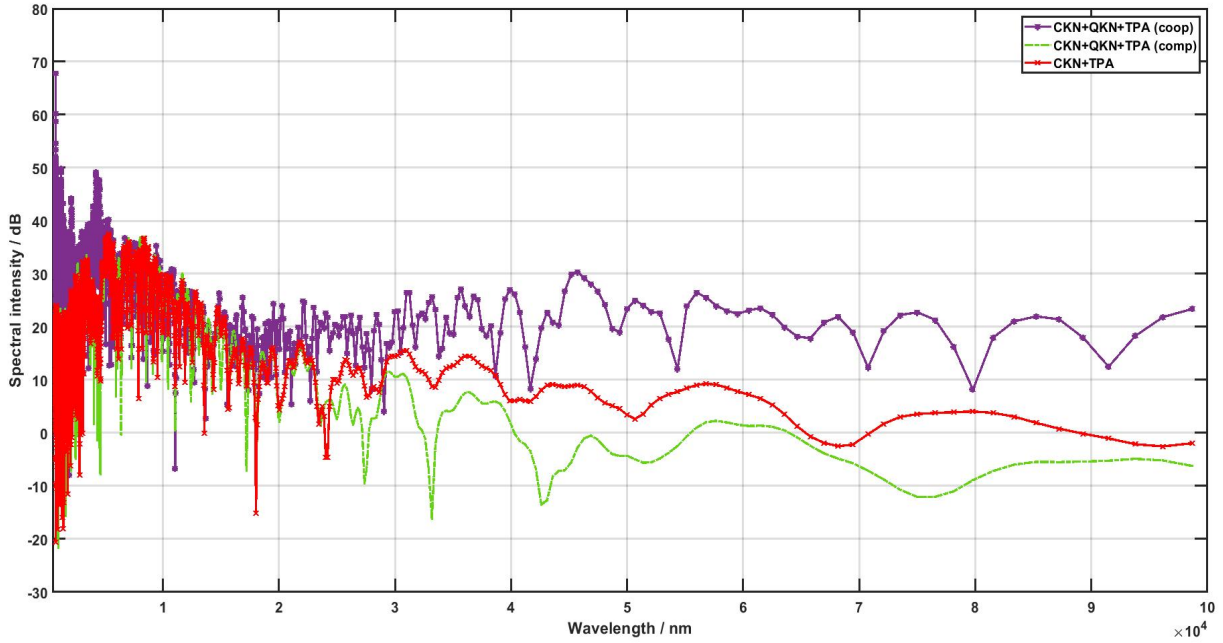


Figure 3.17: Highlight the effect of TPA for the two cases of QKN in the MIR-SCG of FEAP within the considered optical waveguide.

for the SI of the SCG compared with the competition between the CKN and the QKN.

Interaction between the 3PA and the combination of the nonlinearities

The result obtained in Fig. 3.15(d), is very surprising when one considers the effect the 3PA. In fact, the 3PA normally should accentuate the TPA effect as a NPA parameter. Nonetheless, we find here the contrary : the cooperating nonlinearities case resists weakly to the 3PA and collapses beyond $8 \times 10^4 \text{ nm}$ (see the cyan line in Fig. 3.15(d)); so, the competition appears to be more beneficial than the cooperation when the 3PA is considered. This result is very interesting for the management of the QKN in the MIR-SCG of FEAP in the considered waveguide, specially for the great wavelengths. This feature of 3PA can be understood by the following explanation : the cubic nonlinearity could be written as $\gamma_1 = CKN +$

$iTPA$ and the quintic nonlinearity could be written as $\gamma_2 = QKN + i3PA$. Thus, considering a linear analysis of the combination of these phenomena, we can suggest that in the cooperation case : the whole nonlinearity effect combines CKN effect + QKN effect in order to broaden the FEAP spectrum while in the competition case we have CKN effect - QKN effect (QKN thwarts the CKN effect); at the same time the whole NPA effect in the cooperation case combines TPA effect + $3PA$ effect in order to reduce the SI. Hence, as the combined NPA effect is stronger than the whole nonlinearity CKN+QKN, consequently the SI is reduced. Moreover, in the competition case, the whole NPA effect is given as TPA effect - $3PA$ effect, so the $3PA$ fights against the TPA effect. For the considered conditions in the competition case, the $3PA$ resistance against the TPA exceeds the QKN resistance against the CKN effect, that is why the SI does not collapse as in the cooperation case. Therefore, the $3PA$ parameter appears to be a good tool to control the TPA in the MIR-SCG of FEAPs in the considered waveguide. It can also be explained as discussed in ref. [189] for the silicon material, by the TPA forbidden in the MIR region beyond $2.2 \mu m$, while the $3PA$ and the four-photon absorption were found there to dominate in the great wavelengths of the MIR region. Thus, we can suggest here that, in the $AsSe_2/As_2S_5$ -ChRW structure, pumping in the MIR region allows to activate the $3PA$ which is rather beneficial for the SI of the SCG of Airy pulses compared to the TPA effect.

Interaction between the TPA and the $3PA$

As observed in Fig. 3.15(e) for the cooperation case, the NPA (combination of TPA effect + $3PA$ effect) reduces the SI of the MIR-SCG of the FEAP than the single TPA case. On the other hand, in Fig. 3.15(f) for the competition case, the

NPA (competition of TPA effect - 3PA effect) enhances the SI of the MIR-SCG of the FEAP than the single TPA case for the great wavelengths. Thus, as discussed above, the 3PA thwarts the TPA effect, and this resistance exceeds the one of the competing QKN against the CKN (see the green dashed curve of Fig. 3.15(f)).

3.6 conclusion

At the end of this chapter, the different numerical results of regeneration of truncated Airy pulse in fiber optics link through the CDM technique and SCG phenomenon of truncated Airy pulse in a cubic-quintic $AsSe_2/As_2S_5$ optical waveguide with a rib-like structure were presented. Considering the regeneration phenomenon, we have shown that the first model with an initial condition corresponding to the A.I. mechanism $GVD \times chirp < 0$ was the best at yielding interesting regeneration for both a single FEAP and the SFEAPs previously defined by S. Xiaohui et al in [29]. The main parameter that is beneficial for this kind of CDM regeneration of Airy pulses in fiber links was found to be the initial chirp whose dimensionless optimal absolute value $|C|$ should be included, for instance, in the range of $[1; 3]$ in order to combine the quality and good intensity. On the contrary, the temporal gap τ_B and the nonlinearity were shown to have a deleterious impact on regeneration. Moreover, the noise in the regeneration originates from the alternation of the chirp, the simultaneous alternation of GVD and chirp, the drastic increase in chirp, and nonlinearity. Considering the best configuration to obtain regeneration, we have shown that there is a need to realize the A.I. mechanism on each piece of fiber by achieving the condition $s \times C' < 0$, where the GVD sign is changed by alternating the pieces, and C' is the intrinsic chirp

developed by the pulse itself within the current f_i before its injection into the next piece f_{i+1} . Therefore, for weakly nonlinear optical systems with fiber links, considering a fixed absolute optimal value of the initial chirp with an alternation of GVD could be the best choice to achieve convenient regeneration of FEAP starting with the condition of the A.I. mechanism. For symmetric FEAPs, it is necessary to choose a rather small temporal gap. We expect that these features could be interesting for optical applications in zero-TOD systems where the initial chirp is used instead of TOD.

For the SCG phenomenon in the anomalous dispersion using the following pumping conditions describe in chapter 2, we obtained spectral 20 dB-bandwidths have been found to exceed approximately $97250nm$. The effects of the cooperative and competing QKN and NPAs, such as the TPA and $3PA$ is also made. In the case in which the NPA parameters are not taken into account, we show that only the cooperative QKN ($\gamma_1\gamma_2 > 0$) is beneficial for the MIR-SCG of the FEAP within this waveguide. In the temporal domain, the emission of DWs is avoided by the presence of NPAs, while the cooperative nonlinearities perform this emission. Furthermore, considering the cooperative QKN with the TPA when the $3PA$ is neglected is also interesting for the SI of the SCG, compared with the competition between the CKN and the QKN. Surprisingly, we show that the $3PA$ appears to be a good tool with which to control the TPA because, in the competitive case, the SI is less reduced than in the cooperative case. In particular, considering the competing nonlinearities ($\gamma_1\gamma_2 < 0$), the $3PA$ enhances the SI of the MIR-SCG of the truncated Airy pulse compared to the single TPA case for larger wavelengths.

General Conclusion

Summary and Contributions

In this thesis, we have studied truncated Airy pulse regeneration in fiber-optics link through the CDM technique and SCG phenomenon of truncated Airy pulse in a cubic-quintic $AsSe_2/As_2S_5$ optical waveguide with a rib-like structure. As presented in the first chapter, these processes are very useful in nonlinear optics allowing so several applications. In the review of literature, a brief overview on the optical pulse regeneration and the SCG phenomena has been done. In addition, the different waveguides studied in the thesis were described.

To achieve the purpose of the study, we have presented in the second chapter the different models with the numerical method used for the different phenomena studied. For instance, considering truncated Airy pulse regeneration in fiber-optics link through the CDM technique, the FT and the SSFM has been described assuming both the linear and the nonlinear cases of regeneration respectively. For the SCG analyses, the system was also described giving their higher-order CDP. In the last chapter, we have shown the numerical results obtained. Specifically, for CDM process for both single and symmetric FEAPs input pulses, the studies have highlighted the effects of the temporal gap, the CKN and the initial value of frequency chirp. Three models are considered: the first consists of alternation

of the GVD with the chirp being constant, the second consists of alternation of the chirp with a constant GVD, and the third consists of the alternation of both parameters. Assuming the linear regeneration of truncated chirped Airy pulse in fiber-optic links, we have showing that the first model with an initial condition corresponding to the A.I. mechanism $GVD \times chirp < 0$ was the best at yielding interesting regeneration for both a single FEAP and the SFEAPs previously defined by Xiaohui et al [29]. The main parameter that is beneficial for this kind of CDM regeneration of Airy pulses in fiber links was found to be the initial chirp whose dimensionless optimal absolute value $|C|$ should be included, for instance, in the range of $[1; 3]$ in order to combine the quality and good intensity because, increasing the initial chirp also increases the perturbation of the signal that could become more and more unstable; thus, $|C|_{opt}$ should include not only the increase of the intensity but also a good quality of regeneration. Considering the best configuration to obtain regeneration, we have shown that there is a need to realize the A.I. mechanism on each piece of fiber by achieving the condition $s \times C' < 0$, where the GVD sign is changed by alternating the pieces, and C' is the intrinsic chirp developed by the pulse itself within the current f_i before its injection into the next piece f_{i+1} . Assuming the linear regeneration of truncated chirped Airy pulse in fiber-optic links, we are showing that the noise in the regeneration process originates from the alternation of the chirp, the simultaneous alternation of GVD and chirp, the drastic increase in chirp, and nonlinearity. The increase of nonlinear parameter produces a noised regeneration even for the single and symmetric FEAPs.

At the end of this work, we suggest that to achieve efficiently the regeneration

of FEAP through the CDM technique, it is necessary to fulfill only the following points: (a) choose the best model, which is the first one (see Fig. 2.2); (b) use the initial condition of the A.I. mechanism; (c) in the nonlinear context, the value of N should be small; (d) the absolute initial value of the chirp should be a little high but not too high to avoid chirping dominating and destroying the quality of the regeneration [see the inset pictures in Fig. 3.12(a)] (we have chosen to manage $|C| \in [1; 3]$), and (e) for SFEAPs, use a small value of τ_B .

The thesis has also encompassed the study of the SCG in the case of the waveguide modeled by the CQNLSE with non-Kerr terms. Indeed, in this specific part of the work done in thesis, we have observed the different spectral outputs above, we notice that the main discrepancies appear in the high wavelengths of the MIR-region. Firstly, when we considered interaction between CKN and QKN, we observe that the drastic broadening that leads the pulse to explode over the whole bandwidth between 750 nm and 10^5 nm , does not appear at the same distance. For instance, for the case of the single CKN, it appears approximately around 0.024 m , in the case of cooperating nonlinearities, it appears around 0.016 m approximately. For the last case of competing nonlinearities, it appears only around 0.034 m approximately. This can be explained by the intrinsic action of the QKN : when it is positive, the QKN cooperates with the CKN in order to broaden the spectrum of the SCG and the nonlinearity of the medium is sufficiently high to have the appearance of the explosion very sooner than that of the single CKN. However, when the QKN is negative, the nonlinearity becomes smaller and the spectral explosion over the whole bandwidth between 750 nm and 10^5 nm arrives later in the propagation because the nonlinearity acts more weakly than both of the two pre-

vious cases. Therefore, in the case where the NPA parameters (TPA and 3PA) are not taken into account, only the cooperating QKN is beneficial for the MIR-SCG of the FEAP within rib-like structure. Secondly, when we considered interaction between the TPA and the combination of the nonlinearities, we demonstrates that the competition between the two nonlinearities is very detrimental for the MIR-SCG of the FEAP for the great wavelengths. One can note here that the cooperation enhances rather the SI of the SCG and thwarts the deleterious effect of the TPA. Thirdly, when we considered interaction between the 3PA and the combination of the nonlinearities, the $3PA$ normally should accentuate the TPA effect as a NPA parameter. This result is very interesting for the management of the QKN in the MIR-SCG of FEAP in the considered waveguide, specially for the great wavelengths. Thus, we can suggest here that, in the $AsSe_2/As_2S_5$ -ChRW structure, pumping in the MIR region allows to activate the $3PA$ which is rather beneficial for the SI of the SCG of Airy pulses compared to the TPA effect. Finally, when we considered the interaction between the TPA and the 3PA, we observed that for the cooperation case, the NPA (combination of TPA effect + 3PA effect) reduces the SI of the MIR-SCG of the FEAP than the single TPA case. On the other hand, for the competition case, the NPA (competition of TPA effect - 3PA effect) enhances the SI of the MIR-SCG of the FEAP than the single TPA case for the great wavelengths.

Following this analysis, we expect that we have got a good understanding of the impact of TPA, 3PA and interaction between the both on the spectral bandwidth enhancement of the SCG in the studied $AsSe_2/As_2S_5$ optical waveguide with a rib-like structure.

Perspectives

As perspectives, we should in future work conduct the experimental part of the theoretical and numerical studies presented in this thesis for practical confirmations. Furthermore, several paths of research raise from the thesis among which one can quote the investigation of coherence degree of the obtained spectra, birefringent (or polarized) optical waveguides, a nonlinear scattering process as the stimulated Brillouin scattering in the case of mechanisms and phenomena studied in the thesis, the investigation of actual promising waveguides as those based on the study of metamaterials, etc. About truncated Airy pulses regeneration, we want to use higher-order dispersion such that β_4 , β_5 and others with initial frequency chirp and modeling NLSE that includes higher-order effects in zero-TOD system.

Bibliography

- [1] G. P. Agrawal, *Applications of Nonlinear Fiber Optics*, (Academic Press, 1st edn 2008).
- [2] G. P. Agrawal, *Nonlinear Fiber Optics*, (Academic Press, 4th Ed., 2007).
- [3] N. M. Litchinitser, B. J. Eggleton, and D. B. Patterson, "*Fiber Bragg gratings for dispersion compensation in transmission: theoretical model and design criteria for nearly ideal pulse recompression*", *J. Lightwave Technol.* **15**, 1303-1313 (1997).
- [4] L. M. Mandeng and C. Tchawoua, "*Impact of input profile, absorption coefficients and chirp on modulational instability of femtosecond pulses in silicon waveguides under fourth-order dispersion*", *J. Opt. Soc. Am. B* **30**, 1382 (2013).
- [5] A. Sharafali, A.K. Shafeeque Ali, and M. Lakshmanan, "*Modulation instability induced supercontinuum generation in liquid core suspended photonic crystal fiber with cubic-quintic nonlinearities*", *Phys. Lett. A*, **399**, pp. 0375-9601(2021).
- [6] M. V. Berry and N. L. Balazs, "*Nonspreading wave packets*", *Am. J. Phys.* **47**, 264 (1979).

- [7] G. A. Siviloglou and D. N. Christodoulides, "*Accelerating finite energy Airy beam*", Opt. Lett. **32**, 979 (2007).
- [8] G. A. Siviloglou, J. Broky, A. Dogariu, and D. N. Christodoulides, "*Observation of accelerating Airy beams*", Phys. Rev. Lett. **99**, 213901 (2007).
- [9] J. Broky, G. A. Siviloglou, A. Dogariu, and D. N. Christodoulides, "*Self-healing properties of optical Airy beams*", Opt. Express **16**, 12880 (2008).
- [10] T. J. Eichelkraut, G. A. Siviloglou, I. M. Besieris, and D. N. Christodoulides, "*Oblique Airy wave packets in bidispersive optical media*", Opt. Lett. **35**, 3655 (2010).
- [11] P. Polynkin, M. Kolesik, J. Moloney, G. Siviloglou, and D. N. Christodoulides, "*Extreme nonlinear optics with ultra-intense self-bending airy beams*", Opt. Phot. News **21**, 38 (2010).
- [12] Y. Fattal, A. Rudnick, and D. M. Marom, "*Soliton shedding from airy pulses in Kerr media*", Opt. Express **19**, 17298 (2011).
- [13] L. M. Mandeng and C. Tchawoua, "*Chirped self-healing Airy pulses compression in silicon waveguides under fourth-order dispersion*", J. Mod. Opt. **60**, 359-367 (2013)
- [14] W. Liu, D. N. Neshev, I. V. Shadrivov, A. E. Miroshnichenko, and Y. S. Kivshar, "*Plasmonic Airy beam manipulation in linear optical potentia*", Opt. Lett. **36**, 1164-1166 (2011).

- [15] P. Zhang, S. Wang, Y. Liu, X. Yin, C. Lu, Z. Chen, and X. Zhang, "*Plasmonic Airy beams with dynamically controlled trajectories*", Opt. Lett. **36**, 3191-3193 (2011).
- [16] D. Abdollahpour, S. Suntsov, D. G. Papazoglou, and S. Tzortzakis, "*Spatiotemporal Airy light bullets in the linear and nonlinear regimes*", Phys. Rev. Lett. **105**, 253901 (2010).
- [17] A. Chong, W. H. Renninger, D. N. Christodoulides, and F. W. Wise, "*Airy-Bessel wave packets as versatile linear light bullets*", Nat. Photonics **4**, 103-106 (2010).
- [18] W. Cai, M. S. Mills, D. N. Christodoulides, and S. Wen, "*Soliton manipulation using Airy pulses*", Opt. Commun. **316**, 127-131 (2014).
- [19] S. I. Fewo, "*Ultrashort optical solutions in doped nonlinear optical fibers*," (Ph.D thesis, Cameroon, Laboratory of Mechanics, Department of Physics, Faculty of Science, University of Yaoundé, 2008).
- [20] J. Atangana, "*Dynamique des impulsions lumineuses ultra-brèves dans les fibres optiques fortement perturbées*," (Ph.D thesis, Cameroon, Laboratory of Electronics, Department of Physics, Faculty of Science, University of Yaoundé, 2009).
- [21] C. G. L. Tiofack, "*Modulational instability and ultrashort pulse propagation in Erbium doped fiber*," (Ph.D thesis, Cameroon, Laboratory of Mechanics, Department of Physics, Faculty of Science, University of Yaoundé, 2011).

- [22] L. M. Mandeng, "*Ultra-short pulses compression and supercontinuum generation in optical waveguides : cases of SMFs, SOI-waveguides and CS₂ – LCPCFs*," (Ph.D thesis, Cameroon, Laboratory of Mechanics, Department of Physics, Faculty of Science, University of Yaoundé I, 2015).
- [23] R. Driben, Y. Hu, Z. Chen, B. A. Malomed, and R. Morandotti, "*Inversion and tight focusing of Airy pulses under the action of third-order dispersion*", Opt. Lett. **38**, 2499 (2013).
- [24] W. Cai, L. Wang, and S. Wen, "*Evolution of airy pulses in the present of third order dispersion*", Optik **124**, 5833-5836 (2013).
- [25] R. Driben and T. Meier, "*Regeneration of Airy pulses in fiber-optic links with dispersion management of the two leading dispersion terms of opposite signs*", Phys. Rev. A **89**, 043817 (2014).
- [26] L. M. Mandeng and C. Tchawoua, "*Asymmetric inversion of Airy pulses induced by the interaction between the initial chirp and the group-velocity dispersion in a single mode fiber*", in Frontiers in Optics Conference, OSA Technical Digest (online) (Optical Society of America, 2014), paper **FTh4B.5**.
- [27] L. Zhang, K. Liu, H. Zhong, J. Zhang, Y. Li, and D. Fan, "*Effect of initial frequency chirp on Airy pulse propagation in an optical fiber*", Opt. Express **23**, 2566 (2015).
- [28] L. M. Mandeng, C. Tchawoua, H. Tagwo, M. Zghal, R. Cherif, and A. Mohamadou, "*Role of the input profile asymmetry and the chirp on the propagation in highly dispersive and nonlinear fibers*", J. Lightwave Technol. **34**, 5635 (2016).

- [29] S. Xiaohui, H. Xianwei, D. Yangbao, T. Chao, B. Yanfeng, and F. Xiquan, "*Dynamic propagation of symmetric Airy pulses with initial chirps in an optical fiber*", Opt. Commun. **399**, 16 (2017).
- [30] S. Wang, D. Fan, X. Bai, and X. Zeng, "*Propagation dynamics of Airy pulses in optical fibers with periodic dispersion modulation*", Phys. Rev. A **89**, 023802 (2014).
- [31] C. Ament, P. Polynkin, and J. V. Moloney, "*Supercontinuum generation with femtosecond self-healing airy pulses*", Phys. Rev. Lett. **107**, 243901 (2011).
- [32] N. Bonnard et al 2013 Form written by the "*Institut National de Recherche et de Sécurité*" (INRS) (available at: www.inrs.fr)
- [33] R. V. J. Raja, K. Porsezian and K. Nithyanandan; "*Modulational instability-induced supercontinuum generation with saturable nonlinear response*", Phys. Rev. A **82** 013825 (2010).
- [34] R. Cherif, "*Highly nonlinear As₂Se₃-based chalcogenide photonic crystal fiber for mid-infrared supercontinuum generation*", Opt. Eng. **49** 095002 (2010).
- [35] M. Diouf, A. B. Salem, R. Cherif, A. Wague and M. Zghal; "*High power broadband mid-infrared supercontinuum fiber laser using a novel chalcogenide AsSe₂ photonic crystal fiber*", Opt. Mater. **55** 10-16 (2016).
- [36] A. B. Salem, M. Diouf, R. Cherif, A. Wague and M. Zghal ; "*Ultraflat-top mid-infrared coherent broadband supercontinuum using all normal As₂S₅-borosilicate hybrid photonic crystal fiber*", Opt. Eng. **55** 066109 (2016).

- [37] M. Diouf, A. B. Salem, R. Cherif, H. Saghaei and A. Wague; "*Super-flat coherent supercontinuum source in $As_{38.8}Se_{61.2}$ chalcogenide photonic crystal fiber with all-normal dispersion engineering at a very low input energy*", Appl. Opt. **56** 163 (2017).
- [38] M. Diouf, A. Wague, and M. Zghal, "*Numerical investigation of an ultra-broadband coherent mid-infrared supercontinuum in a chalcogenide $AsSe_2 - As_2S_5$ multimaterial photonic crystal fiber*", J. Opt. Soc. Amer. B, vol. **36**, pp. A8-A14, (2018).
- [39] M. Diouf, R. Cherif, A. B. Salem, and A. Wague, "*Ultra-broadband, coherent mid-IR supercontinuum expanding from 1.5 to 12.2 μm in new design of $AsSe_2$ photonic crystal fiber*", J. Modern Opt., vol. **64**, pp. 1335-1341, (2017).
- [40] M. Diouf, L. M. Mandeng, C. Tchawoua, and M. Zghal, "*Numerical investigation of supercontinuum generation through $AsSe_2/As_2S_5$ chalcogenide photonic crystal fibres and rib structures*", J. Lightwave Technol. **37**, 22 (2019).
- [41] M. R. Karim, H. Ahmad, and B. M. Rahman, "*All-normal-dispersion chalcogenide waveguides for ultraflat supercontinuum generation in the mid-infrared region*", IEEE J. Quantum Electron., vol. **53**, no. **2**, Apr. (2017), Art. no. **7100106**.
- [42] T. S. Saini, A. Kumar, and R. K. Sinha, "*Design and modelling of dispersion-engineered rib waveguide for ultra-broadband mid-infrared supercontinuum generation*", J. Modern Opt. **64**, 143-149 (2017).

- [43] T. S. Saini et al., "Coherent mid-infrared supercontinuum generation using a rib waveguide pumped with 200 fs laser pulses at 2.8 μm ", Appl. Opt. **57**, 1689 (2018).
- [44] A. Medjouri, D. Abed, O. Ziane, and L. M. Simohamed, "Design and optimization of As_2S_5 chalcogenide channel waveguide for coherent mid-infrared supercontinuum generation", Optik **154**, 811-820 (2018).
- [45] M. R. Karim, H. Ahmad, S. Ghosh, and B. M. A. Rahman, "Design of dispersion-engineered As_2Se_3 channel waveguide for mid-infrared region supercontinuum generation", J. Appl. Phys. **123**, 213101 (2018).
- [46] H. Saghaei, "Dispersion-engineered microstructured optical fiber for mid-infrared supercontinuum generation", Appl. Opt **57**, 5591 (2018).
- [47] M. Sinobad et al., "Mid-infrared octave spanning supercontinuum generation to 8.5 μm in silicon-germanium waveguides", Optica **5**, 360 (2018).
- [48] M. Sinobad et al., "Dispersion trimming for mid-infrared supercontinuum generation in a hybrid chalcogenide/silicon-germanium waveguide", J. Opt. Soc. Amer. B **36**, A98-A104 (2019).
- [49] S. Dai, Y. Wang, X. Peng, P. Zhang, X. Wang, and Y. Xu, "A review of mid-infrared supercontinuum generation in chalcogenide glass fibers", Appl. Sci. **8**, 707 (2018).
- [50] M. Asorey, P. Facchi, V. I. Man'ko, G. Marmo, S. Pascazio, and E. C. G. Sudarshan, "Generalized quantum tomographic map", Phys. Rev. A **77**, 042115 (2008).

- [51] L. M. Mandeng and C. Tchawoua, "*Nonlinear compression of self-healing Airy pulses in silicon-on-insulator waveguides*", in *Frontiers in Optics Conference*, OSA Technical Digest (online) (Optical Society of America, 2012), paper FW3A.36.
- [52] V. Nathan and A. H. Guenther, "*Review of multiphoton absorption in crystalline solids*", *J. Opt. Soc. Am. B* **2**, 294 (1985).
- [53] F. E. Hernández, K. D. Belfield, I. Cohanoschi, M. Balu, and K. J. Schafer, "*Three- and four-photon absorption of a multiphoton absorbing fluorescent probe*", *Appl. Opt.* **43**, 5394 (2004).
- [54] L. Qian, K. Senthilnathan, K. Nakkeeran, and P.K.A. Wai, "*nearly chirp-and pedestal-free pulse compression in nonlinear fiber Bragg gratings*" *J. Opt. Soc. Am. B* **26**, 432-443 (2009).
- [55] C.E. Shannon, "*A mathematical theory of communication*", *Bell Syst. Technol. J.* **27** (1948) 379-423 623-656.
- [56] C.E. Shannon, W. Weaver, *The Mathematical Theory of Communication*, University of Illinois Press, 1963.
- [57] A. D. Ellis, J. Zhao, Channel capacity of non-linear transmission systems, in: S. Kumar (Ed.), *Impact of Nonlinearities on Fiber Optic Communications*, *Optical and Fiber Communications Reports*, vol. **7**, Springer, 2011.
- [58] R. S. Tucker, K. Hinton, "*Energy consumption and energy density in optical and electronic signal processing*", *IEEE Photon. J.* **3** (5) (2011) 821-833.

- [59] L. K. Oxenløwe, H. C. Hansen Mulvad, H. Hu, H. Ji, M. Galili, M. Pu, E. Palushani, K. Yvind, J. M. Hvam, A. T. Clausen, P. Jeppesen, *Ultrafast nonlinear signal processing in silicon waveguides*, in: Proceedings of the OFC 2012, Los Angeles, California, USA, Paper OTh3H.5, 2012.
- [60] J. Kakande, R. Slavik, F. Parmigiani, P. Petropoulos, D. Richardson, "All-optical processing of multi-level phase shift keyed signals", in: Proceedings of the OFC 2012, Los Angeles, California, USA, Paper OW1I, 2012.
- [61] R. Slavík, F. Parmigiani, J. Kakande, C. Lundström, M. Sjödin, P. A. Andrekson, R. Weerasuriya, S. Sygletos, A. D. Ellis, L. Grüner-Nielsen, D. Jakobsen, S. Herstrøm, R. Phelan, J. O’Gorman, A. Bogris, D. Syvridis, S. Dasgupta, P. Petropoulos, D. J. Richardson, "All-optical phase and amplitude regenerator for next-generation telecommunications systems", *Nat. Photon.* **4** (2010) 690-695.
- [62] P. Andrekson, "Phase sensitive fiber optic parametric amplifiers", in: Proceedings of the ECOC 2011, Geneva, Switzerland, Paper Th.11, 2011.
- [63] E. Palushani, T. Richter, R. Ludwig, C. Schubert, H.C. Hansen Mulvad, A.T. Clausen, L.K. Oxenløwe, *OTDM-to-WDM conversion of complex modulation formats by timedomain optical Fourier transformation*, in: Proceedings of the OFC 2012, Los Angeles, California, USA, Paper OTh3H.2, 2012.
- [64] A. Bogoni, X. Wu, S.R. Nuccio, A.E. Willner, "640 Gb/s all-optical regenerator based on a periodically poled lithium niobate waveguide", *J. Lightwave Technol.* **30** (12) (2012) 1829-1834.

- [65] S. Watanabe, F. Futami, R. Okabe, Y. Takita, S. Ferber, R. Ludwig, C. Schubert, C. Schmidt, H.G. Weber, "160 Gbit/s optical 3R-regenerator in a fiber transmission experiment", in: Proceedings of the OFC 2003, Atlanta, Georgia, USA, vol. **3**, Paper PD16-P1-3 2003.
- [66] F. Parmigiani, L.K. Oxenløwe, M. Galili, M. Ibsen, D. Zibar, P. Petropoulos, D.J. Richardson, A.T. Clausen, P. Jeppesen, "All-optical 160-Gbit/s retiming system using fiber grating based pulse shaping technology", J. Lightwave Technol. **27** (9) (2009) 1135-1141.
- [67] Irène et Michel Joindot et douze co-auteurs, *Les télécommunications par fibres optiques*. DUNOD et CNET-ENST, 1996.
- [68] K. Nakkeeran et al., "Analytical design of densely dispersion-managed optical fiber transmission systems with Gaussian and raised cosine return-to-zero Ansätze", J. Opt. Soc. Am. B **21**, 1901 (2004).
- [69] C. M. Ngabireng et al., "Radiating and nonradiating behavior of hyperbolic-secant, raised-cosine, and Gaussian input light pulses in dispersion-managed fiber systems", Phys. Rev. E **72**, 036613 (2005).
- [70] P. Saari, "Laterally accelerating airy pulses", Opt. Express **16**, 10303 (2008).
- [71] P. Saari, "Airy pulse-a new member of family of localized waves", Laser Physics **19**, 725 (2009).
- [72] I. M. Besieris and A. M. Shaarawi, "A note on an accelerating finite energy Airy beam", Opt. Lett. **32**, 2447 (2007).

- [73] R. Bekenstein and M. Segev, "*Self-accelerating optical beams in highly non-local nonlinear media*", Opt. Express **19**, 23706 (2011).
- [74] M. A. Bandres and J. C. Gutiérrez-Vega, "*Airy-Gauss beams and their transformation by paraxial optical systems*", Opt. Express **15**, 16719 (2007).
- [75] H. I. Sztul and R. R. Alfano, "*The Poynting vector and angular momentum of Airy beams*", Opt. Express **16**, 9411 (2008);
- [76] M. Asorey et al., "*Generalized tomographic maps*", Phys. Rev. A. **77**, 042115 (2008); H. T. Dai et al., "*Airy beams generated by a binary phase element made of polymer-dispersed liquid crystals*", Opt. Express **17**, 19365 (2009); P. Polynkin et al., "*Curved plasma channel generation using ultraintense Airy beams*", Science **324**, 229 (2009); A. V. Novitsky and D. V. Novitsky, "*Non-paraxial Airy beams: role of evanescent waves*", Opt. Lett. **34**, 3430 (2009); A. Salandrino and D. N. Christodoulides, "*Airy plasmon: a nondiffracting surface wave*", Opt. Lett. **35**, 2082 (2010).
- [77] A. V. Gorbach and D. V. Skryabin, "*Soliton self-frequency shift, non-solitonic radiation and self-induced transparency in air-core fibers*", Opt. Express **16**, 4858 (2008).
- [78] Y. Kaganovsky and E. Heyman, "*Airy pulsed beams*", J. Opt. Soc. Am. A **28**, 1243 (2011).
- [79] I. Kaminer, M. Segev, and D. N. Christodoulides, "*Accelerating light beams along arbitrary convex trajectories*", Phys. Rev. Lett. **106**, 213903 (2011).

- [80] I. Kaminer et al., "*Causality effects on accelerating light pulses*", Opt. Express **19**, 23132 (2011).
- [81] A. Rudnick and D. M. Marom, "*Airy-soliton interactions in Kerr media*", Opt. Express **19**, 25570 (2011).
- [82] G. Zhou, R. Chen, and X. Chu, "*Fractional Fourier transform of Airy beams*", Appl. Phys. B **109**, 549 (2012); P. Piksarv et al., "*Temporal focusing of ultrashort pulsed Bessel beams into Airy-Bessel light bullets*", Opt. Express **20**, 17220 (2012); N. Voloch-Bloch et al., Nature **494**, 331 (2013).
- [83] I. M. Besieris and A. M. Shaarawi, "*Accelerating Airy wave packets in the presence of quadratic and cubic dispersion*", Phys. Rev. E **78**, 046605 (2008).
- [84] D. Marcuse, "*Pulse distortion in single-mode fibers*", Appl. Opt. **20**, 3573 (1981).
- [85] O. Leclerc, B. Lavigne, E. Balmefrezol, P. Brindel, L. Pierre, D. Rouvillain, and F. Segueineau, "*Optical regeneration at 40 Gb/s and beyond*", J. Lightw. Technol., vol. **21**, no. 11, pp. 2779-2790, 2003.
- [86] Biswas, Anjan, Daniela Milovic, and Matthew Edwards. "*Mathematical theory of dispersion-managed optical solitons*". Springer Science and Business Media, 2010.
- [87] J. C. Simon, "*GaInAsP semiconductor laser amplifiers for single-mode fiber communications*", J. Lightw. Technol., vol. **5**, no. **9**, pp. 1286-1295, (1987).
- [88] E. Desurvive, "*Erbium-Doped Fiber Amplifiers : Principles and Applications. John Wiley and Sons*", Inc, 1994, vol. **605**.

- [89] P. Becker, N. Olsson, and J. Simpson, "*Erbium-doped fiber amplifiers : fundamentals and technology*". Academic Press, 1999.
- [90] M. Islam, "*Raman amplifiers for telecommunications*", IEEE J. Sel. Topics Quantum Electron., vol. **8**, no. **3**, pp. 548-559, (2002).
- [91] Q. T. Le, "*Contribution à l'étude de fonctions optiques pour la régénération du signal dans les systèmes de transmission à haut débit*", Ph.D. dissertation, ENSSAT - Université de Rennes 1, Lannion, France, 2010.
- [92] G. P. Agrawal, *Fiber-Optic Communication Systems*, 4th ed. (Wiley, 2010).
- [93] A. Hasegawa and Y. Kodama, "*Bistable pulse collisions of the cubic-quintic nonlinear Schrödinger equation*", Proc. IEEE **69**, 145 (1981); Opt. Lett. **7**, 285 (1982).
- [94] Y. Kodama and A. Hasegawa, "*Amplification and reshaping of optical solitons in glass fiber-III. Amplifiers with random gain*", Opt. Lett. **7**, 339 (1982); Opt. Lett. **8**, 342 (1983).
- [95] A. Hasegawa, "*Demonstration of soliton transmission over more than 4000 km in fiber with loss periodically compensated by Raman gain*", Opt. Lett. **8**, 650 (1983); Appl. Opt. **23**, 3302 (1984).
- [96] L. F. Mollenauer, R. H. Stolen, and M. N. Islam, "*Experimental demonstration of soliton propagation in long fibers: Loss compensated by Raman gain*", Opt. Lett. **10**, 229 (1985).
- [97] L. F. Mollenauer, J. P. Gordon, and M. N. Islam, "*Theory of the soliton self-frequency shift*", IEEE J. Quantum Electron. QE-22, **157** (1986).

- [98] L. F. Mollenauer and K. Smith, "*Demonstration of soliton transmission over more than 4000 km in fiber with loss periodically compensated by Raman gain*", Opt. Lett. **13**, 675 (1988).
- [99] M. Nakazawa, Y. Kimura, and K. Suzuki, "*Soliton amplification and transmission with Er/sup 3 + /-doped fibre repeater pumped by GaInAsP diode*", Electron. Lett. **25**, 199 (1989).
- [100] M. Nakazawa, K. Suzuki, and Y. Kimura, "*Nonlinear Phenomena in Optical Fibres*", IEEE Photon. Technol. Lett. **2**, 216 (1990).
- [101] A. Husakou and J. Herrmann, "*Supercontinuum generation, four-wave mixing, and fission of higher-order solitons in photonic-crystal fibers*", J. Opt. Soc. Am. B **19**, 2171 (2002).
- [102] J. P. Gordon and H. A. Haus, "*Theory of the soliton self-frequency shift*", Opt. Lett. **11**, 665 (1986).
- [103] L. F. Mollenauer, J. P. Gordon, and P. V. Mamyshev, *Optical Fiber Telecommunications III*, in I. P. Kaminow and T. L. Koch, Eds. (Academic Press, 1997), Chap. **12**
- [104] E. Iannone, F. Matera, A. Mecozzi, and M. Settembre, *Nonlinear Optical Communication Networks* (Wiley, 1998).
- [105] F. M. Knox, W. Forysiak, N. J. Doran, "*10-Gbt/s soliton communication systems over standard fiber at 1.55/spl mu/m and the use of dispersion compensation*", IEEE J. Lightwave Technol. **13** (1995) 1960-1995.

- [106] M. Suzuki, I. Morita, N. Edagawa, S. Yamamoto, H. Taga, S. Akiba, "*Reduction of Gordon-Haus timing jitter by periodic dispersion compensation in soliton transmission*", Electron. Lett. **31** (1995) 2027-2035.
- [107] H. A. Haus, K. Tamura, L.E. Nelson, E.P. Ippen, "*Stretched-pulse additive pulse mode-locking in fiber ring lasers: theory and experiment*", IEEE J. Quantum Electron. **31** (1995) 591-595.
- [108] N. Smith, F.M. Knox, N.J. Doran, K.J. Blow, I. Bennion, "*Enhanced power solitons in optical fibres with periodic dispersion management*", Electron. Lett. **32** (1996) 54-60.
- [109] I. Gabitov, S. K. Turitsyn, *Preprint Los Alamos*, LAUR-95 (1995) 3633-3635; I. Gabitov, S. K. Turitsyn, "*Averaged pulse dynamics in a cascaded transmission system with passive dispersion compensation*", Opt. Lett. **21** (1996) 327-328.
- [110] V. E. Zakharov, A. B. Shabat, "*Physics and mathematics of dispersion-managed optical solitons*", Sov. Phys. JETP **33** (1971) 77-83.
- [111] A. Hasegawa, Y. Kodama, A. Maruta, "*Recent progress in dispersion-managed soliton transmission technologies*", Opt. Fiber Technol. **3** (1997) 197-200.
- [112] I. Dolev, T. Ellenbogen, and A. Arie, "*Switching the acceleration direction of Airy beams by a nonlinear optical process*", Optics Lett. **35**, 1581 (2010).
- [113] B. J. Eggleton, R. E. Slusher, C. M. de Sterke, P. A. Krug, and J. E. Sipe, "*Bragg grating solitons*", Phys. Rev. Lett. **76**, 1627-1630 (1996).

- [114] W. Xin, Y. Wang, Z. Xin and L. Li, "*Inversion of Airy pulses in nonlinear femtosecond optical system*", Opt. Commun. **489**, 126889 (2021).
- [115] H. Haus, "*Quantum noise in a solitonlike repeater system*", J. Opt. Soc. Am. B **8**, 1122 (1991).
- [116] R. R. Alfano, *The Supercontinuum Laser Source* (Springer-Verlag, New York, 1989).
- [117] H. Takara et al., "*More than 1000 channel optical frequency chain generation from single supercontinuum source with 12.5 GHz channel spacing*", Electron. Lett. **36**, 2089 (2000).
- [118] A. Hasegawa and F. Tappert, "*Transmission of stationary nonlinear optical pulses in dispersive dielectric fibers.* ", Appl. Phys. Lett. **23**, 142 (1973).
- [119] A. V. Gusakov, V. P. Kalosha, and J. Herrmann, "*Ultrawide spectral broadening and pulse compression in tapered and photonic fibers*", QELS, pp. **29** (2001).
- [120] B. Schenkel, R. Paschotta, and U. Keller, "*Pulse compression with supercontinuum generation in microstructure fibers*", J. Opt. Soc. Am. B **22**, 687 (2005).
- [121] J. M. Dudley and J. R. Taylor, 1st ed. Cambridge, U.K.: Cambridge Univ. Press, (2010).
- [122] V. Nathan and A. H. Guenther; "*Review of multiphoton absorption in crystalline solids*", J. Opt. Soc. Am. B **2**, 294 (1985).

- [123] F. E. Hernandez, K. D. Belfield, I. Cohanoschi, M. Balu and K. J. Schafer; "*Three-and four-photon absorption of a multiphoton absorbing fluorescent probe*", Appl. Opt. **43** 5394 (2004).
- [124] W. Chen, S. Bhaumik, S. A. Veldhuis, G. Xing, Q. Xu, M. Grätzel, S. Mhaisalkar, N. Mathews and T. C. Sum; "*Giant five-photon absorption from multidimensional core-shell halide perovskite colloidal nanocrystals*", Nat. Commun. **15198** (2017).
- [125] L. M. Mandeng, A. Mohamadou, C. Tchawoua and H. Tagwo; "*Spectral compression in supercontinuum generation through the higher-order nonlinear Schrödinger equation with non-Kerr terms using subnanjoule femtosecond pulses*", J. Opt. Soc. Am. B **30**, 2555 (2013).
- [126] X. Zhong, X. Du and K. Cheng K; "*Evolution of finite energy Airy pulses and soliton generation in optical fibers with cubic-quintic nonlinearity*", Opt. Express **23** 29467 (2015).
- [127] H. Ebendorff-Heidepriem et al., "*Bismuth glass holey fibers with high nonlinearity*", Opt. Express **12**, 5082 (2004).
- [128] X. Feng et al., "*Single-mode tellurite glass holey fiber with extremely large mode area for infrared nonlinear applications*", Opt. Express **16**, 13651 (2008).
- [129] X. Feng et al., "*Nonsilica glasses for holey fibers*", IEEE J. Lightwave Technol, **23**, 2046, (2005).

- [130] J. M. Dudley, G. Genty, and S. Coen, "*Rogue-wave-like characteristics in femtosecond supercontinuum generation*", Rev. Mod. Phys., vol. **78**, (2006), Art. no. **1135**.
- [131] B. Kibler, "*Propagation nonlinéaire d'impulsions ultracourtes dans les fibres optiques de nouvelle génération*," (Ph.D thesis, France, University of Franche-Comté, Doctoral school of physical sciences for engineers and microtechnics, FEMTO-ST institut, departement of Optics P. M. Duffieux, 2007).
- [132] A. V. Husakou and J. Herrmann, "*Supercontinuum generation of higher-order solitons by fission in photonic crystal fibers*", Phys. Rev. Lett. **87**, 203901 (2001).
- [133] J. Herrmann et al., "*Experimental evidence for supercontinuum generation by fission of higher-order solitons in photonic fibers*", Phys. Rev. Lett. **88**, 173901 (2002).
- [134] L. Tartara, I. Cristiani, and V. Degiorgio, "*Blue light and infrared continuum generation by soliton fission in a microstructured fiber*", Appl. Phys. B **77**, 309 (2003).
- [135] A. Demircan and U. Bandelow, "*Analysis of the interplay between soliton fission and modulation instability in supercontinuum generation*", Appl. Phys. B **86**, 31 (2007).
- [136] J. C. Travers, "*Using the E22 transition of carbon nanotubes for fiber laser mode-locking*", J. Opt., vol. **12**, (2010), Art. no. **113001**.

- [137] S. Roy, S. K. Bhadra and G. P. Agrawal, "*Dispersive waves emitted by solitons perturbed by third-order dispersion inside optical fibers*", Phys. Rev. A **79**, 023824 (2009).
- [138] S. Roy, S. K. Bhadra and G. P. Agrawal, "*Perturbation of higher-order solitons by fourth-order dispersion in optical fibers*", Opt. Comm. **282**, 3798 (2009).
- [139] S. Roy, S. K. Bhadra and G. P. Agrawal, "*Effects of higher-order dispersion on resonant dispersive waves emitted by solitons*", Opt. Lett. **34**, 2072 (2009).
- [140] S. Roy, S. K. Bhadra and G. P. Agrawal, "*Dispersive wave generation in supercontinuum process inside nonlinear microstructured fiber*", Curr. Sci. **100**, 321 (2011).
- [141] L. Yin, Q. Lin, and G. P. Agrawal, "*Optical solitons in a silicon waveguide*", Opt. Lett., vol. **32**, (2007), Art. no. **391**.
- [142] R. J. R. Vasantha, K. Porsezian, and K. Nithyanandan, "*Modulational-instability-induced supercontinuum generation with saturable nonlinear response*", Phys. Rev. A **82**, 013825 (2010).
- [143] R. Zhang, J. Teipel, and H. Giessen, "*Theoretical design of a liquid-core photonic crystal fiber for supercontinuum generation*", Opt. Express **14**, 6800 (2006).
- [144] C. Yu et al., "*Tunable dual-core liquid-filled photonic crystal fibers for dispersion compensation*", Opt. Express **16**, 4443 (2008).

- [145] H. Zhang et al., "*Supercontinuum generation in chloroform-filled photonic crystal fibers*", *Optik* **121**, 783 (2010).
- [146] (a) Y. Sato, R. Morita, and M. Yamashita, "*Study on ultrafast dynamic behaviors of different nonlinear refractive index components in CS₂ using a femtosecond interferometer*", *Jpn. J. Appl. Phys.* **36**, 2109 (1997); (b) Z. Liu et al., "*Nonlinear absorption and optical limiting properties of carbon disulfide in a short-wavelength region*", *J. Opt. Soc. Am. B* **24**, 1101 (2007).
- [147] N. I. Nikolov et al., "*Improving efficiency of supercontinuum generation in photonic crystal fibers by direct degenerate four-wave mixing*", *J. Opt. Soc. Am. B* **20**, 2329 (2003).
- [148] G. Genty, S. Coen, and J. M. Dudley, "*Fiber supercontinuum sources*", *J. Opt. Soc. Am. B* **24**, 1771 (2007).
- [149] A. M. Heidt, "*Pulse preserving flat-top supercontinuum generation in all-normal dispersion photonic crystal fibers*", *J. Opt. Soc. Am. B* **27**, 550 (2010).
- [150] H. Tu et al., "*Nonlinear polarization dynamics in a weakly birefringent all-normal dispersion photonic crystal fiber: toward a practical coherent fiber supercontinuum laser*", *Opt. Express* **20**, 1113 (2012).
- [151] (a) D. Castelló-Lurbe et al., "*Spectral broadening enhancement in silicon waveguides through pulse shaping*", *Opt. Lett.* **37**, 2757 (2012); (b) M. Klimczak et al., "*Impact of steepness of pump temporal pulse profile on spectral flatness and correlation of supercontinuum in all-solid photonic crystal fibers with flattened normal dispersion*", *J. Opt.* **16**, 085202 (2014).

- [152] Z. Zhu, T. G. Brown, "*Effect of frequency chirping on supercontinuum generation in photonic crystal fibers*", Opt. Express **12**, 689 (2004).
- [153] X. Hu et al., "*Nonlinear chirped-pulse propagation and supercontinuum generation in photonic crystal fibers*", Applied Optics **49**, 4984 (2010).
- [154] J. M. Dudley and S. Coen, "*Coherence properties of supercontinuum spectra generated in photonic crystal and tapered optical fibers*", Opt. Lett. **27**, 1180 (2002).
- [155] R. Boyd, *Nonlinear Optics*, (Academic Press, San Diego, CA, 3rd Ed., 2008).
- [156] P. M. Morse and H. Feshbach, *Methods of Theoretical Physics* (McGraw-Hill, New York, 1953), Chap. 9.
- [157] P. V. Mamyshev and S. V. Chernikov, "*Ultrashort-pulse propagation in optical fibers*", Opt. Lett. **15**, 1076 (1990).
- [158] S. V. Chernikov and P. V. Mamyshev, "*Femtosecond soliton propagation in fibers with slowly decreasing dispersion*", J. Opt. Soc. Am. B **8**, 1633 (1991).
- [159] F. DeMartini et al., "*Self-steepening of light pulses*", Phys. Rev. **164**, 312 (1967).
- [160] J. W. Cooley and J. W. Tukey, "*An algorithm for the machine calculation of complex Fourier series*", Math. Comput. **19**, 297 (1965).
- [161] T. R. Taha and M. J. Ablowitz, "*Analytical and numerical aspects of certain nonlinear evolution equations*", J. Comput. Phys. **55**, 203 (1984).
- [162] J. A. Fleck, J. R. Morris, and M. D. Feit, "*Time-dependent propagation of high energy laser beams through the atmosphere*", Appl. Phys. **10**, 129 (1976).

- [163] C. D. Poole and J. Nagel, in *Optical Fiber Telecommunications III*, Vol. A, I. P. Kaminow and T. L. Koch, Eds. (Academic Press, 1997), Chap.6.
- [164] M. Lax, J. H. Batteh, and G. P. Agrawal, "*Channeling of intense electromagnetic beams*", J. Appl. Phys. **52**, 109 (1981).
- [165] M. D. Feit and J. A. Fleck, "*Calculation of dispersion in graded-index multimode fibers by a propagating-beam method*", Appl. Opt. **18**, 2843 (1979).
- [166] G. P. Agrawal, "*Nonlinear Fiber Optics, (Optics and Photonics)*", J. Light-wave Technol. **2**, 537 (1984).
- [167] M. Lax, G. P. Agrawal, M. Belic, B. J. Coffey, and W. H. Louisell, "*Electromagnetic-field distribution in loaded unstable resonators*", J. Opt. Soc. Am. A **2**, 732 (1985).
- [168] B. Hermansson, D. Yevick, and P. Danielsen, "*Propagating beam analysis of multimode waveguide tapers*", IEEE J. Quantum Electron. **19**, 1246 (1983).
- [169] L. Thylen, E. M. Wright, G. I. Stegeman, C. T. Seaton, and J. V. Moloney, "*Beam-propagation method analysis of a nonlinear directional coupler*", Opt. Lett. **11**, 739 (1986).
- [170] G. P. Agrawal and M. J. Potasek, "*Nonlinear pulse distortion in single-mode optical fibers at the zero-dispersion wavelength*", Phys. Rev. A **33**, 1765 (1986).
- [171] R. H. Hardin and F. D. Tappert, SIAM Rev. "*Chronicle*" **15**, 423 (1973).

- [172] O. V. Sinkin, R. Holzlöhner, J. Zweck, and C. R. Menyuk, "*Optimization of the split-step Fourier method in modeling optical-fiber communications systems*", J. Lightwave Technol. **21**, 61 (2003).
- [173] J. Van Roey, J. van der Donk, and P. E. Lagasse, "*Beam-propagation method: analysis and assessment*", J. Opt. Soc. Am. **71**, 803 (1981).
- [174] L. Thylen, "*The beam propagation method: an analysis of its applicability*", Opt. Quantum Electron. **15**, 433 (1983).
- [175] J. Saijonmaa and D. Yevick, "*Beam-propagation analysis of loss in bent optical waveguides and fibers*", J. Opt. Soc. Am. **73**, 1785 (1983).
- [176] D. Yevick and B. Hermansson, "*A guide to electric field propagation techniques for guided-wave optics*", IEEE J. Quantum Electron. **25**, 221 (1989).
- [177] T. Kremp and W. Freude, "*Fast split-step wavelet collocation method for WDM system parameter optimization*", J. Lightwave Technol. **23**, 1491 (2005).
- [178] G. Boudebs, S. Cherukulappurath, H. Leblond, J. Troles, F. Smektala, and F. Sanchez, "*Experimental and theoretical study of higher-order nonlinearities in chalcogenide glasses*", Opt. Commun, **219**, 427 (2003).
- [179] G. S. Parmar, S. Jana, and B. A. Malomed, "*Dissipative soliton fiber lasers with higher-order nonlinearity, multiphoton absorption and emission, and random dispersion*", J. Opt. Soc. Amer. B **34**, 850 (2017).
- [180] M. Sinobad et al., "*Mid-infrared octave spanning supercontinuum generation to 8.5 μm in silicon-germanium waveguides*", Optica **5**, 360 (2018).

- [181] M. Asorey, P. Facchi, V. I. Man'ko, G. Marmo, S. Pascazio, and E. C. G. Sudarshan, "*Generalized tomographic maps*", Phys. Rev. A **77**, 042115 (2008).
- [182] W. Liu, D. N. Neshev, I. V. Shadrivov, A. E Miroshnichenko, Y. S. Kivshar, "*Plasmonic Airy beam manipulation in linear optical potentials*", Opt. Lett. **36**, 1164 (2011).
- [183] Q. Lin, O. J. Painter, and G. P. Agrawal, "*Nonlinear optical phenomena in silicon waveguides: modeling and applications*", Opt. Express **15**, 16604 (2007).
- [184] L. Yin and G. P. Agrawal, "*Impact of two-photon absorption on self-phase modulation in silicon waveguides*", Opt. Lett. **32**, 2031 (2007).
- [185] L. Yin, Q. Lin, and G. P. Agrawal, "*Soliton fission and supercontinuum generation in silicon waveguides*", Opt. Lett. **32**, 391 (2007).
- [186] M. Lipson, "*Guiding, modulating, and emitting light on silicon-challenges and opportunities*", J. Lightwave Technol. **23**, 4222 (2005).
- [187] G. Boudebs, S. Cherukulappurath, H. Leblond, J. Troles, F. Smektala, and F. Sanchez, "*Experimental and theoretical study of higher-order nonlinearities in chalcogenide glasses*", Opt. Commun, **219**, 427 (2003).
- [188] S. Polyakov, F. Yoshino, M. Liu, and G. Stegeman, "*Nonlinear refraction and multiphoton absorption in polydiacetylenes from 1200 to 2200 nm*", Phys. Rev. B **69**, 115421 (2004).

-
- [189] T. Wang, N. Venkatram, J. Gosciniaik, Y. Cui, G. Qian, W. Ji, and D. T. H. Tan, "*Multi-photon absorption and third-order nonlinearity in silicon at mid-infrared wavelengths*", *Opt. Express* **21**, 32192 (2013).

Appendix

A trial MATLAB numerical code for the CDM technique

We give in the next a full version of the MATLAB numerical code for the CDM technique in fiber optics link as discussed in Chapter 2. Please cite this thesis in any publication using this code as : **C. Heuteu, (Ph.D thesis, Laboratory of Mechanics, Department of Physics, Faculty of Science, University of Yaoundé I, Cameroon, 2024).**

1. First model of Fig. 1 : Fixed chirp and alternation of GVD only

`clc; clear all;`

`T0=50; timewidth`

`s2=-1; starting with an anomalous GVD`

`A=1; normalized power`

`L=4.1; dimensionless length of the fiber/distance of propagation`

`b=0; nonlinearity set zero for linear systems ($b = N^2$)`

`C=-0.5; initial chirp`

`N=1000; Number of time step`

`dt=T0/(N); time step`

`t=(-N/2:(N/2)-1)*dt; timewidth grid`

`w = (2 * pi/(T0)) * (-N/2 : N/2 - 1); frequency grid`

$a = 0.05$; *truncation coefficient*
 $u = A * \exp(a * t) * \text{airy}(t) * \exp(-0.5i * C * t^2)$; *definition of the Airy pulse*
 $u_0 = u$; *input pulse*
 $dz = dt$; *we choose equal step for the space and time*
 $tabz = []$; *initializing the table of the propagation distance parameter*
 $tabu = []$; *initializing the table of the pulse amplitude*
 $JJ = 1$; *parameter of incrementation*
 $z_0 = 0$; *initializing the propagation distance parameter*
for $n = 1 : 20$ *start of the ring for the pulse propagation in the fiber links*
 $s_2 = -s_2$; *alternation of the GVD*
for $z = z_0 : dz : z_0 + L - dz$ *propagation within n-th piece of fiber*
 $um(1, JJ) = \max(\max(\text{abs}(u)))$; *recording the JJ-th max value of the pulse amplitude*
 $tabu = [tabu; \text{abs}(u)]$; *recording the current value of pulse amplitude*
 $u = \exp(b * dz * i * \text{abs}(u) * \text{abs}(u)) * u$; *nonlinear part of the SSFM1*
 $c = \text{fftshift}(\text{fft}(u))$; *Fast Fourier Transform (FFT)*
 $c = \exp(dz * s_2 * i * (w.^2)/2) * c$; *dispersive part of the SSFM*
 $u = \text{ifft}(\text{fftshift}(c))$; *inverse of the FFT = temporal profile*
 $tabz = [tabz; z]$; *recording the current propagation distance*
fprintf
 $JJ = JJ + 1$; *incrementation*
end

$z_0 = z + dz$; *incrementation of the propagation distance*

if $n == 5$ *recording the amplitude at the fifth round*

$u_f = u$;

end

$s2 = -s2$; *alternation of the GVD*

end

figure (1); *hold on of the first figure drawing the 3D – contour plot*

$pcolor(t, tabz, tabu^2)$;*shading interp*;

$xlabel('τ')$;

$ylabel('ξ')$;

figure(2); *hold on of the second figure drawing the 2D-plot of $\max(u)$*

versus $ξ$

$plot(tabz, um)$;

$xlabel('ξ')$;

$ylabel('max | u |^2')$;

2. Second model of Fig. 2 : Fixed GVD and alternation of chirp only

clc ; *clear all*;

$T0=50$; *timewidth*

$s2=-1$; *starting with an anomalous GVD*

$A=1$; *normalized power*

$L=4.1$; *dimensionless length of the fiber/distance of propagation*

$b=0$; *nonlinearity set zero for linear systems ($b = N^2$)*

$C=-0.5$; *initial chirp*

$N=1000$; *Number of time step*

```

dt=T0/(N); time step
t=(-N/2:(N/2)-1)*dt; timewidth grid
w = (2 * pi/(T0)) * (-N/2 : N/2 - 1); frequency grid
a = 0.05; truncation coefficient
u = A * exp(a * t). * airy(t). * exp(-0.5i. * C. * t^2); definition of the Airy pulse
u0 = u; input pulse
dz = dt ; we choose equal step for the space and time
tabz = []; initializing the table of the propagation distance parameter
tabu = []; initializing the table of the pulse amplitude
JJ = 1; parameter of incrementation
z0 = 0; initializing the propagation distance parameter
for n = 1 : 20 start of the ring for the pulse propagation in the fiber links
for z = z0 : dz : z0 + L - dz propagation within n-th piece of fiber
um(1, JJ) = max(max(abs(u))); recording the JJ-th max value of the pulse amplitude
tabu = [tabu; abs(u)]; recording the current value of pulse amplitude
u = exp(b * dz * i * abs(u). * abs(u)). * u; nonlinear part of the SSFM1
c = fftshift(fft(u)); Fast Fourier Transform (FFT)
c = exp(dz * s2 * i * (w.^2)/2). * c; dispersive part of the SSFM
u = ifft(fftshift(c)); inverse of the FFT = temporal profile
tabz = [tabz; z]; recording the current propagation distance
fprintf

```

$JJ = JJ + 1$; *incrementation*

end

$z_0 = z + dz$; *incrementation of the propagation distance*

if $n == 5$ *recording the amplitude at the fifth round*

$u_f = u$;

end

$C = -C$; *alternation of the initial chirp value*

$u = u * \exp(-0.5i * C * t^2)$;

end

figure (1); *hold on of the second figure drawing the 3D – contour plot*

$pcolor(t, tabz, tabu^2)$;*shading interp*;

xlabel('τ');

ylabel('ξ');

figure(2); *hold on of the second figure drawing the 2D-plot of max(u)*

versus ξ

plot(tabz,um);

xlabel('ξ');

ylabel('max | u |²');

3. Third model of Fig. 3 : Alternation of both the GVD and the chirp

clc; clear all;

T0=50; *timewidth*

s2=-1; *starting with an anomalous GVD*

A=1; *normalized power*

L=4.1; *dimensionless length of the fiber/distance of propagation*

$b=0$; *nonlinearity set zero for linear systems ($b = N^2$)*
 $C=-0.5$; *initial chirp*
 $N=1000$; *Number of time step*
 $dt=T_0/(N)$; *time step*
 $t=(-N/2:(N/2)-1)*dt$; *timewidth grid*
 $w = (2 * pi/(T_0)) * (-N/2 : N/2 - 1)$; *frequency grid*
 $a = 0.05$; *truncation coefficient*
 $u = A * exp(a * t) . * airy(t) . * exp(-0.5i . * C . * t^2)$; *definition of the Airy pulse*
 $u_0 = u$; *input pulse*
 $dz = dt$; *we choose equal step for the space and time*
 $tabz = []$; *initializing the table of the propagation distance parameter*
 $tabu = []$; *initializing the table of the pulse amplitude*
 $JJ = 1$; *parameter of incrementation*
 $z_0 = 0$; *initializing the propagation distance parameter*
for $n = 1 : 20$ *start of the ring for the pulse propagation in the fiber links*
for $z = z_0 : dz : z_0 + L - dz$ *propagation within n-th piece of fiber*
 $um(1, JJ) = max(max(abs(u)))$; *recording the JJ-th max value of the pulse amplitude*
 $tabu = [tabu; abs(u)]$; *recording the current value of pulse amplitude*
 $u = exp(b * dz * i * abs(u) . * abs(u)) . * u$; *nonlinear part of the SSFM1*
 $c = fftshift(fft(u))$; *Fast Fourier Transform (FFT)*
 $c = exp(dz * s2 * i * (w.^2)/2) . * c$; *dispersive part of the SSFM*

```

u = ifft(fftshift(c)); inverse of the FFT = temporal profile
tabz = [tabz; z]; recording the current propagation distance
fprintf
JJ = JJ + 1; incrementation
end
z0 = z + dz; incrementation of the propagation distance
if n == 5 recording the amplitude at the fifth round
uf = u;
end
C = -C; alternation of the initial chirp value
s2 = -s2 alternation on GVD
u = u * exp(-0.5i * C * t^2);
end
figure (1); hold on of the third figure drawing the 3D – contour plot
pcolor(t, tabz, tabu^2) ;shading interp;
xlabel('τ');
ylabel('ξ');
figure(2); hold on of the second figure drawing the 2D-plot of max(u)
versus ξ
plot(tabz,um);
xlabel('ξ');
ylabel('max | u |^2');

```

List of Publications

Regular journal papers

1. **C. Heuteu**, L. M. Mandeng and C. Tchawoua, "*Chirp-dispersion management inducing regeneration of truncated Airy pulses in fiber optics links*", J. Opt. Soc. Am. B **37**, A121-A129 (2020).
2. **C. Heuteu**, S. K. Boukar, L. M. Mandeng and C. Tchawoua, "*Supercontinuum generation of truncated Airy pulse in a cubic-quintic $AsSe_2/As_2S_5$ optical waveguide with rib-like structure*", J. Opt. **23**, 095503 (2021).